OPTIMIZATION OF ZINC OXIDE SURGE ARRESTER DESIGN IN REDUCING LEAKAGE CURRENT

NURUL AIN BINTI ABDUL LATIFF

FACULTY OF ENGINEERING
UNIVERSITY OF MALAYA
KUALA LUMPUR

2018

OPTIMIZATION OF ZINC OXIDE SURGE ARRESTER DESIGN IN REDUCING LEAKAGE CURRENT

NURUL AIN BINTI ABDUL LATIFF

THESIS SUBMITTED IN FULFILMENT OF THE REQUIREMENTS FOR THE DEGREE OF DOCTOR OF PHILOSOPHY

FACULTY OF ENGINEERING
UNIVERSITY OF MALAYA
KUALA LUMPUR

2018

UNIVERSITY OF MALAYA

ORIGINAL LITERARY WORK DECLARATION

Name of Candidate: Nurul Ain binti Abdul Latiff [redacted]

Registration/Matric No: KHA 140011

Name of Degree: Doctor of Philosophy

Title of Project Paper/Research Report/Dissertation/Thesis ("this Work"):

Optimization of zinc oxide surge arrester design in reducing leakage current

Field of Study: High Voltage Engineering

I do solemnly and sincerely declare that:

(1) I am the sole author/writer of this Work;
(2) This Work is original;
(3) Any use of any work in which copyright exists was done by way of fair dealing and for permitted purposes and any excerpt or extract from, or reference to or reproduction of any copyright work has been disclosed expressly and sufficiently and the title of the Work and its authorship have been acknowledged in this Work;
(4) I do not have any actual knowledge nor do I ought reasonably to know that the making of this work constitutes an infringement of any copyright work;
(5) I hereby assign all and every rights in the copyright to this Work to the University of Malaya ("UM"), who henceforth shall be owner of the copyright in this Work and that any reproduction or use in any form or by any means whatsoever is prohibited without the written consent of UM having been first had and obtained;
(6) I am fully aware that if in the course of making this Work I have infringed any copyright whether intentionally or otherwise, I may be subject to legal action or any other action as may be determined by UM.

Candidate's Signature Date:

Subscribed and solemnly declared before,

Witness's Signature Date:

Name:

Designation

OPTIMIZATION OF ZINC OXIDE SURGE ARRESTER DESIGN IN REDUCING LEAKAGE CURRENT

ABSTRACT

A surge arrester diverts lightning surge to earth, preventing damage on electrical systems. Under normal operating condition, surge arresters do not conduct current but there is a leakage current flow across surge arresters. Leakage current is one of the factors, which contributes towards degradation of surge arresters. Numerous works on improving surge arrester designs have been conducted since the past. However, works on improvement on surge arrester design using optimisation methods are less likely to be found in literature. Therefore, improvement on surge arrester design by minimising the leakage current across the arrester using optimisation methods is proposed in this work. The main advantage of using optimisation methods is the most suitable solutions can be obtained without trial and error method, which can reduce the simulation time. A three-dimensional (3D) 11kV surge arrester model in finite element method (FEM) was developed and used to simulate the leakage current under normal operating condition. Evolutionary computation methods, imperialist competitive algorithm (ICA) and gravitational search algorithm (GSA) were employed to optimise the arrester designs, which can minimise the leakage current. Measurements of surge arrester leakage current under different conditions were also performed and were used to compare with the simulation results to validate the models that have been developed. Comparison between different optimisation methods allows the most suitable method for surge arrester design optimisation to be identified. The results from this work can also help in improving the design of surge arresters in reducing 15.63% of resistive leakage current in industries.

Keywords: Surge arrester, optimization, evolutionary computation, leakage current measurement, finite element analysis

OPTIMASI REKABENTUK PENANGKAP KILAT JENIS OKSIDA ZINK UNTUK MENGURANGKAN KEBOCORAN ARUS

ABSTRAK

Alat yang melindungi talian penghantaran dari kilat voltan adalah penangkap kilat. Ia mengalihkan lonjakan kilat ke bumi dan mencegah kerosakan pada sistem elektrik. Di bawah keadaan operasi biasa, penangkap kilat tidak menjalankan arus elektrik tetapi terdapat aliran arus bocor. Arus elektrik yang bocor adalah salah satu faktor yang menyumbang ke arah kerosakan penangkap kilat. Banyak kerja untuk memperbaiki reka bentuk penangkap kilat telah dijalankan sejak masa lalu. Walau bagaimanapun, kerja penambahbaikan kepada reka bentuk penangkap kilat menggunakan kaedah pengoptimuman kurang dijumpai dalam kesusasteraan. Oleh itu, peningkatan reka bentuk penangkap kilat dengan meminimumkan kebocoran arus di seluruh penangkap menggunakan kaedah pengoptimuman adalah dicadangkan dalam kerja ini. Kelebihan utama menggunakan kaedah pengoptimuman adalah penyelesaian yang paling sesuai boleh diperolehi tanpa percubaan dan kesilapan kaedah, yang boleh mengurangkan masa simulasi. Tiga dimensi model 11kV penangkap kilat (3D) dalam kaedah unsur terhingga (FEM) telah digunakan untuk mensimulasikan arus bocor di bawah keadaan operasi biasa. Kaedah optimasi iaitu algoritma imperialis kompetitif (ICA) dan carian graviti algoritma (GSA) telah digunakan untuk mengoptimasi reka bentuk penangkap yang boleh mengurangkan kebocoran arus. Pengukuran kebocoran arus terhadap penangkap kilat pada keadaan yang berbeza juga telah dilaksanakan dan digunakan untuk membandingkan dengan keputusan simulasi untuk mengesahkan model yang telah dibangunkan. Perbandingan antara kaedah pengoptimuman yang berbeza boleh membenarkan kaedah yang paling sesuai untuk lonjakan penangkap pengoptimuman reka bentuk yang akan dikenal pasti. Hasil daripada kerja-kerja ini juga boleh membantu dalam

meningkatkan reka bentuk penankap kilat dalam mengurangkan kebocoran rintangan semasa dalam industri sebanyak 15.63%.

Kata kunci: penebat kilat, zinc oxide, kebocoran arus, optimasi

ACKNOWLEDGEMENTS

Thanks to Allah SWT, the most gracious, most merciful, for His blessing who has helped me to manage throughout this project. This research project is conducted as fulfilment of the requirements for the degree of Doctor of Philosophy in University Malaya.

I would like to take this opportunity to express my gratitude to my supervisor, Assoc. Prof. Ir. Dr Hazlee Azil bin Illias for giving me guidance and advice as well as time that he spent on supervising this project. I am truly grateful for his patient in proof reading and language editing, both for my thesis and my research papers. Because of his help, the message can be expressed more clearly and hence make this thesis more readable.

Besides, I truly appreciate and thankful to my second supervisor, Prof. Ir. Dr. Ab Halim bin Abu Bakar for the understanding, patience and trust he vested on me. This thesis would not have been possible without his experience and deep knowledge in high voltage, which added great value to this research.

Special thanks to my colleagues from the University of Malaya High Voltage Research Group (UMHVRG) members, Sameh Dabbak, who is also my husband for assisting me with the experiment setup and Dr. Syahirah binti Abdul Halim for guiding me in using COMSOL Multiphysics software and sharing valuable knowledge. Finally, I would like to convey my gratitude to my families for their prayers and supports.

TABLE OF CONTENTS

LIST OF FIGURES

LIST OF TABLES

LIST OF SYMBOLS AND ABBREVIATIONS

σ	:	Electrical conductivity (S/m)
ρ	:	Density of the material (kg/m3)
k	:	Thermal conductivity (W/mK)
$\mathcal{E}o$	:	Permittivity in vacuum
$\mathcal{E}r$	:	Relative permittivity of the material
T	:	Time (s)
f	:	Frequency (Hz)
A	:	Area (m2)
C	:	Specific heat capacity of the material (J)
C_1	:	Coupling capacitor (nF)
E	:	Electric field (kV)
F	:	Frequency of the applied voltage (Hz)
I	:	Current (A)
I_r	:	Resistive current (μA)
I_c	:	Capacitive current (μA)
I_t	:	Total leakage current (μA)
I_n	:	Nominal discharge current (kA)
J	:	Current density (A)
J_e	:	Externally generated current density (A)
K	:	Temperature in Kelvin (K)
Q	:	Heat source density (W)
Q_j	:	Current source (A)
R	:	Resistance (Ω)
R_s	:	Protective resistor (MΩ)
R_{sh}	:	Shunt resistor (kΩ)

T	:	Temperature (°C)
T_x	:	Transformer (0.22/100kV)
V_{app}	:	Applied voltage (kV)
V	:	Electric potential (kV)

AC	:	Alternating current
FEA	:	Finite Element Analysis
FEM	:	Finite Element Method
FFT	:	Fast Fourier transform
GSA	:	Gravitational Search Algorithm
ICA	:	Imperialist Competitive Algorithm
ITDAM	:	Improved time delay addition method
PDE	:	Partial Differential Equation
RMS	:	Root mean square
TNB	:	Tenaga Nasional Berhad
VI	:	Voltage-Current
ZnO	:	Zinc oxide
2D	:	Two diemension
3D	:	Three dimension

CHAPTER 1: INTRODUCTION

1.1 Overview

Electrical power is transferred by transmission network from generating units at many locations to distribution systems. There are two types of AC transmission networks, underground and overhead transmission lines. The main supporting unit of overhead transmission lines is transmission tower. The protection of transmission towers is very important to avoid instrument from damage. One of the natural phenomena that always occur on transmission towers is lightning overvoltage. The most effective way to protect transmission lines from lightning is by using surge arresters. The purpose of a surge arrester is to limit the peak voltages to a value that will not damage the equipment.

There are many types of surge arresters available since 1965 (Woodworth, 2010). These overvoltage are limited by the use of nonlinear resistive elements. In conventional surge arresters, silicon carbide elements are used. To prevent the continuous flow of leakage currents, spark gaps are required but for modern metal oxide and zinc oxide, gaps are not necessary because they have low leakage current elements. However, leakage current still flows through a surge arrester during normal condition and increases under some circumstances (Hoang, Cho, Alam, & Vu, 2018). Leakage current can be classified as capacitive and resistive component current. Capacitive component current is created from the permittivity of Zinc Oxide (ZnO) elements, stray capacitance or grading capacitor. Resistive component current is created from ZnO element or pollution and is increasing with time, ambient temperature and applied voltage (Bok-Hee Lee, Sung-Man Kang, Ju-Hong Eom, & Kawamura, 2003).

The increasing leakage current across the surge arrester can lead to degradation of surge arrester and it is one of the main sources of disruption and failures in electrical system (Metwally, Eladawy, & Feilat, 2017). Breakdown in electrical system equipment

can result in time consuming and high maintenance cost as the whole equipment is required to be changed (Said, 2018). Along these lines, it is very important to avoid this breakdown in high voltage protective equipment before failures happen (Lu, Xie, Fang, & Hu, 2018). This can be succeeded by having consistent maintenance on the surge arrester by monitoring the leakage current in the surge arrester and analyzing the source of rising leakage current (Latiff, Illias, Bakar, & Dabbak, 2018). On the other hand, the design of surge arrester can also be improved in order to reduce the leakage current (Abdul Latiff, Illias, Abu Bakar, Abd Halim, & Dabbak, 2018). Consequently, the maintenance cost can be minimized and the reliability and consistency of the protection system can be enhanced.

In previous works, the researchers are focused on how to measure leakage current, however, they have limited technique available in developing the exact model of surge arrester and the technique used was restricted in analyse the source of increasing of leakage current. Therefore, in my research, these problem can be solved to achieve the best optimised design of surge arrester to reduce the leakage current by using the proposed FEA model, experiments and optimization techniques that support the engineers and designers in evaluating the reduction of leakage current on new surge arrester designs before being fabricated.

1.2 Problem Statement

Nowadays, gapless surge arrester, which is zinc oxide (ZnO) surge arresters are widely used in power systems since there are many advantages compared to other types of arrester. However, leakage current commonly flows across ZnO to ground during normal condition. Since increasing leakage current value is one of the main factors of weakening of the surge arrester, monitoring of the leakage current behaviour has turned out to be important in assessing the performance of the surge arrester. Thus, the modelling of ZnO

surge arrester is essential in assisting a better understanding of leakage current phenomenon.

Modern improvements related to the ZnO varistors technology have brought in great design enhancements of the surge arresters. However, there is still room for improvement on reducing the leakage current that flows across the ZnO surge arrester under normal condition. Improvement using numerical technique such as finite element analysis (FEA) allows researchers to construct a surge arrester model based on real physical dimensions. Therefore, the developed FEA model can be used to evaluate various factors affecting leakage current across surge arresters.

Although many studies on surge arrester leakage current behavior have been performed since the past, works on improvement on surge arrester design using optimisation methods are less likely to be found in literature. Thus, surge arrester models were developed using actual physical dimensions in finite element method (FEA) in this work and used to simulate the leakage current under different conditions. The developed FEA models were interfaced with a MATLAB programming code to find the optimized design of ZnO surge arrester in reducing the leakage current using optimization methods. The methods include imperialist competitive algorithm (ICA) and gravitational search algorithm (GSA).

1.3 Objectives

In this work, the measurement and simulation of leakage current behaviour through surge arrester have been performed under various conditions and the design of surge arrester was optimised by altering the size and dimension of the arrester in order to reduce the value of leakage current. The main objectives of this project are:

1. To develop a model of leakage current in zinc oxide surge arrester in three-dimensional geometry using finite element analysis method.
2. To investigate the influence of surge arrester parameters on the behaviour of leakage current through the FEA model.
3. To perform measurement of leakage current in zinc oxide surge arrester under various conditions.
4. To apply optimization methods on zinc oxide surge arrester designs to reduce the leakage current.

1.4 Scope of study

In this work, zinc oxide surge arrester was used because it has simple construction and can handle very small to very large current, with almost constant voltage across them. However, there is a leakage current flows from terminal to ground, which can reduce the performance of the surge arrester. Hence, laboratory experiment and simulation work were performed to measure the leakage current. A three-dimensional (3D) 11kV surge arrester model of zinc oxide surge arrester was developed using finite element analysis method to simulate the leakage current across the arrester. The developed FEA model was used to study the effect of surge arrester parameters on behaviour of leakage current.

In order to validate the simulation model, the simulated results were compared with measurement results of leakage current across the surge arrester in various conditions. Then, the developed model was used to find the optimized design of zinc oxide surge arrester in reducing the leakage current. The main advantage of using optimisation methods over trial and error method is the most suitable solutions can be obtained within shorter time. The optimization techniques used to optimize the design are Imperialist Competitive Algorithm (ICA) and Gravitational Search Algorithm (GSA). The results gathered from this techniques were used in the FEA model to redesign the surge arrester.

This work shows the benefit of using FEA-based model in simulating the surge arresters with actual physical dimensions in order to assess the performance of leakage current during normal condition. Furthermore, the conducted study using the FEA model and optimization methods could be beneficial and could increase the confidence among surge arrester designers in designing suitable protection device. This can improve the performance of transmission lines, mainly in terms of reducing the leakage current on surge arresters during normal condition. Through this work, a better understanding of leakage current across ZnO arrester can be attained, which may help in condition monitoring analysis on surge arrester in electrical utilities.

1.5 Contributions of the Thesis

The contributions of the thesis are:

1. Works on reducing leakage current in surge arrester through evaluation of surge arrester design were performed.

One of the factors of surge arrester degradation is the flowing of leakage current through the arrester. Hence, the arrester will damage, resulting in maintenance cost to increase. Therefore, by reducing the leakage current through evaluation of various surge arrester designs, the design which can reduce the leakage current in surge arrester can be identified.

2. Measurement and modelling of leakage current in zinc oxide surge arrester under various conditions were performed.

Measurement and modelling of leakage current in zinc oxide surge arrester under various conditions were performed in this work. The measurement results were replicated by simulation results through a surge arrester model that has been developed using Finite

Element Analysis (FEA) software. The advantage of this software is the model can be precisely developed and yields small error between measurement and simulation results. From comparison of measurement and simulation results, the factors that affect the mechanism of leakage current in surge arresters can be identified.

3. Surge arrester design was optimised by reducing leakage current using optimisation methods.

The developed model of surge arrester using FEA method was used to optimise the surge arrester design by interfacing the model with a MATLAB programming code. The optimization methods used to optimize the design of surge arrester in reducing leakage current in this work are Imperialist Competitive Algorithm (ICA) and Gravitational Search Algorithm (GSA). No research has been undertaken in designing surge arrester with leakage current reduction using these algorithms. Also, GSA and ICA are two recent optimization techniques. In addition, the FEA and optimization techniques can support in evaluating the reduction of leakage current on new surge arrester designs before being fabricated.

1.6 Outline of Thesis

This thesis is organised into five chapters as follows:

Chapter 1 is the introduction section. In this chapter, the overview of the effects of lightning overvoltages on transmission line are described and the leakage current that flows through a surge arrester is briefly explained. At the end of this chapter, the objectives of the study and the thesis outline are stated.

Chapter 2 is the literature review section. This chapter contains explanations on several types of lightning protection devices on transmission lines and details on zinc oxide surge arresters. Moreover, this chapter includes literature review on previous works related to

the leakage current in surge arresters and optimization methods used of designing surge arresters.

Chapter 3 is the methodology section. This section describes in details the development of the models in finite element analysis (FEA), leakage current measurement setup and resistive leakage current extraction method. This chapter also explains in details on the optimisation methods used in this work, which are imperialist competitive algorithm (ICA) and gravitational search algorithm (GSA).

Chapter 4 is the results and discussion section. The simulation and measurement results of surge arrester leakage current under various conditions are presented and discussed in this chapter. The parameters of the surge arrester that influence the performance of leakage current are analysed and explained. The optimised design of the surge arrester based on GSA and ICA is also presented in this section.

Chapter 5 consists of conclusions and recommendation for future wrk. Conclusion are made based on the findings of the work and some recommendations are listed for future work.

CHAPTER 2: LITERATURE REVIEW

2.1 Introduction

This chapter focuses on the types of transmission line protection, features of zinc oxide surge arrester including structure, working principle and degradation, concept of leakage current measurement and parameters related to leakage current performance. The equivalent circuit models that represent surge arresters used by researchers including IEEE model, PINCENTTI model, Fernandez-diaz model are also described in this chapter. Additionally, this chapter contains literature review on previous works which are related to the leakage current in surge arresters and optimization methods used in designing surge arresters.

2.2 Protection of transmission lines

Electricity supply industry always has a problem with overhead transmission lines, the lightning interference problem. Lightning interference can be minimized by shielding the overhead lines by using grounding rods and counter-poise wires and also by including protective devices at the line terminations (Naidu & Kamaraju, 2006). In heavy lightning regions, surge arresters are used.

2.2.1 Ground wires

Ground wire, also known as shielded wires is a conductor which is parallel to the main conductor of transmission lines. This conductor runs above the main conductor of the lines. It is supported on the same tower and grounded at every equally spaced tower (Naidu & Kamaraju, 2006). The ground wire protects the transmission line conductor from lightning discharge and induced charges. The effectiveness of the ground wire depends on the height of the ground wire from the ground and shielding angle. However, the ground wire is not suitable for high voltage transmission lines since the tower height

is more than 50m and lightning strokes occur directly to the line wires. Figure 2.1 shows the shielding arrangement of ground wires, where *h* is height of the ground wire from the earth surface, *G* is ground wire, *P-P* is phase wires and *Θs* is shielding angle.

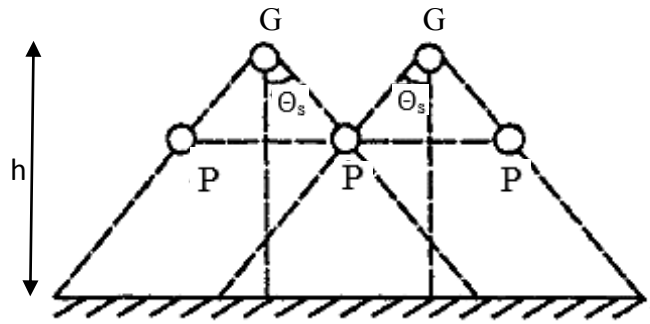

Figure 2.1: Shielding arrangement of ground wires (Naidu & Kamaraju, 2006)

2.2.2 Ground rods and counter poise wires

Ground rod is a rod driven into the ground. Normally, ground rods are made from galvanized iron or copper bearing steel. The standard size of a ground rod is around 3m in length with diameter of 15mm. However, if the rod is used in hard soils, the size will be longer. The depth of the ground wire that is driven depends on the type of the soils and the desired tower footing resistance. Counter poise wires are wires connected to tower legs and running parallel to the conductor of the transmission lines. The length of the wire is normally around 50 to 100m. It can reduce the surge impedance as low as 25Ω. Different from ground rods, the depth of counter poise wires does not affect the resistance but it is more difficult to lay the wires compared to ground rods.

2.2.3 Protective devices

Many types of protective devices can be connected to overhead transmission lines in heavy lightning strokes region. Expulsion gaps and protector tubes are used on the line itself while surge arresters are used at line terminations, junction of lines and substations.

(a) ***Protector tubes***

Protector tube is a device comprises of a rod or spark gap in air formed by a line conductor and its terminal voltage. Protector tubes are mounted on a tower underneath a line conductor. Figure 2.2 shows the position of protector tubes on transmission lines. Nonlinear elements are used in the hollow gap of protector tubes, which gives very high impedance at low currents and during high lightning currents, it offers low impedance.

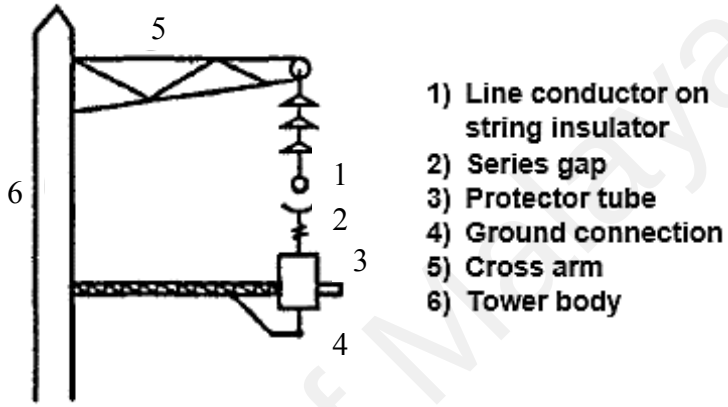

Figure 2.2: Protector tube (Naidu & Kamaraju, 2006)

(b) ***Rod gaps***

Rod gap is the simplest and effective protection device. However, the requirement of this device is not complete, where sparkover voltage depends on atmospheric conditions. Since the rod gaps have no series resistance and very high sparking current, it is dangerous to equipment that needs to be protected. Rod gaps are suitable to be used in lower lightning region and the lines sheltered by ground wires.

(c) ***Expulsion gaps***

The construction and principle of expulsion gaps are similar to protector tubes. It consists of a spark gap together with arc quenching device. The function of arc quenching device is to extinguish the current arc when the gap breaks down due to overvoltages.

Figure 2.3 shows the assembly of expulsion gaps, which consists of a rod gap in series with a second gap enclosed with electrode in a fibre tube.

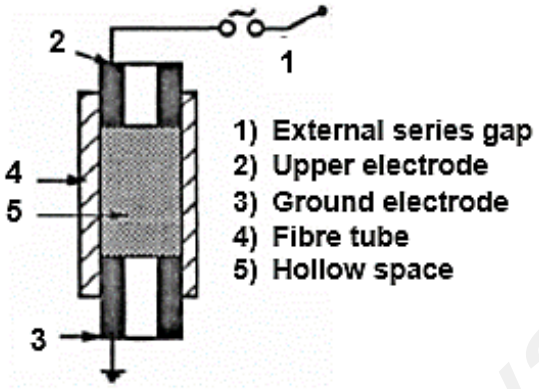

Figure 2.3: Expulsion gap (Naidu & Kamaraju, 2006)

(d) ***Surge arresters***

There are many types of surge arresters, depending on the materials, sizes and rated voltages. Different types of housing can be designed in many forms and this allows optimum surge arrester can be provided for every possible application. All surge arresters are planned for years of operation in their design and provide a contribution towards the protection of the environment. Figure 2.4 shows the location of a surge arrester for transmission and distribution lines. Due to the excellent chemical and physical properties of silicone rubber, it is always used as a shed material.

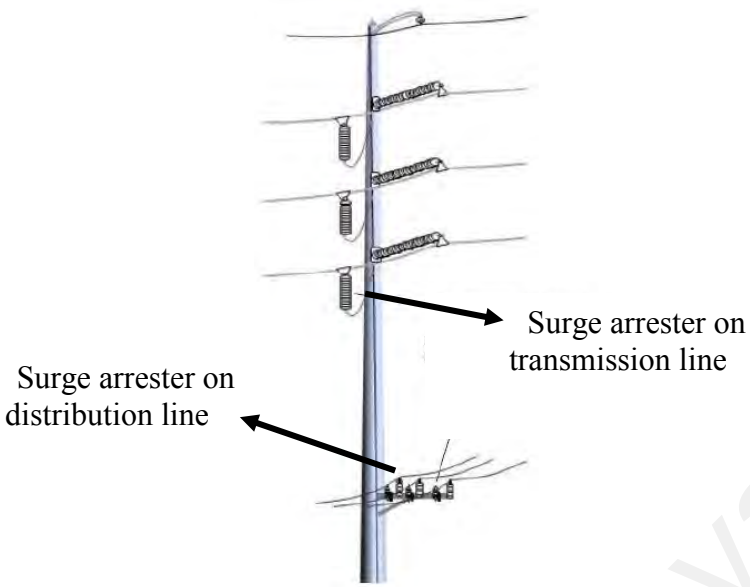

Figure 2.4: Surge arrester on transmission and distribution lines (Woodworth, 2010)

Figure 2.5 shows the types of surge arresters used with different housing materials and design. The housing of a surge arrester is designed with sheds. There are two designs of sheds for arrester housing; alternating shed profile and normal shed profile as shown in Figures 2.6 (a) and (b). The design of the shed including distances, overhang and angle of inclination must follow IEC 60815 regulation. The alternating shed profile can prevent continuous conductive layers from appearing on the surface. Therefore, the ratio of creepage distance to total length can be increased.

(a) **(b)** **(c)**

Figure 2.5: (a) Porcelain housing (b) Silicone housing and (c) Composite housing

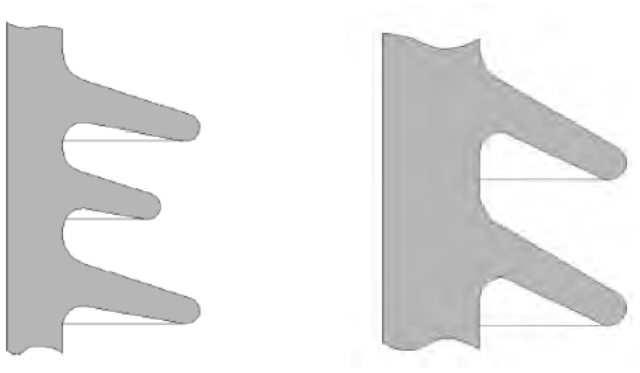

(a) **(b)**

Figure 2.6: Sheds profile (a) Alternating and (b) Normal (Hinrichen, 2006)

Withstanding the internal pressure and arc heat is the important characteristic in designing porcelain housing to avoid damage during internal flow of short circuit current and pressure relief. According to a study, polymer tube design arresters are better than porcelain because they have higher cantilever strength and headload (K.Steinfeld, 2000). Figures 2.7 (a) and (b) show the result of porcelain and polymer housing after short circuit test was conducted. Porcelain housing falls into pieces but not risking the surrounding equipment but polymer shows that arrester housing has kept its full mechanical strength. Hydrophobic effect of a material is a unique advantage of silicon rubber polymer tube design compared to porcelain tube design (Gubanski, S. M., Vlastos, & E, 1990). The risk of surface flashover or thermal instability due to field distortion can be reduced by self-restoring hydrophobicity of the sheds.

For a better protection of equipment and plant, a proper selection of surge arresters is needed. There are three basic characteristics required in selecting the most suitable surge arrester. They are maximum continuous operation voltage, rated voltage and fault current levels. In this study, zinc oxide surge arrester is used since it is the latest type of surge arrester which has low resistance path. An example of typical zinc oxide (ZnO) surge arrester comprises ZnO blocks, FRP rods, and aluminium end fitting, which is stored in a housing as shown in Figure 2.8.

(a) **(b)**

Figure 2.7: Short circuit test (a) Porcelain and (b) Polymer (Steinfeld K., Gohler R., & D, 2003)

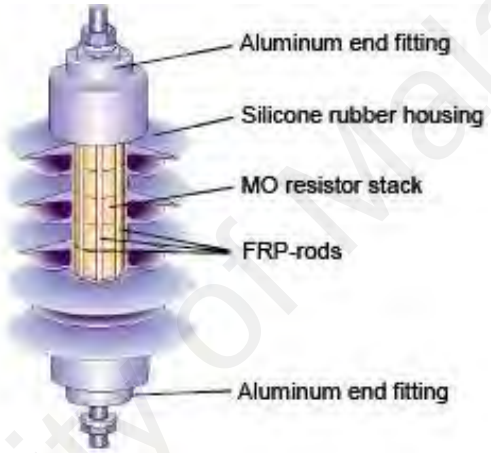

Figure 2.8: Typical arrangement of zinc oxide (ZnO) surge arrester

2.3 Zinc oxide surge arrester

The usual types of surge arresters are silicon carbide arrester with spark gaps, silicon carbide arresters with current limiting gaps and gapless metal oxide arresters. Unfortunately, arresters with spark gaps are not very well suited to limit the switching overvoltages. Therefore, new developments in solid state technology have led to the development of non-linear resistors. With this new technology, new class of surge arresters named zinc oxide (ZnO) has been developed, which can handle very small to very large current with almost constant voltage across them (Naidu & Kamaraju, 2006). The performance of ZnO surge arresters is determined by the thermal and electrical

properties of the metal oxide elements, the material of the insulator and the design of the surge arrester. The advantages of ZnO arresters are simple in construction, no spark gap which produces steep voltage gradient during sparking and have flat VI characteristic over a wide range.

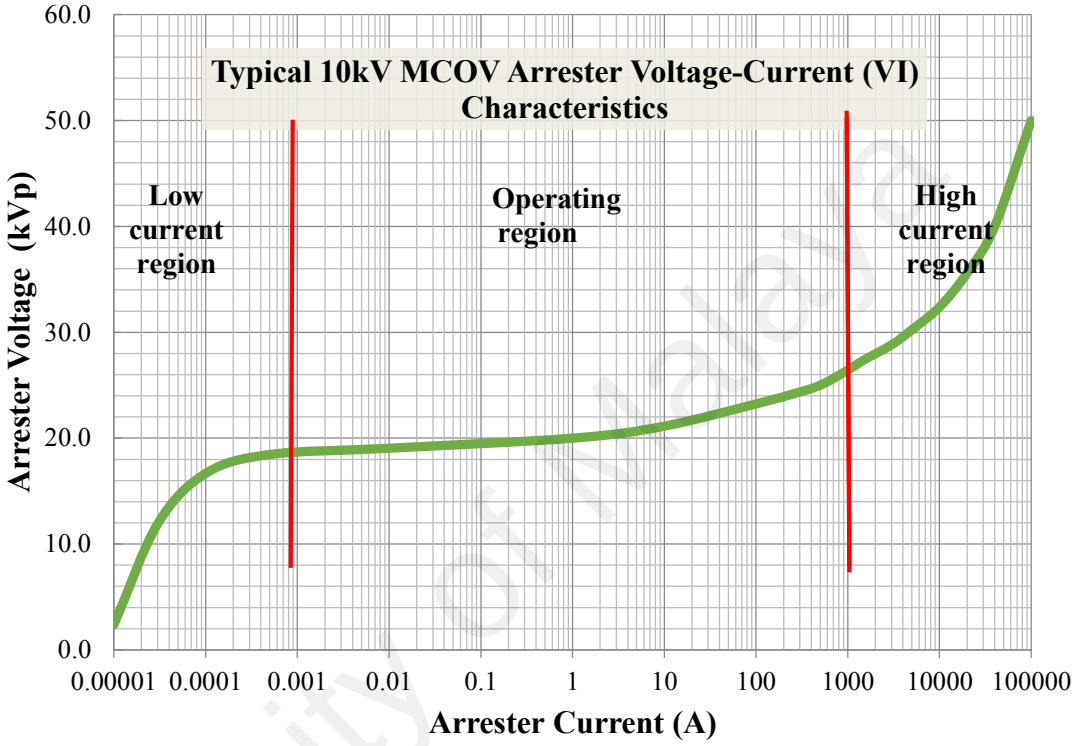

Figure 2.9: VI characteristic of 10kV MCOV surge arrester

Figure 2.9 show an example of VI characteristice curve of a typical ZnO surge arrester for surge arrester with maximum continuous operating voltage (MCOV) of 10kV and class 2, which is also used in this study. Once a VI curve is determined for a ZnO disk, the full arrester characteristics can be predicted. This curve is the fundamental and modest way to show the resistance changes as a function of voltage. The important parts which consists of three regions; they are low current region, operating region and high current region are stated in this figure.

2.3.1 Structure of ZnO varistor

The main component in ZnO surge arrester is ZnO varistor, which is normally produced in a cylindrical block comprises of numbers of solid zinc oxide disc. The voltage rating of the system will decide the number of zinc oxide discs to be used in each surge arrester (Martinez & Durbak, 2005). The block contains a high nonlinear resistance material that is zinc oxide and mixed with other metal oxides, such as small amount of bismuth, cobalt, manganese. In order to obtain high nonlinear conductivity of ZnO varistor, these combinations of metal oxides are sintered at 1000°C. The size of ZnO particles, which is also called microvaristors is between 50-100μm in diameter as shown in Figure 2.10 (Shinji Ishibe, Masafumi Mori, Masahiro Kozako, & Hikita, 2014).

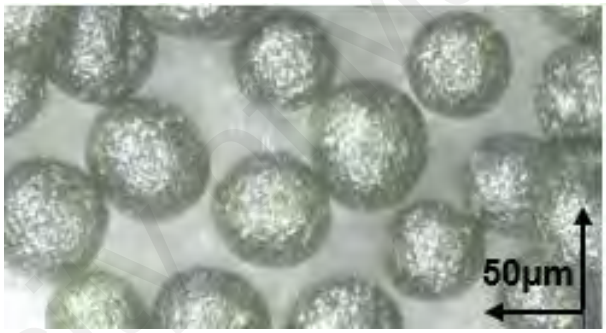

Figure 2.10: Sintered microvaristors (Shinji Ishibe et al., 2014)

ZnO varistor is a semiconductor and represents the protective characteristics of the surge arrester. It is very sensitive to voltage. It is an insulator which does not conduct current at normal voltages. When overvoltage occurs, the voltage will be very high and ZnO becomes a conductor. The ZnO block is a very fast performing electronic switch. It will be an open switch to standard system AC voltages and a closed switch to overvoltages (Coleman, 2000). Figure 2.11 shows an example of surge arrester that uses zinc oxide (ZnO) blocks. They are arranged in parallel to each other.

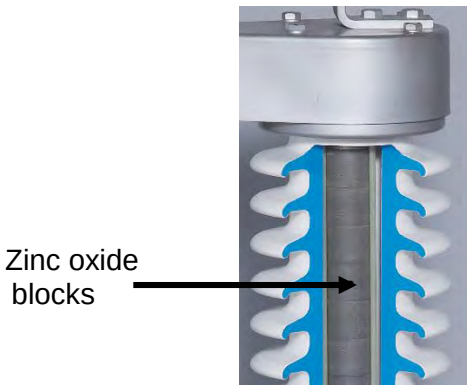

Figure 2.11: ZnO blocks in surge arrester

Each ZnO disk contains billions of ZnO grains. These grains divert the surge current to ground, similar to the operation of an electronic switch (Woodworth, 2010). By enlarging the ZnO material 5000 times, the switches at the junctions between the grains can be discerned as shown in Figure 2.12. The grain junction looks like an open circuit during low voltage. These grains will close when overvoltage happens and causes a rise in the voltage across the terminal. The voltage across it is limited and current can flow through the switches. Therefore, the equipment is protected.

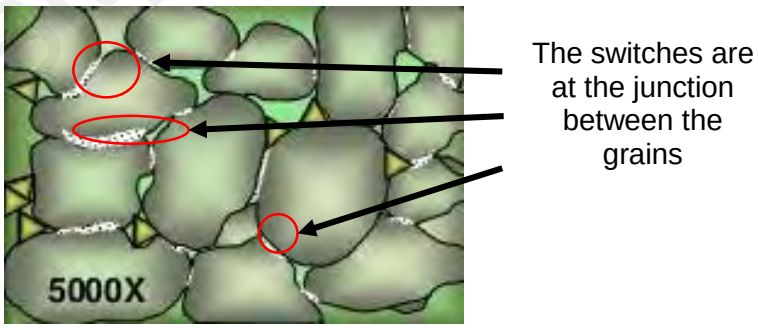

Figure 2.12: Structure of ZnO disk (Woodworth, 2010)

2.3.2 Working principle of ZnO surge arrester

The ZnO surge arrester is connected between phase and ground of transmission line to protect any equipment from damage that is caused by rapid, long term lightning strikes. The working operation of ZnO surge arrester under normal operating voltage and under

overvoltage is shown in Figure 2.13(a). The ZnO varistor plays an important role in protecting the equipment. During normal operation, the impedance of varistor is very high, which is up to megaohms. Because of that, it can be considered as an open circuit. Therefore, the current bypasses the varistor and flows through the equipment.

During overvoltages, the ZnO impedance is very low and the current is very high, which is up to the range of kiloampere. Since the impedance is very low, large current will not flow through the equipment as shown in the Figure 2.13(b). The varistor returns to its normal condition, which is high impedance immediately after the surge absorption is completely finished. The advantage of the varistor is the non-linear characteristics that can demolish the power flowing through it after the overvoltage has disappeared and reduces the residual voltage at high current.

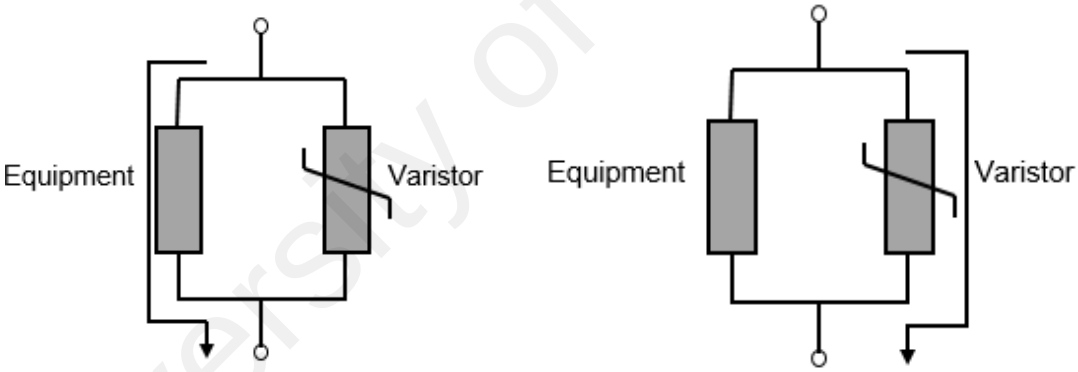

(a) **(b)**

Figure 2.13: Working operation of varistor (a) under normal operating voltage and (b) under high voltage

2.4 Degradation of ZnO surge arrester

The degradation of ZnO surge arrester is caused by many factors. A possible factor of surge arrester degradation is moisture ingress due to weakening of the housing sealing, which can lead to internal discharge (Ohki, 2014). However, varistors in surge arrester are not affected at low humidity level since it is sealed by glaze layers. The internal flashover will be initiated if the humidity level increases (Chrzan, 2004).The performance

of surge arrester housing can be improved with new polymer improvement; high density polyethylene (HDPE) that is lately studied by many researchers (F. Tian, Q. Lei, & Wang, 2011; Ivan Paulo de Faria, Manuel Luis Barreira Martinez, & Queiroz, 2015; T. Takada, Y. Hayase, & Okamoto, 2008; X. Wang, D. M. Tu, & Du, 2008). The material properties such as excellent dielectric, good resistance to weathering, suitable hydrophobicity surface and high thermal and oxidative stability are suitable for medium voltage surge arresters (G. Heger, H.J. Vermeulen, J.P. Holtzhausen, & Vosloo., 2010; R. Arora & Mosch, 2011; Teyssedre & Laurent, 2013).

Moreover, partial discharge that occurs on a surge arrester also increases the internal current of the surge arrester, which will lead to degradation of the surge arrester (Chrzan, 2004). The surge arresters with clean and dry housing surface are normally free from internal partial discharge, where the standard level of acceptable partial discharges is 15pC. For surge arresters with polluted surface, a non-uniform voltage distribution is created. However, the voltage distribution is nearly uniform along the varistor column. The partial discharge is instigated with high radial field on the housing and varistor surface. The electrical properties of varistor can recover within 1 to 2 years even though it is extremely degraded by partial discharge.

Since ZnO varistor is the main component of a surge arrester, many researchers have studied on the structure of ZnO. The increasing of ZnO varistor temperature will increase the leakage current and consequently lead to degradation and cracking of the surge arrester (Sp et al., 2016). By using dielectric characterization, the failure of the surge arrester can be predicted earlier by altering the grain size and formulation of ZnO (Bassi & Tatizawa, 2016). The studies show that actual degradation in actual operation is predictable to encourage the conductivity of the metal oxide to increase. The complexity of voltage-current (VI) characteristics, which is caused by current routes and inadequate links between microvaristors has been conveyed (C. Lin, W. Lee, & W.Whu, 2008).

Additionally, tough manufacture processes for high stacking of microvaristors have also been reported (Shinji Ishibe et al., 2014).

The ZnO surge arrester also degraded due to pollution on external housing. The lessening of oxygen during burning of plastic materials affects the VI characteristic of ZnO blocks (Akbar & Ahmad, 1999). The sealing defects of ZnO blocks results in the excessive leakage current to flow through the arrester. This phenomenon will change the characteristics of the ZnO blocks and resulting in thermal run-away of the surge arrester that leads to failure of the entire surge arrester.

During normal operating conditions, ZnO surge arrester absorbs electrical energy, which increases the temperature of the surge arrester. This will affect the performance of the surge arrester (Reza Shariatinasab, Farid Ajri, & Daman-Khorshid, 2013). Thermal runaway can occur if the surge arrester fails to disperse the absorbed energy to ambient, which can cause the temperature to exceed the operating temperature limitation (Mohammad Ali Atefi, Majid Sanaye-Pasand, & Bahari, 2013). This phenomenon can cause malfunction of the surge arrester. Therefore, surge arresters should operate stably under normal operating voltage and under transient condition (Seyyedbarzegar & Mirzaie, 2016). The aging condition of surge arrester has been investigated using thermal imaging data (Novizona, Maleka, Nouruddeen Bashira, & Asilah, 2013). The studies show the relation between thermal image data and third harmonic of resistive leakage current is applied to monitor the surge arrester condition (Almeida, 2009).

Another renowned factor of surge arrester degradation is overheating of the surge arrester. The heat will increase the temperature of the surge arrester and therefore, increases the leakage current. Thus, it is very important to monitor the leakage current behaviour in order to reduce the degradation time of ZnO surge arrester. There are many studies on monitoring technique for surge arrester based on analysis of leakage current

(M. Khodsuz & Mirzaie, 2015; Masume Khodsuz & Mirzaie, 2016; Masume Khodsuz, Mirzaie, & Seyyedbarzegar, 2015).

2.5 Leakage current in ZnO surge arrester

The purpose of a surge arrester is to limit the peak voltage to a value that will not damage the equipment. ZnO surge arrester has good surge absorption ability with tremendous nonlinear characteristics. However, leakage current continuously flows across ZnO under non-conducting condition from terminal to ground, which affects the electrical performance of ZnO surge arrester. The resistance will drops to a low value when overvoltage occurs and a large current will flow through the surge arrester. The arrester will return to its normal condition after draining the surge energy (G. R. S. Lira & Costa, 2013).

Leakage current can be affected by many parameters of surge arresters. Many researchers have studied on the behaviour of leakage current in various conditions. One of the reasons for increasing and decreasing leakage current is the ambient conditions. The studies also show the difference of leakage current behaviour for different types of surge arresters (Bhattacharya & Roy, 2012). Surge arresters were investigated with different stresses of mechanical, electrical and humidity (Miguel, 2014). It shows that different housing of surge arresters affects the time of leakage current to flow. Studies on surge arrester condition, which is based on the third harmonic leakage current has been conducted by many researchers (A. Gakiya Kanashiro & al., 2011).

2.6 Leakage current measurement techniques

There are many methods to measure and monitor the leakage current on surge arresters. Generally, two methods can be conducted to assess the performance of surge arrester leakage current, which are off-line (requires intruding operation) and on-line (does not

require interrupted operation) methods. By comparing these two methods, the off-line method is more accurate than on-line methods. However, the expenses of this method are more difficult for transportation, disassembly and laboratory testing. Therefore, most researchers have studied on on-line monitoring method, which is more economic.

Leakage current can be classified as capacitive or resistive component current (George R. S. Lira, Costa, & Ferreira, 2014). Capacitive component current is created from permittivity of ZnO elements, stray capacitance or grading capacitor. Resistive component current is created from ZnO element or pollution. However, the resistive current will increase with time, ambient temperature and applied voltage (Bok-Hee Lee et al., 2003). The measurements on extracting the resistive and capacitive leakage current have become very popular among researchers. Many ways have been used to extract the leakage current (Masume Khodsuz & Mirzaie, 2016; G. R. S. Lira & Costa, 2013).

Therefore, several methods on extracting resistive leakage current from the total leakage current have been proposed by many researchers (Masume Khodsuz et al., 2015; G. R. S. Lira & Costa, 2013). There are point-on-wave method, current compensation method, current orthogonality method (Xu, Zhao, Ding, & Lu, 2013), resistive current waveshape-based method (Heinrich & Hinrichsen, 2001), harmonic analysis method (Liao et al., 2000), time delay addition method (Abdul-Malek, Novizon, & Aulia, 2008; Lee & Kang, 2005; M.K. Yalla1, 2012) and improved time delay addition method (Masume Khodsuz & Mirzaie, 2016). An example of extraction waveform of surge arrester leakage current is as shown in Figure 2.14. These methods are basically explained in the next subsection.

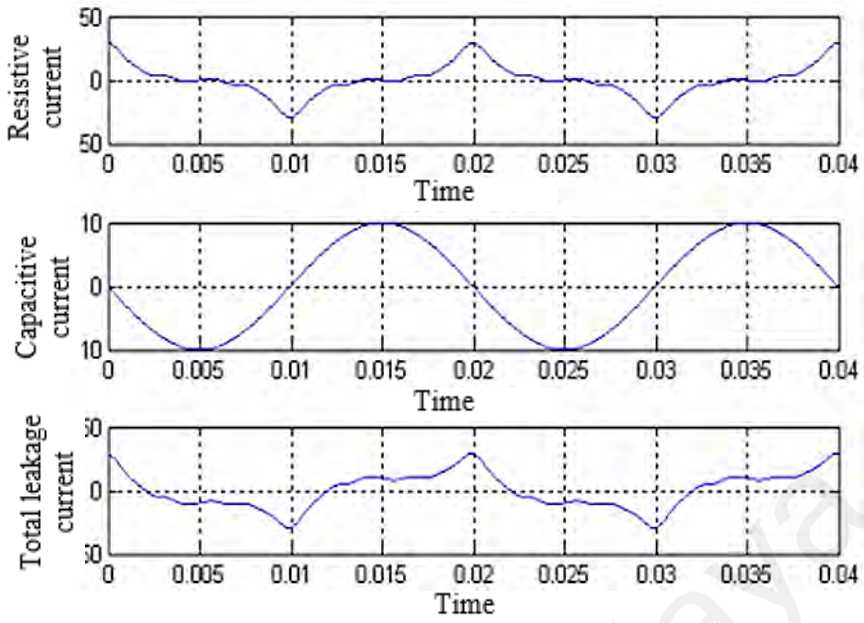

Figure 2.14: Waveform of total, resistive and capacitive leakage current (Abdul-Malek et al., 2008)

2.6.1 Current compensation method (CCCM)

Current compensation method (CCCM) is used by many researchers to obtain resistive leakage current by using compensation technique (Lundquist, Stenstrom, Schei, & Hansen, 1990; Luo, 2003; Shirakawa et al., 1988). The resistive current is attained by using voltage signal, which phase is shifted by 90° (same phase as the capacitive current) in order to compensate the capacitive current component. This method was modified to consider the voltage harmonics (Lundquist et al., 1990) but the results lead to significant error.

2.6.2 Point-on-wave method (POWM)

Same as CCCM, point-on-wave method (POWM), proposed in (Luo, 2003), used capacitive current compensation technique to extracts the resistive current. In this method, the waveform of capacitive current is symmetric at the point of $\pi/2$ and at the half period, it can be eliminated. The advantage of this method is that the measurement

of applied voltage is not required. However, this method ignores the harmonics of the voltage and this leads to inaccuracies or errors.

2.6.3 Resistive current waveshape-based method (RCWM)

The advantage of resistive current waveshape-based method (RCWM) method is the measurement of the applied voltage is not calculated. The capacitive component (only fundamental component) is subtracted from the total sinusoidal leakage current signal and hence, the resistive current contains harmonic components from the capacitive current. However, the measurement of the third harmonic only can be used in detecting particular kinds of degradation.

2.6.4 Harmonic analysis method (HAM)

In the harmonic analysis method (HAM), the voltage and current are decomposed into harmonics for all frequencies by using fast Fourier transform (FFT) algorithm. In FFT, the same phase of harmonic voltage and resistive current are assumed, which is suitable for presenting metal oxide surge arrester (MOSA) parallel with a capacitor and a linear resistor. However, the evidence and clarification of accuracy are not shown.

2.6.5 Current orthogonality method (COM)

Current orthogonality method (COM) is a method improved from CCCM, POWM and HAM. It is used to extract the resistive current based on simulated voltage and leakage current signal, which is created on low current region equivalent circuit of MOSA. The real capacitance can be obtained orthogonality between resistive and capacitive currents even if the applied voltage is unidentified. By multiplying the real capacitance and the differential voltage signal results, the capacitive current is attained. Then, by subtracting the capacitive component from the total leakage current, the resistive current is obtained.

2.6.6 Time delay addition method (TDAM)

Similar to COM method, time delay addition method (ITDAM) is also based on the orthogonality between resistive and capacitive currents. The capacitive current is obtained by shifting the total leakage current as 90° and resistive current is attained by subtracting the capacitive current from the total leakage current. However, the disadvantage of this method is the applied voltage should be pure sinusoidal and therefore the voltage harmonics are ignored. For this reason, there are errors in extracting resistive current particularly in higher order harmonics.

2.6.7 Improved time delay addition method (ITDAM)

Since TDAM is not accurate for non-pure applied voltage, the improved time delay addition method is introduced. This method is also used in this study to extract the resistive leakage current from the total leakage current since it is more precise compared to other methods. The steps in extracting the resistive leakage current are explained in Chapter 3.

2.7 Leakage current measuring device

Normally, more resistive current is allowed by ZnO surge arresters to leak with time and surge degradation, which resistive current increases with the applied voltage and ambient temperature (Lee & Kang, 2005). Hence, the interruption of power supply must be avoided in detecting surge arrester leakage current by using new leakage current detection device. The function of the device is to discriminate the resistive and capacitive currents by using the time-delay addition method. The same researcher has also designed and fabricated a device to diagnosis the weakening of surge arresters. The resistive leakage current with a compensation circuit and third harmonic current component are the methods used. They used current transducer with a ferrite core, which has higher

precision and greater reliability of current detectors to improve the detection sensitivity (Bok-Hee Lee et al., 2003).

Presently, surge arrester commercial monitoring devices are available but they are not suitable for continuous monitoring applications, which can be self-powered. New wireless systems have been studied by N.Harid to monitor the leakage current in electrical substation equipment (Harid, Bogias, Griffiths, Robson, & Haddad, 2016). The continuous data can be provided and the system can be used in a variety of equipment. There are another types of devices used to measure leakage current. One of the devices has been developed to isolate resistive leakage current from the total leakage current. The device which is based on analysis of harmonics of the resistive leakage current has also been developed by other researchers (Novizona et al., 2013).

In this study, the leakage current measuring device is used only to verify the leakage current of experimental setup since it is not capable to load a leakage current waveform, which is very important to be used in extracting the resistive leakage current. This device is used by main energy provider in Malaysia, Tenaga Nasional Berhad (TNB), which is called as SCAR10 to diagnose the condition of surge arresters.

SCAR10 comprises of one measuring instruments and one special clip-on current transformer. It can be used while surge arresters are in service. The clip-on current transformer is used to take the value of the leakage current while clamping it to the ground connection of a surge arrester. The value of this current is normally in the range from fractions of milliampere to a few milliampere and is characterized by a third harmonic distortion, which is an indicator of the deterioration of the surge arrester. The resistive component of this leakage current can increase due to different stresses causing ageing and finally causing arrester failures.

2.8 Model of surge arrester

There are several surge arrester models suggested by researchers to explain the performance of surge arresters. The challenging part of these models is the classification of the surge arrester parameters to determine sufficient values. The renowned used models based on electrical circuit are IEEE, Pinceti-Gianettoni, Fernandez-Diaz, Popov and P-K models.

2.8.1 IEEE model

The most conventional and famous model in representing metal oxide surge arrester is IEEE model, which recommended by IEEE 3-4-11 working group (3-4-11, 1992). This model is based on electrical circuit consisting of two non-linear resistances; A_0 and A_1, R_0 is used to alleviate the numerical integration, L_0 is related to magnetic fields in the area of the arrester and C symbolizes the terminal-to-terminal capacitance. These resistances (A_0 and A_1) are part of the resistor-inductor (RL) filter as shown in Figure 2.15.

This filter is neglected for arrester discharge currents with slow rising time. Hence, A_0 and A_1 are in parallel and describe the static behaviour of the metal oxide surge arrester. The RL filter turns out to be more substantial during fast front currents. In fact, inductance L_1 develops more current into the non-linear branch A_0. The model creates a greater voltage among its input terminals as A_0 has a higher voltage than A_1 that agrees with the dynamic characteristics of the metal oxide surge arrester (Hosseini & Gharadaghi, 2017).

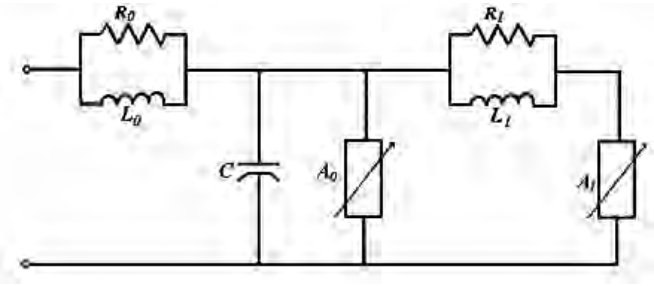

Figure 2.15: IEEE model (Nafar, Gharehpetian, & Niknam, 2011)

2.8.2 Pinceti-Gianettoni model

With some modification on IEEE model, Pinceti-Gianettoni was obtainable as presented in Figure 2.16 but the operating principle is still similar to IEEE model. The modifications are by removing the capacitance since the influence on the model is neglected. The two resistances, A_0 and A_1, which are parallel with inductances, are substituted with one resistance R between the input terminals in order to evade from numerical problems. In this model, only electrical data are required and there are no physical characteristics taken into consideration.

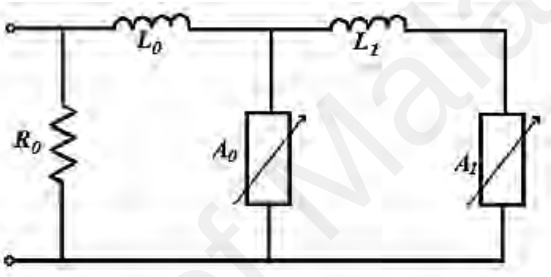

Figure 2.16: Pinceti-Gianettoni model (Nafar et al., 2011)

2.8.3 Fernandez-Diaz model

In 2001, Fernandez-Diaz has proposed another model which also based on IEEE model as shown in Figure 2.17. In this model, the currents across A_0 and A_1 ratio are called I_0 and I_1. The ratio of these currents are assumed to remain constant all over the voltage range of their protection characteristics. The percentage of the voltage increases depending on the inductance L_1.

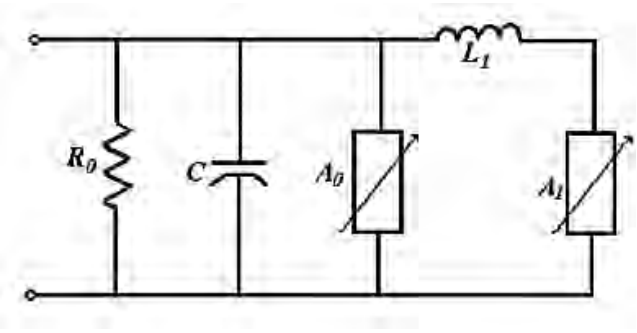

Figure 2.17: Fernandez-Diaz model (Nafar et al., 2011)

2.8.4 P-K model

The P-K model was proposed by (Hosseini & Gharadaghi, 2017) and is shown in Figure 2.18, which is also originated from IEEE. The model is similar to Fernandez-Diaz model but neglecting the effect of capacitance *C*. It is envisioned for the simulation of the dynamic characteristics for discharge currents having front times begining from 0.5 to 8μs.

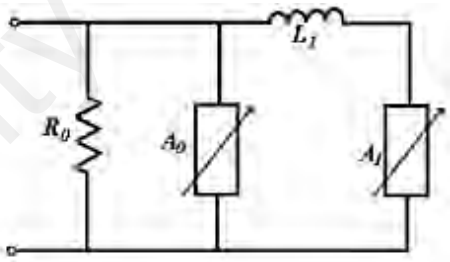

Figure 2.18: P-K model

2.8.5 Popov model

In 2002, Popov has proposed a model that is suitable for switching studies (M & G.C, 2002) as presented in Figure 2.19. An iterative trial and error was needed in order to estimate its parameters. The disadvantage of this model is it does not always obtain the best parameters but by following the procedures, a good estimation of starting point can be achieved.

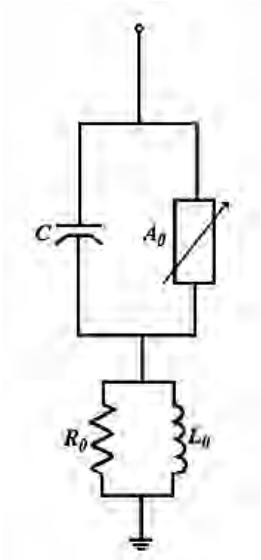

Figure 2.19: Popov model (Nafar et al., 2011)

2.8.6 MOSA wide-range (MWR) model

The MWR model is newly proposed and is suitable for a wide range of amplitude and frequencies (Mousavi, Feizifar, & Onal, 2017). In order to achieve this target, twelve ZnO varistors have been tested with different characteristics from five different companies. The equivalent circuit is presented in Figure 2.20. As mentioned by the authors, the calculation of the parameters are simpler and straight forward compared to other methods. However, the most accurate model is IEEE because it provides the smallest deviation compared to the manufacturer's datasheet.

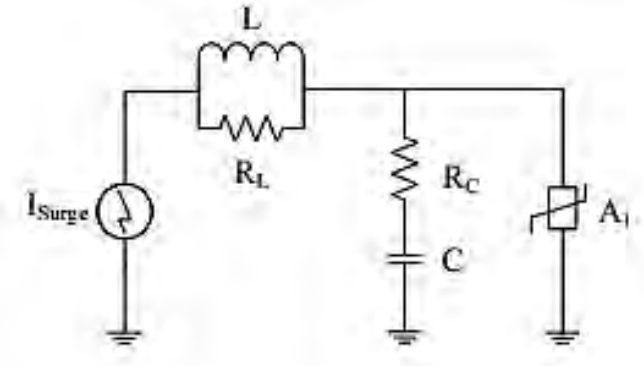

Figure 2.20: Wide-range model (Mousavi et al., 2017)

2.9 Finite element analysis (FEA) model

Finite element analysis (FEA), also called the finite element method (FEM), is a method for numerical solution of field problems and used in this study instead of using equivalent electrical system. By using this model, the accurate parameters of surge arrester can be developed and hence can produce precise results. FEA has advantages over most other numerical analysis methods, including versatility and physical appeal.

The advantages of FEA are applicable to any field problem such as heat transfer, stress analysis, magnetic fields, etc. There is no geometric restriction where the body or region analysed can have any shape. Material properties are not restricted to isotropy and may change from one element to another or even within an element. Many FEA software can be used, such as ANSYS, Star CCM+, COMSOL, Strand7, etc. In this work, COMSOL Multiphysics software was selected because it can be interfaced with other software, which is MATLAB, which was used to optimise the design of surge arrester.

Jose Americo Dias Pinto published a work on thermal analysis of a ZnO surge arrester using the finite element approach. ZnO surge arrester was performed using CAD technique under two different conditions. The transient heat transfer phenomena was also occupied into the explanation. The importance of heating and cooling was discussed and the authors concluded that thermal runaway of ZnO surge arrester can be expected for different temperature, voltage and weather conditions (Pinto, Coimbra, Antunes, & e Moura, 1998). In 2010, Chao Zhang has simulated the surge arrester electric field distribution using FEA by Maxwell software. It shows the electric field distribution on an optimized design of grading ring that has obtained from the Maxwell software (Zhang, Kester, Daley, & Rigby, 2010).

Previous studies have used FEA to calculate the inductance using magnetic flux linkage and capacitance for various transmission line configurations (Hazlee Azil Illias,

Bakar, Mokhlis, & Halim, 2012). The study shows that the results obtained by using FEA is practical with other analytical method and is applicable in general. The same authors also used this method to study on discharge energy capabilities during fast-front surge events on a surge arrester (Hazlee Azil Illias, 2014).

Another researcher, Mohammad R.Meshkatodinni used COMSOL Multiphysics software to analyse the electric field inside regular and bushing-integrated arresters. In his work, the maximum field intensity was found to be on the surface of the varistor blocks (Meshkatoddini, 2018). This shows that the method is applicable in many types of study.

2.10 Design optimization of surge arrester

In order to have better performance of surge arresters, many researchers have studied on optimizing the design of surge arresters. The optimization used to increase the effectiveness of surge arresters are by residual voltage value, surge arrester location, system reliability, lightning performance, insulation coordination studies, etc. From previous researches, the design of 500kV polymeric housed arrester has been discussed in (Jinliang, Shuiming, Rong, Jun, & Chenggang, 2006). The discussion of the arrester includes structure design, selection of ZnO varistor, parameter determination, polymeric housing design and mechanical structure design. From the results, it shows that two-ring shape discharging electrodes were added to the series gap on two ends of a composite insulator. By this new addition, the lightning withstand level of a compact transmission line is improved.

The equivalent circuit parameter model of surge arrester was used to represent the effectiveness of an arrester and to minimize the relative peak residual voltage error between simulation and manufacture data (C.A. Christodoulou, L. Ekonomou, G.P. Fotis,

P. Karampelas, & Stathopulos, 2009). Three arrester models frequently used are IEEE model (Group, 1992), the Pinceti–Gianettoni (PINCETI P. & M, 1999) and the Fernandez–Diaz model. The difference between the current models and the proposed model is the parameter estimation procedure.

Since all models are efficient in simulating frequency-depended behaviour of the arresters (B., 2008), the proposed model is able to simulate curve fit as a real waveform. The gas-discharge arrester's model (GDA) has been studied by another researchers in 2010 (Glotic, Joze Pihler, Janez Ribic, & Stumberger., 2010). The purpose of this study is to determine sufficient parameter values of the model in order to create better performance of a surge arrester.

In 2011, P. Valsalal proposed a few modifications on 198kV arrester design against very fast transient overvoltages in order to improve the dynamic performance. In his study, finite element method (FEM) and electromagnetic transient program (EMTP) were used. FEM was used to compute the block and stray capacitance values of the arrester (Valsalal, Usa, & Udayakumar, 2011).

FEM was also used by another researchers combined with intelligent algorithms to determine the optimal dimension of a grading ring of a metal oxide surge arrester in order to minimize the value of the electric field distribution, inside and outside of the surge arrester (M.R. Aghaebrahimi, Shariatinasab, & Ghayedi, 2012). Therefore, the lifetime of the surge arrester can be increased. Both algorithms were verified with particle swarm optimization (PSO) and differential evolution (DE) techniques. In 2013, PSO method was used by Hamed to prove the accuracy of surge arresters in minimizing the residual peak voltage for lightning surge, switching surge and steep front surge (Hamed Zeinoddini-Meymand, Behrooz Vahidi, Ramezan Ali Naghizadeh, & Moghimi-Haji, 2013).

There are numerous types of optimization techniques used by previous researchers to optimize the design of surge arresters. In this study, optimization techniques have also been used to optimise the design of surge arrester in reducing the leakage current.

2.11 Optimization techniques

The interest in algorithms has been increasing among researchers. The behaviours of natural phenomena have motivated researchers to explain complex computational difficulties (D.H. Kim, A. Abraham, & Cho, 2007; J.D. Farmer, N.H. Packard, & Perelson, 1986; M. Dorigo, V. Maniezzo, & A. Colorni, 1996). Examples of complex computational problems are objective functions (W. Du & Li, 2008), control objectives, pattern recognition, image processing and filter modelling.

Numerous optimization methods have been developed by researchers. The methods are Genetic Algorithm (K.S. Tang, K.F. Man, S. Kwong, & He, 1996), Simulated Annealing, Ant Colony Search Algorithm and Particle Swarm Optimization. Different kinds of optimization problems can be solved by these algorithms, depending on the type of problems since there is no specific algorithm suitable for all kinds of problems (Esmat Rashedi, Hossein Nezamabadi-pour , & Saryazdi, 2009).

In this research work, ICA and GSA were used to optimize the surge arrester design in reducing the leakage current that flows through a surge arrester during normal condition. The result of the leakage current was obtained from the simulation using FEA software, which is COMSOL Multiphysics and interfaced with MATLAB.

2.11.1 Imperialist competitive algorithm (ICA)

Imperialist competitive algorithm (ICA) is an optimization method recently used to deal with different optimization problems. This algorithm was announced in 1989 by

Baran (Baran & Wu, 1989). It is inspired based on the imperialist competition. Vahid Korani has used ICA in his research to efficiently control the traffic of metropolises (Khorani, Razavi, & Disfani, 2011). Mathematical models for traffic have been used to reduce the traffic and also to prevent any kind of traffic standstill in the city. The researchers found out that ICA is the most suitable method because it can solve continuous-optimization problems, similar to traffic problems. The simulation results show that the traffic can be controlled and flexible for all kinds of infrastructure.

In 2013, Masoud Safari published a paper on a strategy of load sharing for a wind/diesel/battery hybrid power system (Safari & Sarvi, 2014). Three optimization methods were used in the research including ICA and other two methods; ant colony optimisation (ACO) and particle swarm optimisation (PSO). These methods were used to optimise load sharing and the results show that it can reduce fuel consumption and the battery lifetime can be increased.

ICA was also used to deal with distribution system reconfiguration in minimizing power losses, branches current constraint violations and deviation of nodes voltages (Jazebi, Hadji, & Naghizadeh, 2014). In order to solve these combination problems, ICA was compared with Discrete Particle Swarm Optimization (DPSO) and Shuffled Frog Leaping Algorithm (SFLA). From the obtained results, ICA is more effective in exploring the search space and produces more promising results. This makes ICA the best optimization technique for long-term reconfiguration problems.

2.11.2 Gravitational search algorithm (GSA)

Another optimization method recently used by researchers is gravitational search algorithm (GSA). Esmat Rashedi first introduced this algorithm in 2009. This algorithm is based on the law of gravity and mass interactions. Based on the Newtonian gravity and

the laws of motion, a collection of masses, which is called agents, are cooperating with each other. The method shows that it can solve various nonlinear functions by comparing with other recognised heuristic methods (Esmat Rashedi, Hossein Nezamabadi-pour , et al., 2009).

Esmat Rashedi also used GSA to present a new linear and nonlinear filter modeling. In the study, the author considered unknown filter parameters as a vector to be optimized. In order to verify the efficiency of the proposed GSA-based filter modeling, genetic algorithm (GA) and particle swarm optimization (PSO) were used to compare the obtained results (Rashedi, Nezamabadi-pour, & Saryazdi, 2011).

S. Duman used GSA in his work to reduce the problem in reactive power system (RPS) (Duman et al., 2012). This problem can decrease grid congestion with minimising active power loss. GSA was used in the problem to find the settings of control variables in order to minimize power losses in transmission system. The results show that GSA is an effective method to solve RPS problem compared to other methods.

In planning and operating stage of power system operation, optimal power flow (OPF) is very important. GSA has been used by A. Bhattacharya to solve OPF problems (Bhattacharya & Roy, 2012). The researchers used laws of gravity and motion of Newton. GSA was used to minimize fuel cost, reduce active power loss and minimize voltage deviation. The results were compared with other optimization methods. The methods are particle swarm optimisation (PSO), evolutionary programming (EP), genetic algorithm (GA) and biogeography-based optimisation (BBO). From the results, it shows that GSA is more effective than others in terms of convergence speed and global search ability.

2.12 Summary

Degradation of surge arresters has been studied by many researchers to increase the performance of surge arresters. A better understanding of surge arrester leakage current phenomena can be achieved through modelling that have been used by past researchers that have been summarized in Table 2.1. The design of surge arresters has been studied to increase the accuracy of surge arresters. Previous researchers have used many ways to measure leakage current of surge arresters as shown in Table 2.2.

Table 2.1: Model of surge arrester

No.	Surge arrester model	Proposed by	Year
1	IEEE model	IEEE working grop 3-4-11	1992
2	Pinceti-Gianettoni model	Pinceti-Gianettoni	1999
3	Fernandez-Diaz model	Fernandez-Diaz	2001
4	P-K model	Pramuk Unahalekhaka	2014
5	Popov model	Popov	2001
6	MOSA wide-range (MWR) model	Mousavi	2017

Table 2.2: Leakage current measuring techniques

No.	Technique	Researcher	Year
1	Current compensation method (CCCM)	S. Shirakawa, F. Endo, H. Kitajima, S. Kobayashi, K. Goto, M. Sakai	1988
2	Point-on-wave method (POWM)	Y.F. Luo	2003
3	Resistive current waveshape-bassed method (RCWM)	C. Heinrich, V. Hinrichsen	2001
4	Harmonic analysis method (HAM)	R.J. Liao, Z.Y. Wang, C.X. Sun, L.G. Gu, P. Yan, B. Yang	2000
5	Current orthogonality method (COM)	X. Zhi-Niu, Z. Li-Juan, A. Ding, L. Fang-Cheng	2013
6	Time delay addition method (TDAM)	B.H. Lee, S.M. Kang	2005
7	Improved time delay addition method (ITDAM)	Masume Khodsuz & Mirzaie	2015

CHAPTER 3: LEAKAGE CURRENT MEASUREMENT, MODELLING AND OPTIMISATION

3.1 Introduction

This section explains the methodology used in this project. The design of the surge arrester using finite element analysis (FEA) software and its simulation are shown in this section. This section also describes leakage current measurement setup in order to validate the FEA model. Various conditions of the surge arrester have also been created. The surge arrester used in this study is 11kV zinc oxide (ZnO) surge arrester without spark gap with silicone housing produced by ABB as shown in Figure 3.1. The type of this arrester is MWK10, which is fabricated and tested according to IEC 60099-4. It is a gapless MOV test standard. The arrester consists of two ZnOs with diameter, height of 47mm respectively, a glassfibre between insulator and ZnO blocks, four silicone sheds and aluminum caps at both ends. The dimensions and parameters of the ZnO surge arrester used in this work are shown in Table 3.1.

Figure 3.1: 11kV zinc oxide surge arrester with silicone rubber housing

Table 3.1: Dimensions and parameters of the surge arrester

Characteristics	Data
Height	227 mm
Housing material	Silicon rubber
Creepage distance	344 mm
Dimensions (L x B x H)	39 x 29 x 26 cm
Net weight	1.86 kg
Number of sheds	4
Maximum continuous operating voltage (MCOV)	10 kV_{rms}
Rated voltage	12.5 kV_{rms}
Nominal discharge current I_n 8/20 µs	10 kA peak

This section also describes in details the optimisation methods used in this work, which are imperialist competitive algorithm (ICA) and gravitational search algorithm (GSA). There are six parameters adjusted on the surge arrester. The parameters are the dimension of the aluminum block, aluminum base, curve of the housing shed, thickness of the silicone rubber, permittivity of the silicone rubber and glassfibre, as shown in Figure 3.2.

These parameters were optimised in order to achieve the lowest leakage current that flows through the arrester. These parameters were selected because they have strong influence on the leakage current in the surge arrester. The size of the design can be changed while for the material permittivity, there is variation in the permittivity value of the glassfibre and silicone rubber available in the market. The objective function of the problem is defined as the minimum leakage current that flows through the arrester. The optimized leakage current through the surge arrester must be less than the leakage current through the original surge arrester design, which is 408µA.

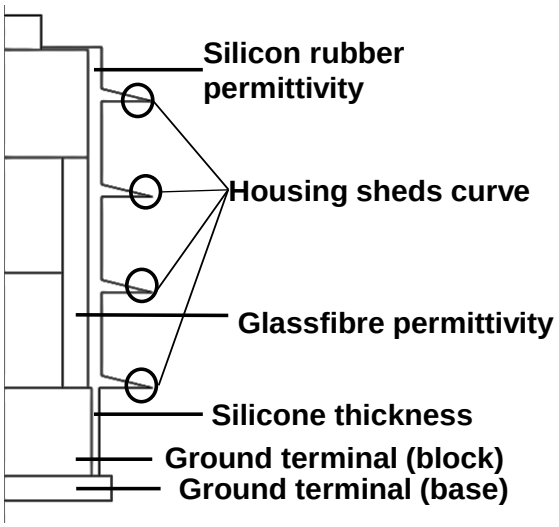

Figure 3.2: Optimised parameters of 11kV surge arrester

3.2 Modeling of surge arrester

A surge arrester was modelled in three-dimensional (3D) by using finite element analysis (FEA) software. Two physics were used in this simulation under 'AC/DC Module'. They are 'electric current' and 'heat transfer in solids' module. The electric current was used to generate the current density and electric field on the surge arrester model while the heat transfer in solids module was used to solve temperature distribution in the model.

3.2.1 Model geometry

An 11kV ZnO surge arrester was modelled in three-dimensional (3D) by using finite element analysis (FEA) software as shown in Figure 3.3. The surge arrester is modelled based on the dimensions from the actual surge arrester that was used in the measurement. The arrester comprises of two zinc oxide blocks with diameter of 47mm and height of 47mm, a glassfibre between insulation and ZnO with width and height of 10mm and 90mm respectively and the aluminum caps at each end. The insulation material is made of silicone rubber and the whole model geometry was surrounded by a layer of air.

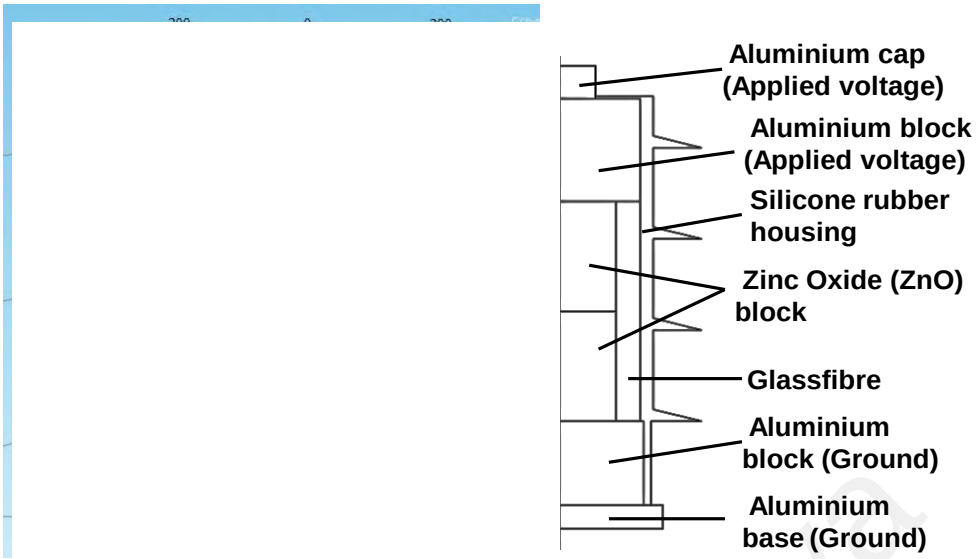

(a) **(b)**

Figure 3.3: Surge arrester model; (a) drawn in 3D and (b) detailed structure of the model

3.2.2 Material and boundary settings

The electrical conductivity σ and relative permittivity ε_r of each material in the model were assigned as listed in Table 3.2. Since ZnO is a nonlinear element, the electrical conductivity of the ZnO blocks was assigned according to the measured V-I characteristics curve of the surge arrester as shown in Figure 3.4 during normal condition, where their electrical conductivity is voltage-dependent. This curve is a fundamental approach of displaying the changing of resistance as a function of the voltage. Generally, the ZnO varistors spends its whole life in this region where conduction is very near to zero by means of minimal leakage current flowing through arrester.

The boundary conditions of the model were set with relevant interface settings as shown in Table 3.3. The terminal of the arrester was applied with a voltage with presence of harmonic components while the bottom of the arrester was grounded, which zero electric potential was applied. The outer side of the arrester was enclosed by air. All interior boundaries were set to continuity.

Table 3.2 Properties of each material in the electric current physic

Material	Relative Permittivity, ε_r	Electrical Conductivity, σ (Sm^{-1})
Air	1	0
Silicon rubber	11.7	$1x10^{-12}$
Zinc Oxide	2250	From V-I characteristics
Glassfibre	4.2	$1x10^{-14}$
Aluminum	1	$3.77x10^{7}$

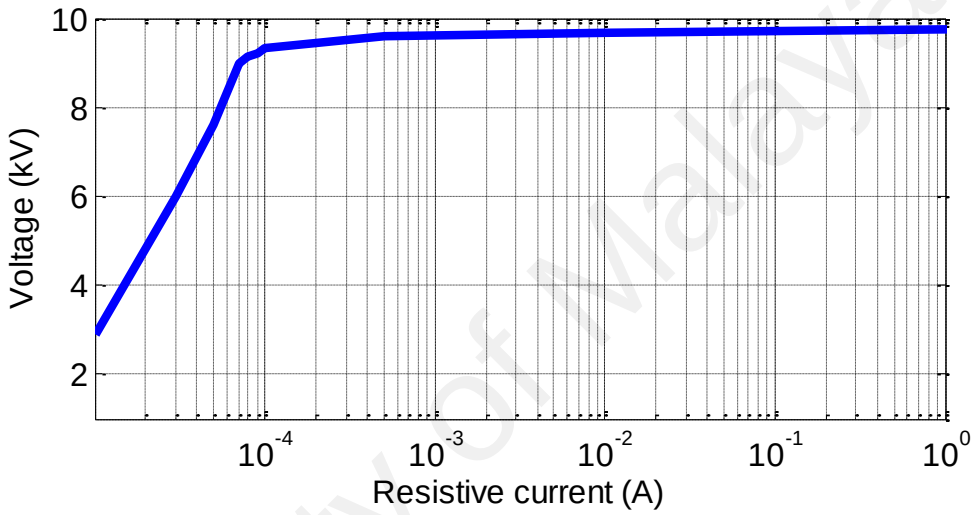

Figure 3.4: V-I characteristics curve of ZnO varistor

Table 3.3: Boundary setting of the electric current physic

Boundary	Boundary condition	Expression
Terminal	Applied voltage	$V = V_0 + \sum_{k=1}^{K} V_k \sin(kwt + \alpha_k)$
Air	Electric insulation	$n.J = 0$
Ground	0V	$V = 0$
All interior boundary	Continuity	$n.(J_1 - J_2) = 0$

3.2.3 Meshing

After the boundary and material of the model were assigned, the model was meshed. The FEA model estimates the solution of domain, boundary, edge and point of surge arrester model by using some elementary shape functions, which include tetrahedral,

triangular, edge and vertex elements. The shape function can be either constant, linear, or of higher order. In order to obtain accurate results, a finer or coarser mesh is required depending on the element order in the surge arrester model. Since the size of the triangular elements has substantial effect on the simulation time, the size of the triangular elements used was normal for air, finer for all domains of the model except for ZnO, which is extremely fine because it is the important element of the model (BAKAR et al., 2016; Hazlee Azil Illias, 2014; H. Illias, Chen, & Lewin, 2017; Hazlee A Illias, Chen, & Lewin, 2011). During constraining the potential on edges, it it can produce a current outflow that is mesh-dependent.

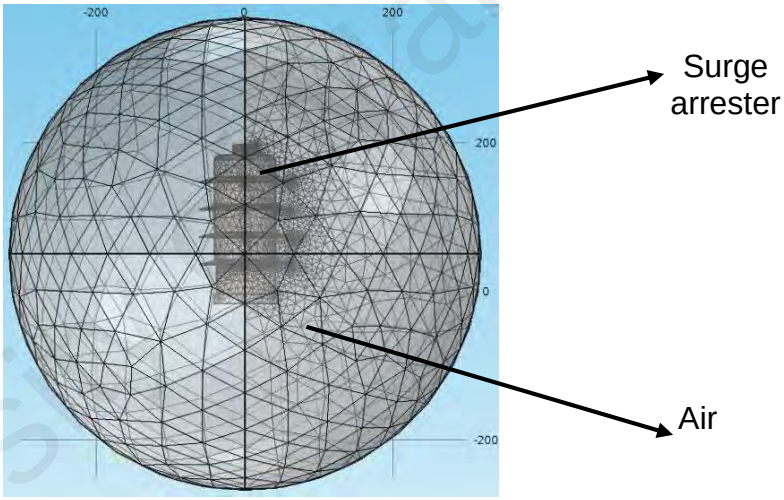

(a)

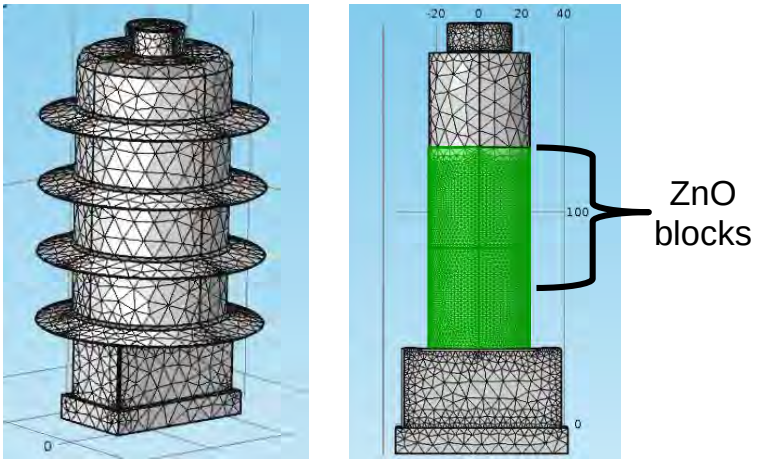

(b) **(c)**

Figure 3.5: Meshing elements in the model; (a) normal elements for air, (b) finer elements for all domains of surge arrester and (c) extremely fine elements for ZnO

The number of elements used in this model are 106194, 14943, 2792 and 245 for tetrahedral, triangular, edge and vertex elements respectively. For domain of the surge arrester, the elements of tetrahedral were used, triangular elements for boundary, edge elements for all edges and vertex for all points. The meshing elements of the surge arrester are illustrated in Figure 3.5 and the statistics of the mesh elements for each type of the elements are specifies in Table 3.4.

Table 3.4: Statistic of mesh elements of surge arrester model

Geometric entity level	Type of element	Number of element	Element statistic
Domain	Tetrahedral	106194	Minimum element quality : 1.351×10^{-4} Average element quality : 0.6143 Element volume ratio : 2.89×10^{-7} Mesh volume : 1.116×10^{8} mm^3
Boundary	Triangular	14943	Minimum element quality : 0.02004 Average element quality : 0.8325 Element area ratio : 3.119×10^{-5} Mesh face area : 1434000 mm^2
Edge	Edge	2792	Element length ratio : 0.006671 Mesh edge length : 20150 mm Maximum growth rate : 9.865 Average growth rate : 2.032
Point	Vertex	245	-

3.2.4 Electric current equations

The geometry of the surge arrester model was solved using partial differential equations (PDE). The module employed in the model is the electric current module to obtain the electric field and current density distributions on the surge arrester. In the electric current model, current conservation is the main point which inserts the electric potential equations and offers a settings window to define electrical conductivity, constitutive relation for the electric displacement field and its related material properties. In the surge arrester model, the leakage current was calculated through surface integration

of the current density, which was attained on the ground surface. Eqs. (3.1) to (3.5) were used by the FEA model to solve the problem,

$$\nabla . J = Q_j \tag{3.1}$$

$$J = \left(\sigma + \epsilon_0 \epsilon_r \frac{\partial}{\partial_t}\right) E + J_e \tag{3.2}$$

where J is the current density, Q_j is the current source, ε_r is the relative permittivity of the material, σ is the electrical conductivity, E is the electric field, J_e is the externally generated current density, which equals to zero in the surge arrester model and V is the electric potential.The problem to be solved in the model is governed by Maxwell's equation as follows,

$$\nabla \times E + \frac{\partial B}{\partial t} = 0 \tag{3.3}$$

By applying quasi-static assumptions, Eq. (3) becomes

$$\nabla \times E = 0 \tag{3.4}$$

Since the electric field E is conservative and irrotational, E can be written as

$$E = -\nabla V \tag{3.5}$$

The resistive and capacitive currents from the obtained leakage current were extracted by improved time-delay addition method (ITDAM) because it is more precise compared to other extraction methods (Masume Khodsuz & Mirzaie, 2016).

3.3 Measurement setup using leakage current measuring equipment

This section focuses on leakage current experimental arrangement and preparation of the test samples. Figure 3.6 and Figure 3.7 show the leakage current measurement setup on ZnO surge arrester used in the laboratory. The measurement setup consists of a sinusoidal variable voltage source, a high voltage step-up transformer (T_x) of 0.22/100kV, a 2.4 MW protective resistor (R_s) to prevent short circuit, a 1 nF measuring capacitor (C_1) to observe the applied voltage, a measuring circuit, a 20 kW shunt resistor (R_{sh}) to

measure the leakage currents by measuring the voltage drop from the current built across the resistance and a two channel digital storage oscilloscope to capture the applied voltage and current through a silicone rubber-housed surge arrester.

The experiment was performed under various applied voltage amplitudes, different wetness conditions and several artificial pollution conditions. A leakage current measuring equipment, SCAR10 was used. SCAR10 is an equipment used by Malaysia main company of energy provider, Tenaga Nasional Berhad (TNB) to measure leakage current across surge arresters in service.

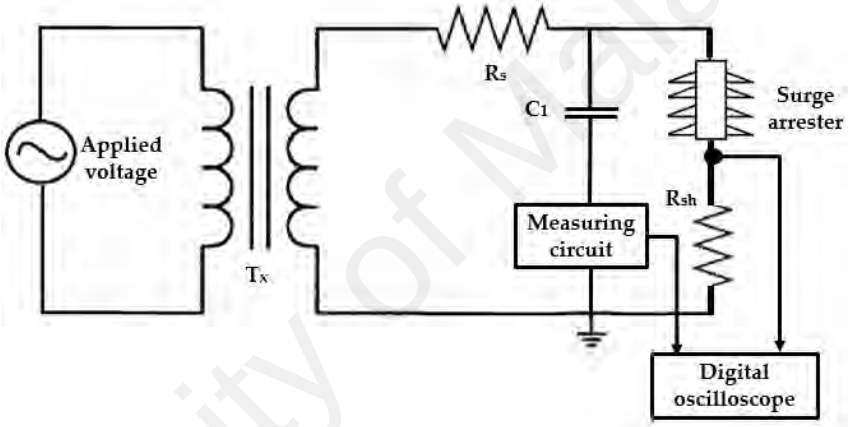

Figure 3.6: Experimental set up for leakage current measurement

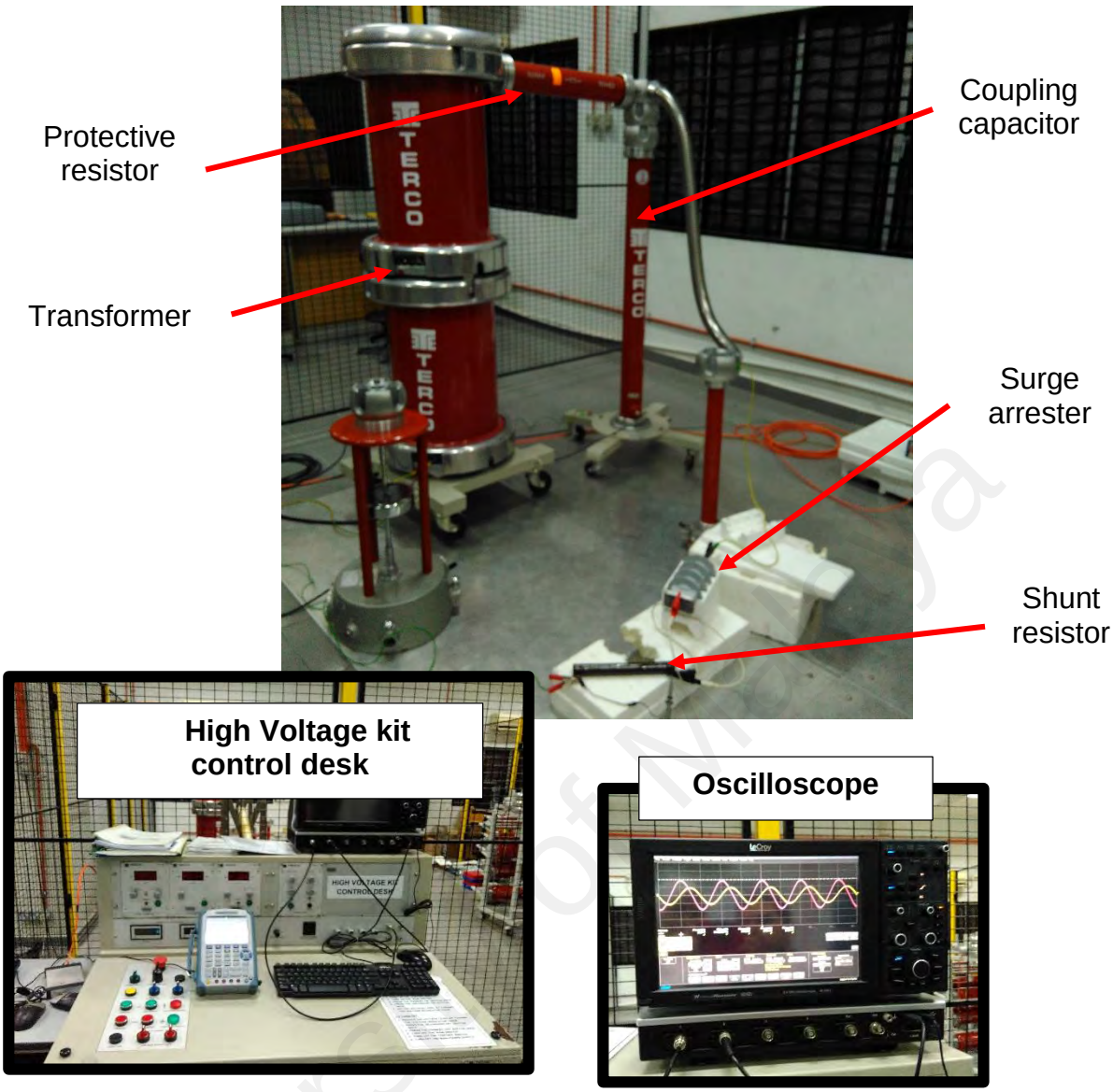

Figure 3.7: The actual experiment setup

SCAR10 is used to diagnose the condition of leakage current surge arresters by using clip-on current transformer, which is C 47-IS. It is specially invented to measure leakage current losses in the existence of high magnetic and electric fields as the windings are circulated on the magnetic circuit and reduces the exterior effect. Moreover, the handle of the transformer is built in with signal pre-amplifier to minimize the inaccuracy. The clip-on current transformer is used by clamping it to the ground connection of a surge arrester. The value of the current is normally in the range from fractions of milliampere

to a few milliampere. It is characterized by the third harmonic distortion, which is an indicator of the deterioration of the surge arrester.

Figure 3.8 and Figure 3.9 illustrate the SCAR10 equipment and experiment setup. The calibration was done before using the equipment. The output of the calibration test generates a triangular waveform current output of 1 mA peak at 50Hz, which flows on a short-circuit wire supplied with RMS current value of 0.606 mA ± 5%. The effective value of the third harmonic component is 65μA ± 5%. The obtained measurement results for different conditions are compared with the simulation results. This allows physical mechanisms affecting leakage current activity for various stress conditions to be identified.

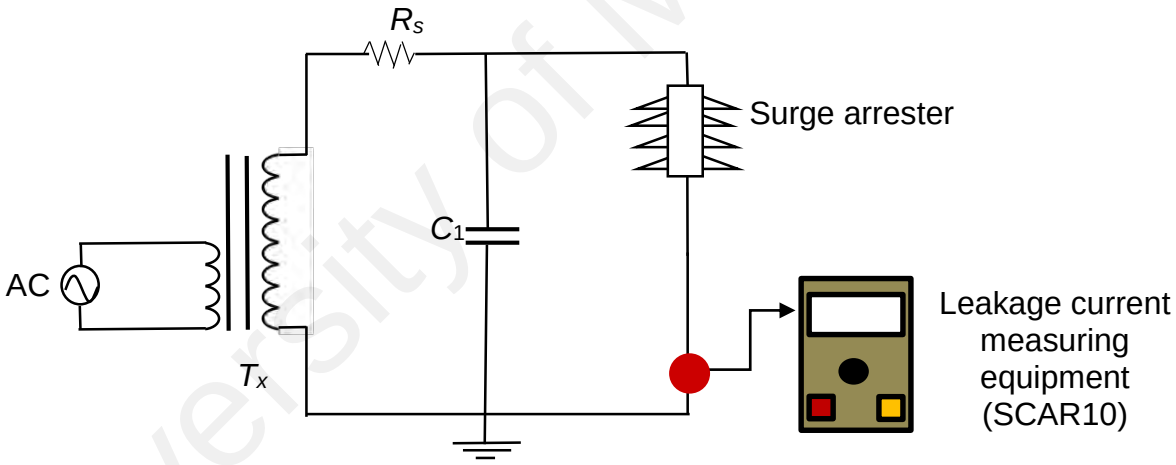

Figure 3.8: Experimental set up for leakage current measurement using SCAR10

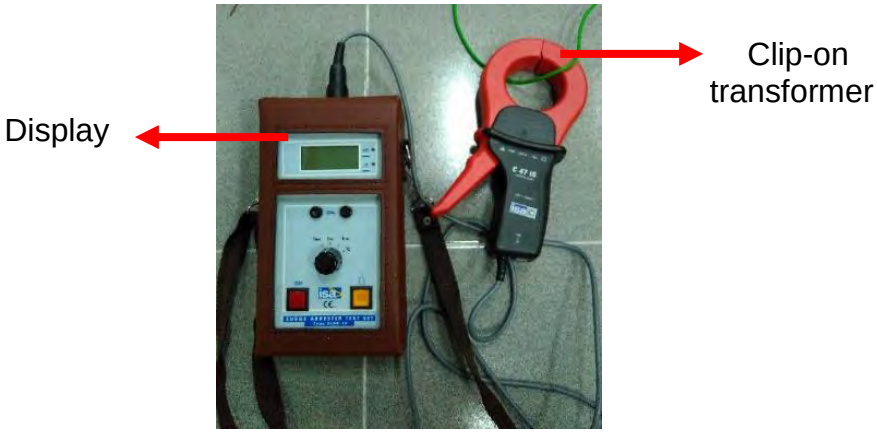

Figure 3.9: Leakage current equipment (SCAR10)

3.3.1 Variable applied voltage amplitude measurement

The surge arrester used in this experiment is 11kV with zinc oxide varistor, which is housed using silicone rubber manufactured by ABB. For experiments of leakage current activity under different applied voltage, the applied voltage amplitude of 50 Hz AC sinusoidal was varied at 6, 6.5, 7, 7.5, 8, 8.5, 9, 9.5 and 10 kV_{rms} while maintaining its temperature at 26°C. This allowed observation of whether the sequence influences the leakage current measurement or not. The surge arrester was stressed for 30 minutes at 5kV_{rms}, 50 Hz before any measurement was taken to ensure that quasi-static conditions were reached.

3.3.2 Variable wetness condition measurement

One of the objectives of this work was to inspect the effect of pollution on the leakage current of the surge arrester. Hence, test samples 2 and 3 were prepared based on the pollution related to natural and anthropogenic sources. For test sample 2, the uncontaminated arrester was sprayed with water of 100Vm resistivity. Different wetness of the arrester was prepared by adding water on the arrester surface in different quantity (50ml, 100ml, 150ml) and tested under applied voltage of 8kV_{rms} at 26°C as shown in Figure 3.10.

(a) **(b)**

(c) **(d)**

Figure 3.10: Different wetness conditions of the surge arrester; (a) Dry (b) Lightly wet (5oml) (c) Wet (100ml) and (d) Very wet (150ml)

3.3.3 Variable artificial pollution condition measurement

For test sample 3, the surge arrester was polluted by anthropogenic source as showsn in Figure 3.11. The outer layer of the surge arrester was contaminated with dry sand, wet sand, salt sand and salt water and tested under applied voltage of 50 Hz, $8kV_{rms}$ AC sinusoidal at 26ºC. The wet sand was prepared by adding 200g of sand into 150mL of distilled water. The salt sand is combination of 50g of NaCl and 100g of sand while for salt water, the solution consists of 100g NaCl and 100mL distilled water. For every artificial pollution type, the arrester was cleaned and rinsed with water thoroughly before another type of artificial pollution was applied.

At the end of the experiment, the leakage current waveform recorded by the oscilloscope was used to extract the resistive and capacitive current using an improved time-delay addition method (ITDAM), which is explained in Section 3.3 (Masume Khodsuz & Mirzaie, 2016). The summary of the conducted measurements is presented in Table 3.5.

(a)

(b)

(c)

(d)

(e)

Figure 3.11: Different artificial pollution conditions of the surge arrester; (a) clean, (b) dry sand (100g of sand), (c) wet sand (200g of sand & 150ml water), (d) salt sand (50g of salt & 100g of sand) and (e) salt water (100g of salt & 100ml water)

Table 3.5: Conditions of each test sample

Test sample	Condition	
	Applied voltage amplitude	**Surface condition**
1	50 Hz AC sinusoidal: 6, 6.5, 7, 7.5, 8, 8.5, 9, 9.5 and 10kV_{rms}	Clean
2	50 Hz, 8kV_{rms} AC sinusoidal	Dry, lightly wet (50ml), wet (100ml), very wet (150ml)
3	50 Hz, 8kV_{rms} AC sinusoidal	Clean, dry sand (100g of sand), wet sand (200g of sand & 150ml water), salt sand (50g of salt & 100g of sand) and salt water (100g of salt & 100ml water)

3.3. Resistive leakage current extraction method

Since the resistive current has a smaller value, which is around twenty percent from the total leakage current, extracting resistive leakage current turns out to be complicated. During normal operating voltage, the range of resistive current value is 100μA whereas the capacitive current value is in the range of 1mA, which is dominant in the range of operating voltage. Since surge arresters consist of high nonlinearity region, resistive component is highly distorted and non-sinusoidal.

There are several techniques to compute the value of resistive leakage current from the total of leakage current. The method used to extract resistive leakage current in this study is improved time delay addition method (ITDAM) (Masume Khodsuz & Mirzaie, 2016). This method is chosen since it is more precise compared to other previous algorithm. This method is capable to extract resistive and capacitive currents under applied harmonic voltages and based on the study, ITDAM is able to be utilized in offline or online measuring process.

This technique is based on the orthogonality between resistive and capacitive currents. The advantage of this method is that the harmonic components of the applied voltage is not ignored. The resistive current is extracted from the total leakage current under applied harmonic voltages. The capacitive current is attained by shifting the total leakage current by 90^0.Then, the resistive leakage current is obtained by subtracting the capacitive leakage current from the total leakage current. In this method, only the third and fifth harmonics of the applied voltage were measured. Since the upper harmonics comprise of only small values, they are not considered. The steps used for this method are as follows:

Step 1 : Obtaining signals

The first step in extracting resistive leakage current using ITDAM is obtaining the signals of applied voltage and total leakage current of the measurement and simulation.

Step 2 : Determine the phase angles and amplitudes of current signals

The Fast Fourier Transform (FFT) was used to determine the phase angles and amplitudes of total leakage current to the measured current signal (I_{t1m} - θ_{1i}, I_{t3m} - ϑ_{3i}, I_{t5m} - ϑ_{5i}).

Step 3 : Determine the phase angles of voltage signals

The phase angle of voltage harmonics was determined by applying FFT to the voltage signals (ϑ_{1v}, ϑ_{3v}, ϑ_{5v}).

Step 4 : Shifting the phase leakage current

The lagging phase ($2\vartheta_{1i}$ - $2\,\vartheta_{1v}$) was used to shift I_{t1}.

Step 5 : Inserting the phase shifted leakage current

I_{t1} was inserted with the phase-shifted leakage current ($I_{t1shifted}$).

Step 6 : Determine the peak time

The peak time of added current waveforms (T_{p1}) was determined.

Step 7 : Obtaining the capacitive leakage current

Based on the T_{p1}, the fundamental harmonic peak value of the capacitive leakage current (I_{c1m}) can be obtained from the I_{t1} waveform. The fundamental capacitive leakage current is formed as follows:

$$I_{c1}(t) = I_{c1m} \cos(wt + \vartheta_{1v}) \tag{3.6}$$

Step 8 : Repeat step 4 and 7

For other harmonics, steps (d) and (g) are repeated.

Step 9 : Attaining resistive leakage current

The fundamental, third and fifth capacitive currents are added and capacitive current is obtained. Finally, by subtracting the obtained capacitive current from the total measured current, the resistive current can be found.

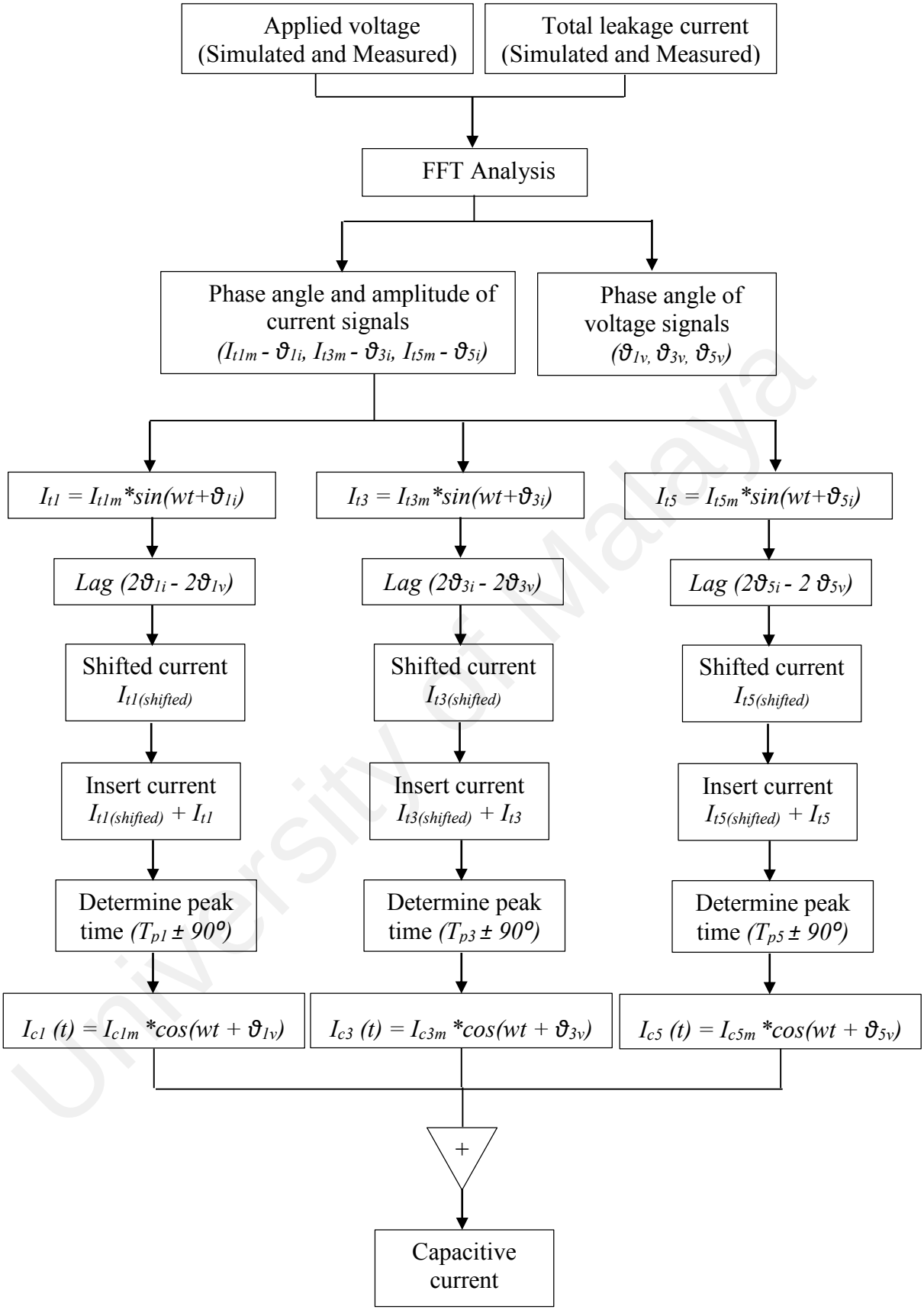

Figure 3.12: Block diagram of ITDAM steps

3.4 Gravitational search algorithm (GSA)

GSA is an optimisation technique motivated by the Newton law of motion and gravity. E. Rashedi first introduced this algorithm in 2009 (Esmat Rashedi, Hossein Nezamabadi-pour *, & Saryazdi, 2009). In GSA, the performance of the objects, called as agents, are measured by their masses. The solution of the problem is the position of the mass and the objective function is used to specify its gravitational and inertial masses. The steps involved in GSA in optimising the surge arrester design in this work are as follows:

Step 1: Initializing agents

The first step is agent initialization, which determines the upper and lower limit of the independent variables. The parameters of surge arrester that will be optimised are called as agents which are permittivity of glassfibre and silicone rubber, silicone rubber thickness, aluminium block and base, silicone housing curve. The positions of N parameters to be optimised are initialized, where x_i^d represents the positions of i^{th} agent in d^{th} dimension and n is the space dimension, where

$$X_i = (x_i^1,..,x_i^d,...,x_i^n), \text{ where } i \text{ is 1 to } N \tag{3.7}$$

Step 2: Evolution of fitness and best fitness computation

The evolution of the fitness is performed to minimize or maximize the dimensions of the surge arrester's parameters by determining the worst and best value of the leakage current for each combination of the parameters.

Step 3: Computation of constant of gravitational (G)

G is determined by

$$G(t) = G_0^{(-\alpha t/T)} \tag{3.8}$$

where $G_0 = 100$ and $\alpha = 10$ control the search accuracy, t is iteration and T is the total iteration.

Step 4: Calculation of masses of the agents

Gravitational and inertia masses for every agent (parameters) are determined at each iteration. M_{ii} is the inertia mass of i^{th} parameters and M_{pi} and M_{ai} are the passive and active gravitational masses, where

$$M_{ai} = M_{pi} = M_{ii} = M_i, \text{ where i is 1 to } N \tag{3.9}$$

In this step, every iteration will decide the position and dimension of the parameters.

Step 5: Calculation of agents' accelerations

At t-th iteration, the acceleration of i^{th} parameter a_i^d is computed by

$$a_i^d\,(t) = F_i^d\,(t) / M_{ii}\,(t) \tag{3.10}$$

where $F_i^d(t)$ is the total force on i^{th} parameter whereas the total force that acts on mass.

Step 6: Position and velocity of agents

In this step, the next position of each parameter is updated. The position and velocity of the agents (parameters) at t+1 iteration are calculated by

$$x_i^d\,(t+1) = x_i^d\,(t) + v_i^d\,(t+1) \tag{3.11}$$

$$v_i^d\,(t+1) = rand_i\, v_i^d\,(t) + a_i^d\,(t) \tag{3.12}$$

where t is the current iteration, t+1 is the next iteration, v_i^d is the i^{th} agent (parameter) velocity, x_i^d is the i^{th} agent (parameter) position, $rand_i$ is a random number between 0 and 1 and a_i^d is the i^{th} agent (parameter) acceleration.

Step 7: Convergence check

Steps 2 to 6 are repeated until the final iteration is reached. The lowest leakage current value at the final iteration is taken as the global fitness while the parameters' position with the lowest leakage current is taken as the global solution of the problem.

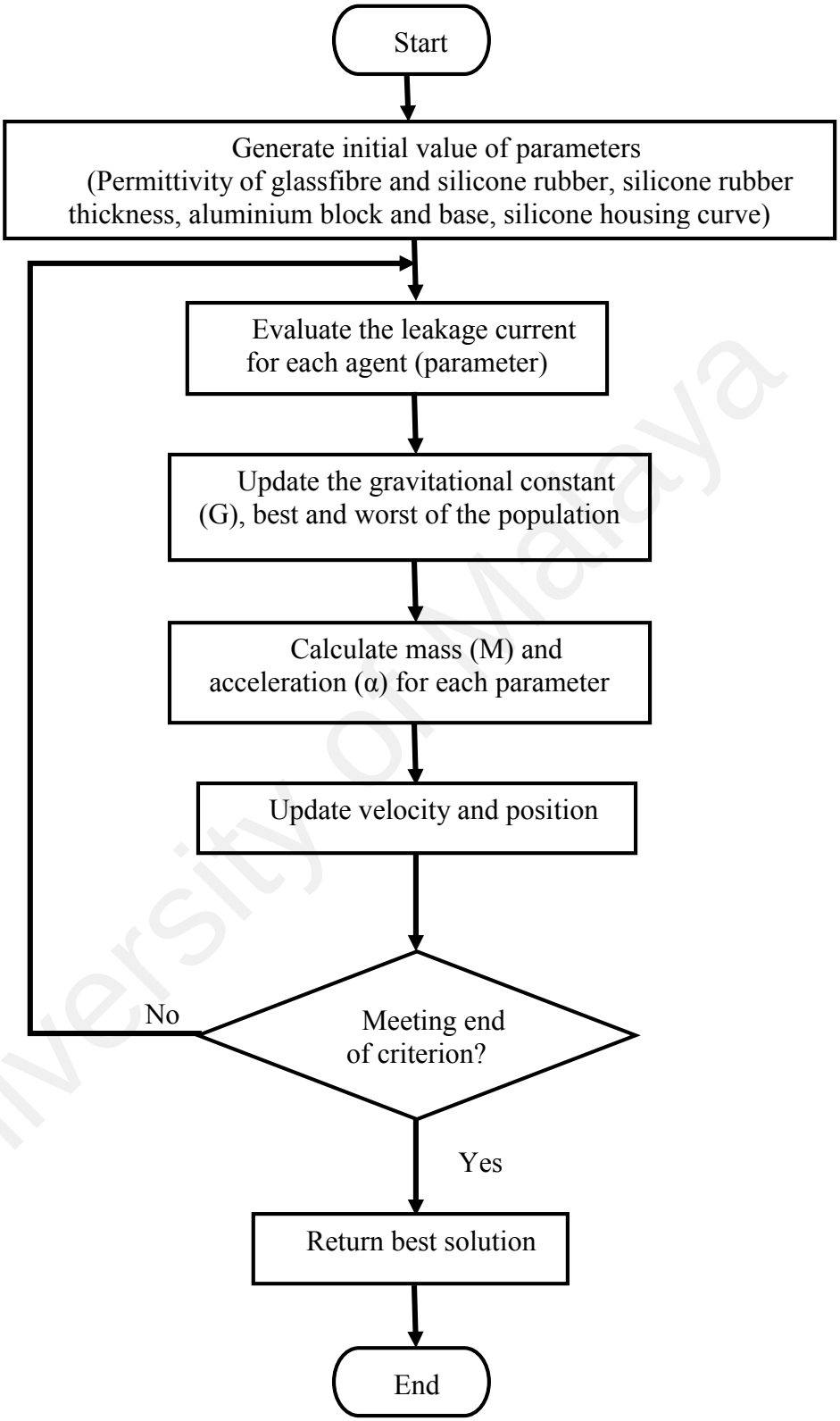

Figure 3.13: GSA Flowchart

3.5 Imperialist competitive algorithm (ICA)

Imperialist Competitive Algorithm, (ICA) is a method recently used to deal with different optimization problems. This algorithm was announced since 1989 by Baran (Baran & Wu, 1989). It is inspired based on the imperialist competition. The empires comprise of imperialists and colonies. The imperialists are chosen from the best countries in the empires and the remaining forms the colonies of those imperialists. The steps involved in ICA in reducing the leakage current in the surge arrester are as follows:

Step 1: Initial empires generation

The first step is to form an empire, which is determined by the parameters of the surge arrester to be optimized. The number of parameters (permittivity of glassfibre and silicone rubber, silicone rubber thickness, aluminium block and base, silicone housing curve) of the surge arrester is equal to the number of cells in each country's array. The value of every cell is 0 or 1, depending on the width or length of the arresters. The array for n parameters to be optimized c is formed, which is written as

$$Country = [c_1, c_2 c_3, ..., c_n] \tag{3.13}$$

The parameters with the best objective function are chosen as the imperialists and the rest of the parameters are colonies.

Step 2: Assimilation and revolution

Assimilation is when the imperialists try to move forward to their colonies and make them a part of themselves. This step is applied to the parameters of the arrester in the colonies' array. The colony moves towards the imperialist as shown in Figure 3.14 by

$$x \sim U(0, \beta \text{ x } d) \tag{3.14}$$

where d is the distance between the imperialist and colony and β is a constant larger than one.

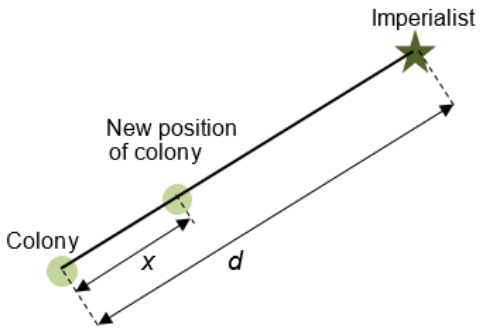

Figure 3.14: Colony move to a new position by x units toward its imperialist

Some of the colonies are chosen randomly in order to pursuit different points around their imperialist to endure revolution. Therefore, a random sum of deviation as shown in Figure 3.15 is added to the path of movement. This deviation from the original direction is attuned by Υ which is defined by

$$\theta \sim U(-\gamma, \gamma) \tag{3.15}$$

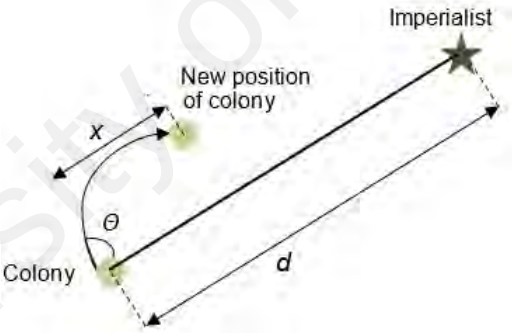

Figure 3.15: Colony moves to a new position by *x* units with a random deviation θ towards its imperialist

Step 3: Position exchange of imperialist and colony

If a colony (dimension/permittivity of parameter) reaches a position with more powerful (lower leakage current) than an imperialist (existing dimension/permittivity of parameter), the colony and the imperialist exchange their positions. In this step, the colony and imperialist will exchange their position if it reaches a lower leakage current value as shown in Figure 3.16.

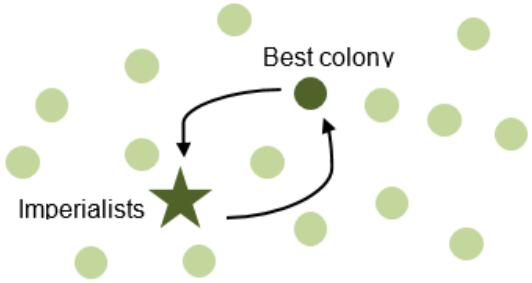

Figure 3.16: Exchange position between an imperialist and a colony

Step 4: Empire total cost calculation

The cost of imperialist country affects the total cost (TC) of an empire where in other words, the value of the leakage current will be computed for all parameters using

$$TC_n = \mathcal{E}mean[cost(empire\ colonies_n)] + Cost(imperialist_n) \quad (3.15)$$

Step 5: Competition of imperialistic

The power of weaker empires decreases while the power of powerful empires becomes greater. In the weakest empire, the weakest colony, which has the highest leakage current, is sent to other empires. The normalized total cost (NTC) of each empire is determined by

$$NTC_n = TC._n = max[TC._i] \quad (3.16)$$

Step 6: Convergence check

Steps 2 to 5 are repeated until all of the empires collapse except the most powerful empire, which has the lowest value of the leakage current

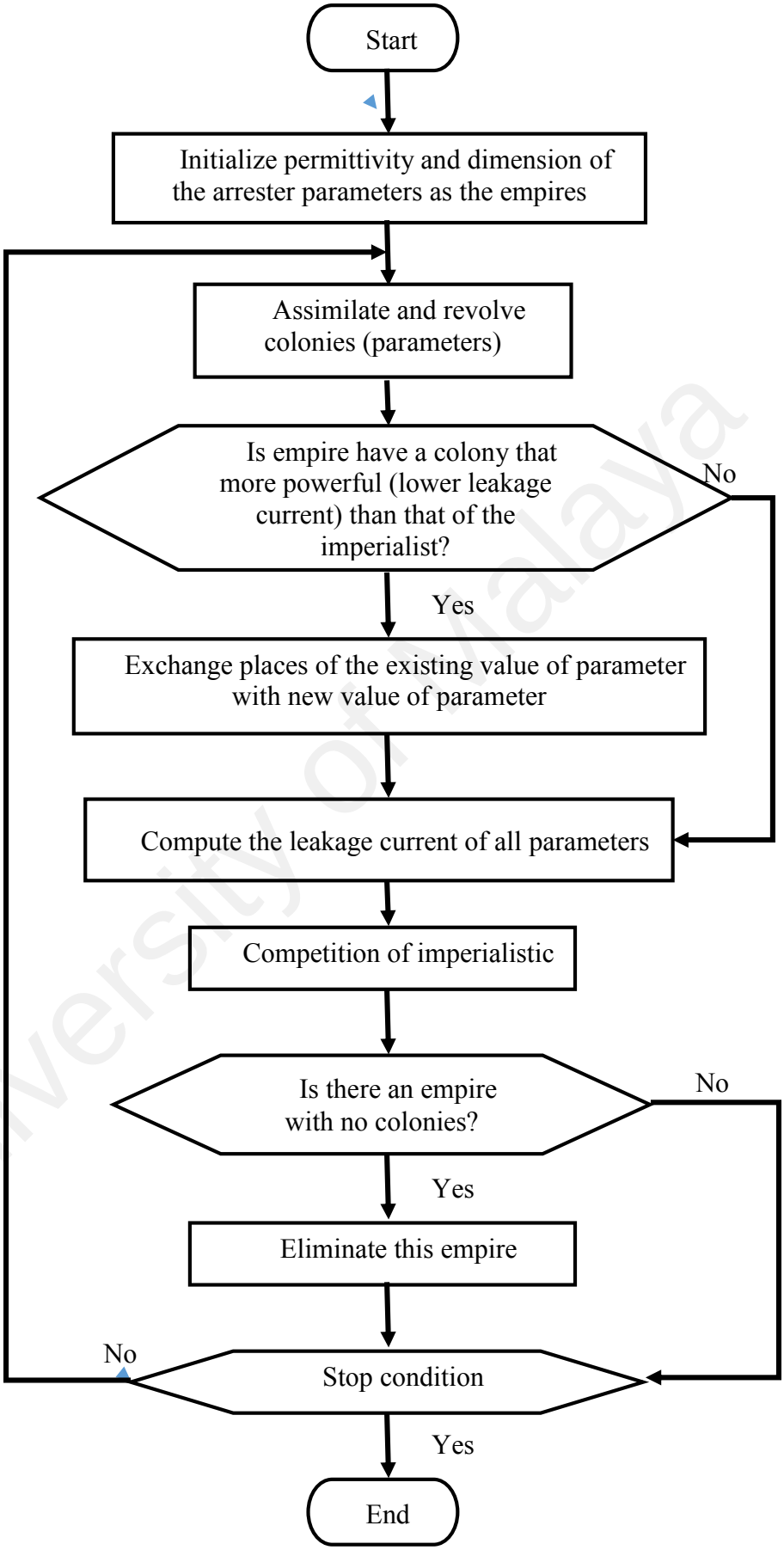

Figure 3.17: ICA Flowchart

3.6 Chapter summary

A model describing an 11kV ZnO surge arrester with silicone rubber housing has been developed using the Finite Element Analysis (FEA) method. The benefits of this method over previous methodologies are any shape of the geometry can be modelled easily, has the ability to generate electric field distribution, current distribution and temperature distribution without analytical equations. The surge arrester model has been developed and analyzed in different voltage amplitude, wetness conditions and polluted conditions. The results of the FEA method were compared with the measurement results using leakage current measurement equipment. The obtained waveforms were used to extract the resistive leakage current by using Improved Time Delay Addition Method (ITDAM).

The surge arrester model, which is developed using FEA was used to optimise the surge arrester design in order to achieve the lowest leakage current that flows through the arrester. The parameters of the surge arrester were optimized by using GSA and ICA. These optimization methods are based on Newton law of motion and gravity for GSA and imperialist competition for ICA. The best parameter results with the lowest leakage current value are used to improve the design of the surge arrester.

CHAPTER 4: RESULTS AND DISCUSSION

4.1 Introduction

This section presents the results that have been obtained from this work and the explanations of each result. These include the electric potential distribution and current density distribution in the surge arrester models. The comparison between the leakage current measurement and simulation results are also presented. The usefulness of the proposed optimisation methods in optimising the design of the surge arrester, which are GSA and ICA are demonstrated.

4.2 Electric potential, electric field and current density distribution of the surge arrester using FEA model

The distribution of electric potential, electric field and current density of the 11kV surge arrester can be determined from the FEA model. Figures 4.1, 4.2 and 4.3 present the electric potential, current density and electric field distributions obtained from the FEA model at $9kV_{rms}$ applied voltage amplitude and temperature of 26^0C. Referring to Figures 4.1 and 4.2, the potential and current density distributions show that the highest potential is located at the top terminal of the arrester due to the applied high voltage but decreases towards the bottom terminal, which is grounded. According to Figure 4.3, the electric field magnitude is the highest at the top terminal of the arrester due to the applied high voltage (Hazlee Azil Illias, 2014). There is also relatively higher electric field magnitude on the top and bottom surfaces of each housing shed than the surrounding housing.

In order to evaluate the practicality of the developed FEA model, the result attained was then compared with the measurement and manufacturer's data as illustrated in Figure 4.4. The applied voltages of the FEA, measurement and manufacturer's data were

computed at the magnitude of 9kV$_{rms}$. In general, FEA model exhibit similar residual voltage patterns, which are in good agreements with the manufacturer's data and measurement (B., 2008). With a small relative error mostly caused by non-linear V-I characteristic settings, it can be assumed that the developed FEA model is sufficient in term of approximating the voltage distribution and current density of the surge arrester during normal opertion.

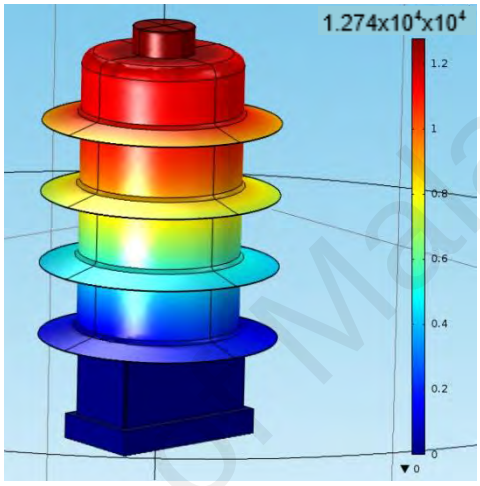

Figure 4.1: Electric potential distribution from the surge arrester FEA model

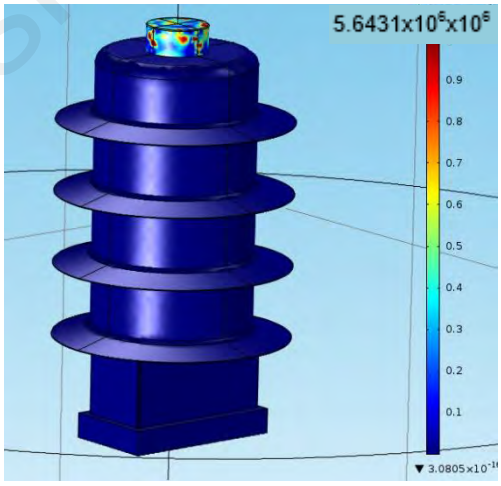

Figure 4.2: Current density distribution from the surge arrester FEA model

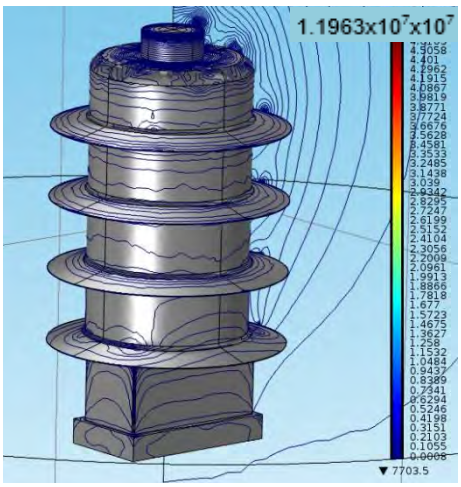

Figure 4.3: Electric field distribution from the surge arrester FEA model

The simulation processes were then repeated for different design of surge arresters, which is explained in Section 4.3, since there is a good agreement between simulation results and actual measurements. It can be concluded that the arrester model developed using FEA is an effective option for future arrester development, which can solve the problem easily using triangular fundamentals. Following are the assumptions made in the proposed FEA method in COMSOL Multiphysics software:

i. A layer of air is added surrounding the surge arrester model with permittivity $\mathcal{E}_r$ equals to 1 to allow the electric potential and leakage current distribution along the surface of surge arrester to be calculated.

ii. The complexity of the surge arrester model was reduced by removing the small scale elements of the surge arrester model. The elements including disc string, drilled holes and the wall of ZnO varistors since these elements do not affect the simulation results.

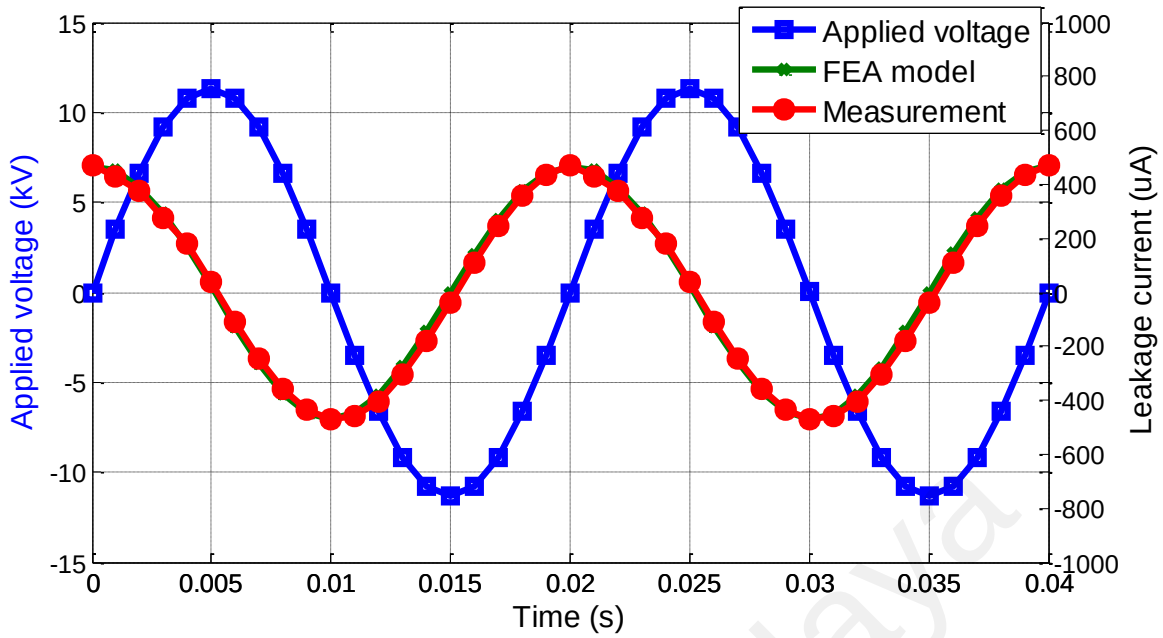

Figure 4.4: Comparison of electric potential and current density distribution between FEA model and measurement at 50 Hz, 9kV$_{rms}$ and 26^{o}C

4.3 Parametric assessment using FEA model

The practicability of the developed surge arrester model by using FEA software has been effectively validated by having an excellent agreement between the simulation results and the measurements data. Additional assessments were conducted on the effect of different design amendments related to the leakage current of the surge arrester. The parameters that have been altered are the width of ZnO, glassfibre, insulation layer (silicone rubber) and dielectric constant of the insulation layer.

4.3.1 Influence of the ZnO width on leakage current

The influence of the width of ZnO block on leakage current was recognised by increasing and decreasing the value of ZnO width. This can enhance a better understanding on the theoretical feature of ZnO dimensions towards leakage current. In this assessment, four values of ZnO widths were used to examine the effect of changing the widths on leakage current behavior at 9kV$_{rms}$. The initial value of ZnO width is 47mm and was changed to 35mm, 40mm, 50mm and 55mm. Referring to Figures 4.5, the

leakage current in the surge arrester decreases when the ZnO block width increases. This is due to larger ZnO radius produces larger cross sectional area that contains billions of ZnO grains that act as electronic switch. During normal condition, these grain junctions is open circuit which lower the resistance of ZnO block and hence reducing the current flow through the arrester. Therefore, ZnO radius has a significant influence on the leakage current in the surge arrester. Since the height of ZnO block affects the residual voltage of the arrester, which proportionally increases with the height of the arrester, the height of ZnO block is not observed in this study. Besides, manufacturing procedure for greater height of the ZnO block is tougher in order to attain adequate homogeneity of the material.

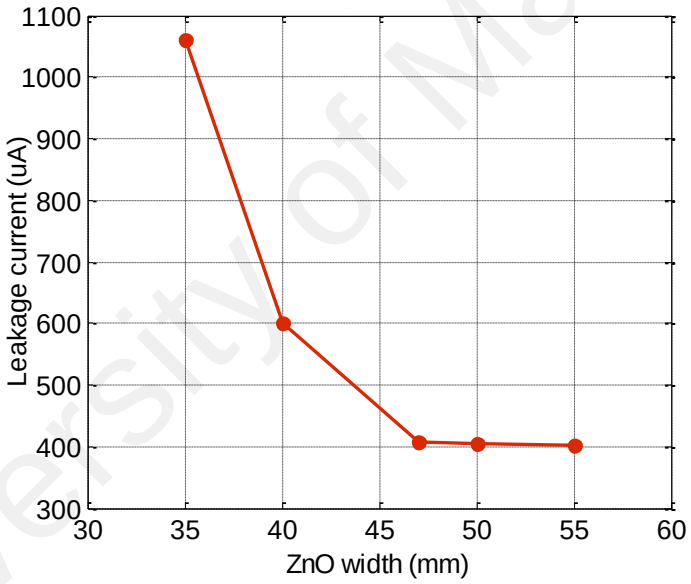

Figure 4.5: Leakage current in the surge arrester for different ZnO width

4.3.2 Influence of the glassfibre width on leakage current

In general, ZnO blocks are arranged on top of each other to be mechanically immovable in the housing. The intention of the arrangement is to make sure that the most important part of the surge arrester cannot be moved out from its current position during transportation or installation. Additionally, a certain contact pressure, where in this type of surge arrester is fiber glassfibre, is needed in axial position so that the current stress

that occurs can be simply controlled. Moreover, the glassfibre that is located between ZnO and housing can reduce possible sagging towards the wall of the housing. For that reason, an assessment on the width of glassfibre rod was evaluated with 5mm, 7mm, 10mm (initial size), 12mm and 15mm. Referring to Figure 4.6, there is a great reduction on the value of leakage current with increasing width of the glassfibre. When the glassfibre width is increased, there is more volume for heat from the ZnO blocks to dissipate into the glassfibre width and consequently reduces the value of leakage current. In addition, if the width of glassfibre is too large, a pressure will built-up which result in crushing the housing, whereas, if the width is smaller, the mechanical resistance may occur towards external forces.

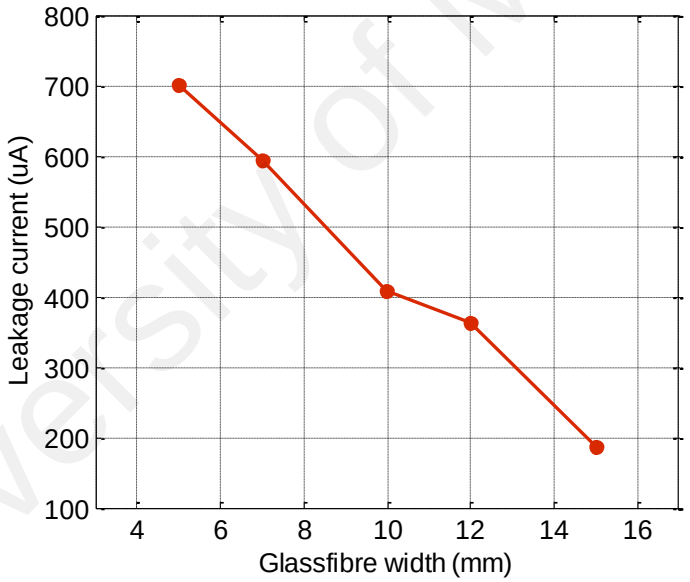

Figure 4.6: Leakage current in the surge arrester for different glassfibre width

4.3.3 Influence of the silicone housing thickness on leakage current

In a surge arrester configuration, an insulation layer that is silicone rubber house has an important duty to shield the essential parts of surge arrester from the environment and affords an adequate creepage distance by fitting with sheds either alternatingly or uniformly. Therefore, in this study, different thickness of silicone housing was simulated

to find out the effect on leakage current behavior of the surge arrester. The initial thickness value of the silicone housing is 3mm and another four values were tested at 1mm, 2mm, 5mm and 7mm. According to the obtained results in Figure 4.7, there is a small difference in leakage currents where the leakage current increases with lower value of the silicone thickness. However, a small decrement of the leakage current is able to increase the lifespan of the surge arrester and at the same time reduces the electric field intensity of the surge arrester housing (Hazlee Azil Illias, 2014).

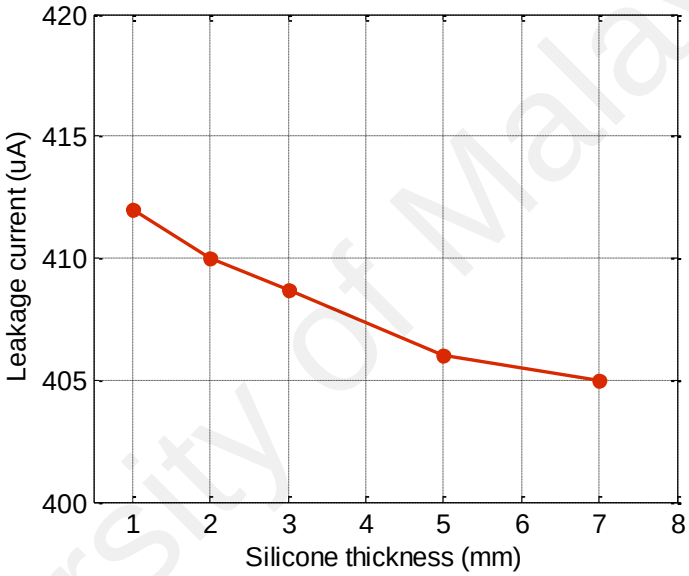

Figure 4.7: Leakage current in the surge arrester for different silicone thickness

4.3.4 Influence of the insulation layer relative permittivity on leakage current

In general, an insulation layer, glassfibre and silicone rubber housing are used to protect the surface of ZnO blocks in a surge arrester. The behavior of insulation layer relative permittivity shows an important role in controlling the withstand capability of ZnO blocks with respect to surface flashover. Therefore, the weakening of surge arrester attributable to moisture ingress and partial discharges could be avoided. In this parametric analysis, the effect of silicone rubber and glassfibre relative permittivity on leakage current was observed. Figure 4.8 and Figure 4.9 present the leakage current results for

different relative permittivity value of glassfibre and silicone rubber respectively. The initial relative permittivity value for glassfibre was 4.2 and additional four values of relative permittivity simulated were 2, 3.5, 5.5 and 7. As well as glassfibre, the relative permittivity of silicone rubber was also simulated at initial value of 11.7 and another four values at 8, 10, 13 and 15.

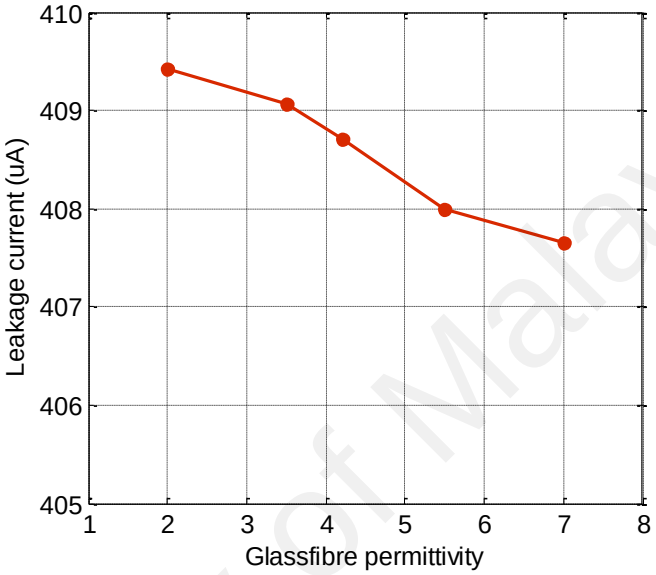

Figure 4.8: Leakage current in the glassfibre material for different relative permittivity

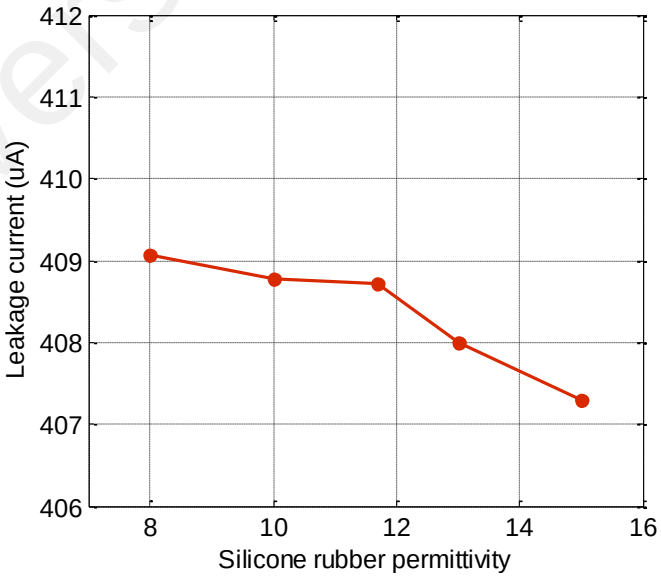

Figure 4.9: Leakage current in the silicone rubber for different relative permittivity

Referring to Figure 4.8 and Figure 4.9, the leakage current is affected by the housing materials. By increasing the relative permittivity of insulation layers by means of glassfibre and silicone rubber, the value of leakage current is decreasing in a very small amount. With high value of relative permittivity, the leakage current can be aligned easier within the material that leads to lower leakage current. This enlightens the importance of the insulation layer in avoiding the weakening of ZnO surface. The accurate values of relative permittivity and other parameters can be obtained by using optimization method as discussed in Section 4.8.

4.4 Comparison between simulation and measurement results

Comparison of leakage current measurement and simulation results was made for different applied voltage amplitudes, wetness conditions and artificial pollution conditions to study leakage current behaviour under these conditions. From the comparison, the effectiveness of the FEA model can be shown. The comparison includes the resistive and capacitive leakage current extracted by using ITDAM and harmonic components revealed from FFT analysis.

4.4.1 Leakage current under different applied voltage amplitude

Comparison between measurement and simulation results of the surge arrester total leakage current under different applied voltage amplitude is shown in Figure 4.10 while the resistive and capacitive leakage current extracted using ITDAM are shown in Figure 4.11(a) and Figure 4.11(b) respectively. The voltage was applied from 6kV to 10kV with a step size of 0.5kV. It was found that the leakage current increases when the applied voltage is increased. This is fundamentally due to the direct proportionality between the voltage and current with an equivalent impedance, which is produced by the constant capacitive impedance Z ($I=V/Z$). The percentage error between the measurement and

modelling was calculated and is stated in Figures 4.10 and 4.11. The percentage errors of the leakage current were determined based on equation (4.1) to evaluate the accuracy of the FEA model.

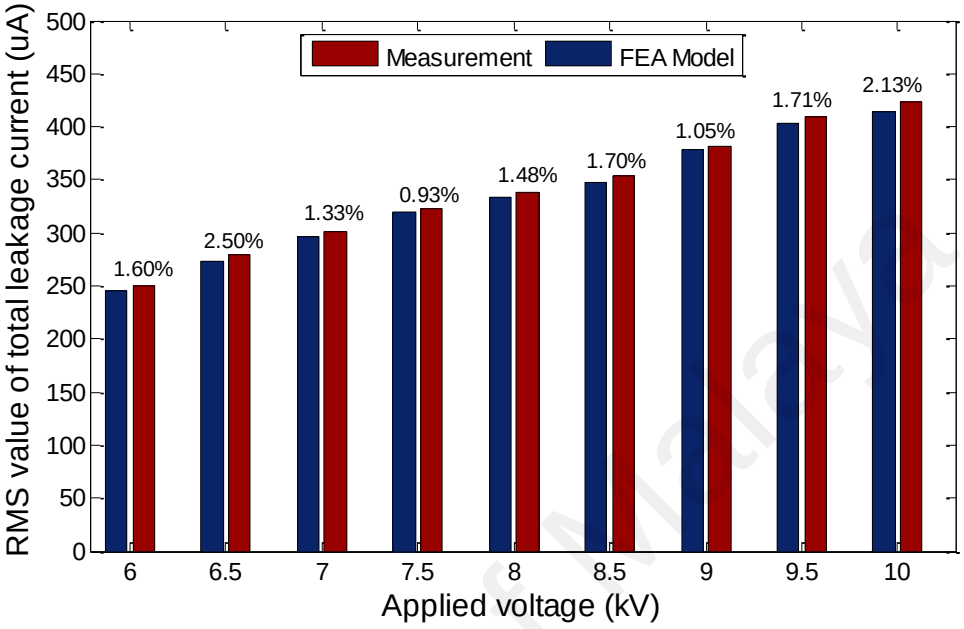

Figure 4.10: Comparison of RMS value of total leakage current between measurement and FEA model under different applied voltage amplitudes

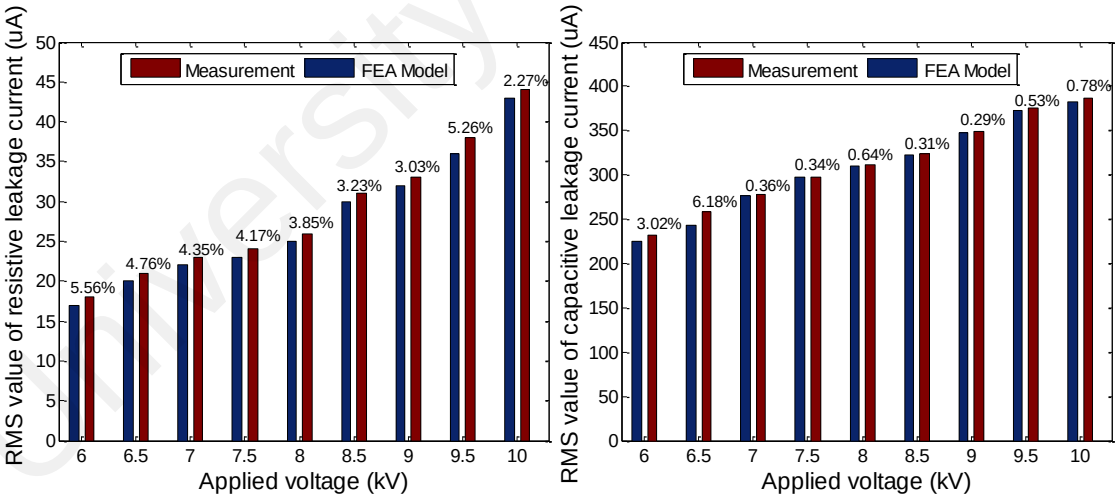

(a) **(b)**

Figure 4.11: Comparison of RMS value of (a) resistive and (b) capacitive leakage current between measurement and FEA model under different applied voltage amplitudes

Table 4.1 represents the values of errors which were calculated for 6kV, 6.5kV, 7kV, 7.5kV, 8kV, 8.5kV, 9kV, 9.5kV and 10kV respectively. The percentage of error is calculated using equation (4.1).

$$\text{Percentage of error (\%)} = \left|\frac{V_{FEA} - V_m}{V_m}\right| \times 100 \quad (4.1)$$

where V_{FEA} is the simulated value of the surge arrester leakage current in μA and V_m is the measurement value of the surge arrester in kV. According to the results, the average errors between the measurement and simulation for the total, resistive and capacitive leakage current are 1.60%, 4.05% and 1.38% respectively, as shown in Table 4.1. This indicates that the measurement and simulation results are in good agreement with each other. Therefore, the proposed model of the surge arrester in this work under various applied voltage amplitudes can be considered reasonable.

Table 4.1: Percentage error of FEA model leakage current compared to measurement

Applied voltage (kV_{rms})	Error compared to measurement (%)		
	Total leakage current	Resistive current	Capacitive current
6	1.60	5.56	3.02
6.5	2.50	4.76	6.18
7	1.33	4.35	0.36
7.5	0.93	4.17	0.34
8	1.48	3.85	0.64
8.5	1.70	3.23	0.31
9	1.05	3.03	0.29
9.5	1.71	5.26	0.53
10	2.13	2.27	0.78
Average	**1.60**	**4.05**	**1.38**

In Figure 4.12 (a) and (b), the waveforms of the applied voltage, total leakage current, capacitive leakage current and resistive leakage current with harmonic components of

total leakage current were obtained using ITDAM and FFT methods. Figure 4.12 (a) represents the results from the measurement while Figure 4.12 (b) represents the FEA model results. According to the obtained measurement and simulation results, it can be seen that the developed FEA model is able to include harmonic components, producing reasonable results compared to the measurement results.

The value of resistive leakage current at $8kV_{rms}$ is 26μA from the measurement, which is around 7.7% of the total leakage current. The value of the resistive leakage current at $8kV_{rms}$ from the FEA model is 25μA. This indicates that the difference between the measured and simulated resistive leakage current is only 3.8%. Similar waveforms of the applied voltage, total leakage current, capacitive leakage current and resistive leakage current with harmonic components of the total leakage current were obtained from the measurement and simulation at $10kV_{rms}$, as shown in Figure 4.13 (a) and (b). The resistive leakage current at $10kV_{rms}$ from the measurement is 44μA while from the simulation, the value is 43μA.

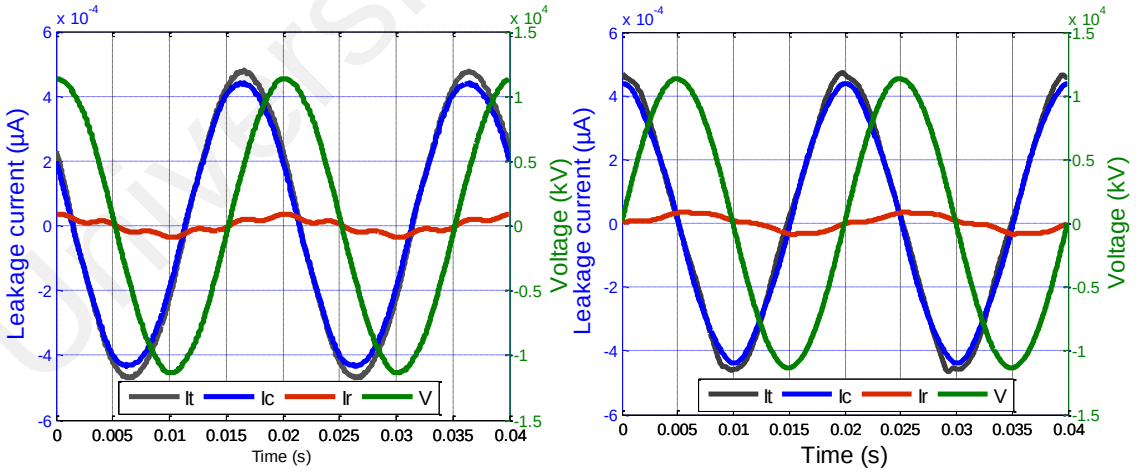

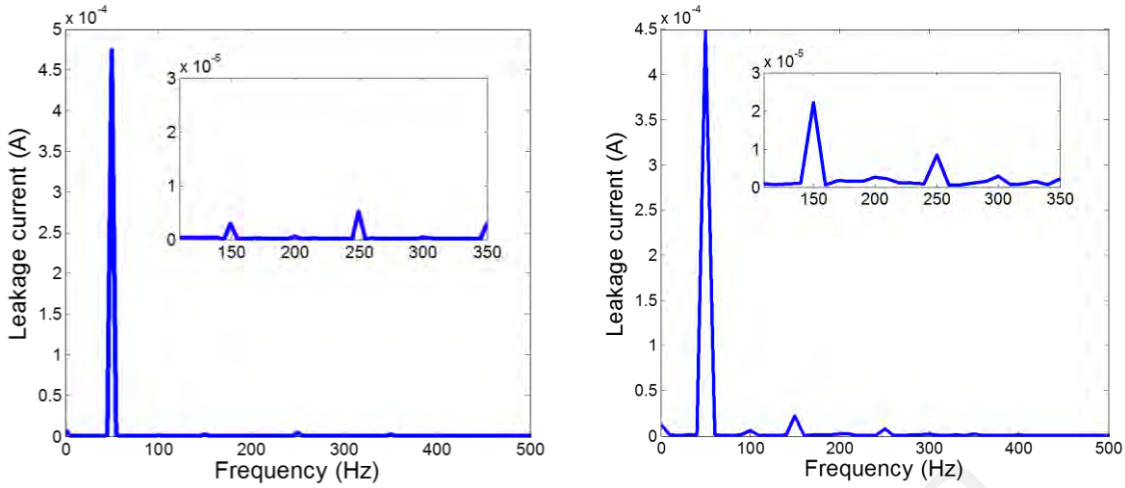

(a) (b)

Figure 4.12: Leakage current waveforms and harmonic components at 8kV$_{rms}$ applied voltage from the (a) measurement and (b) FEA model

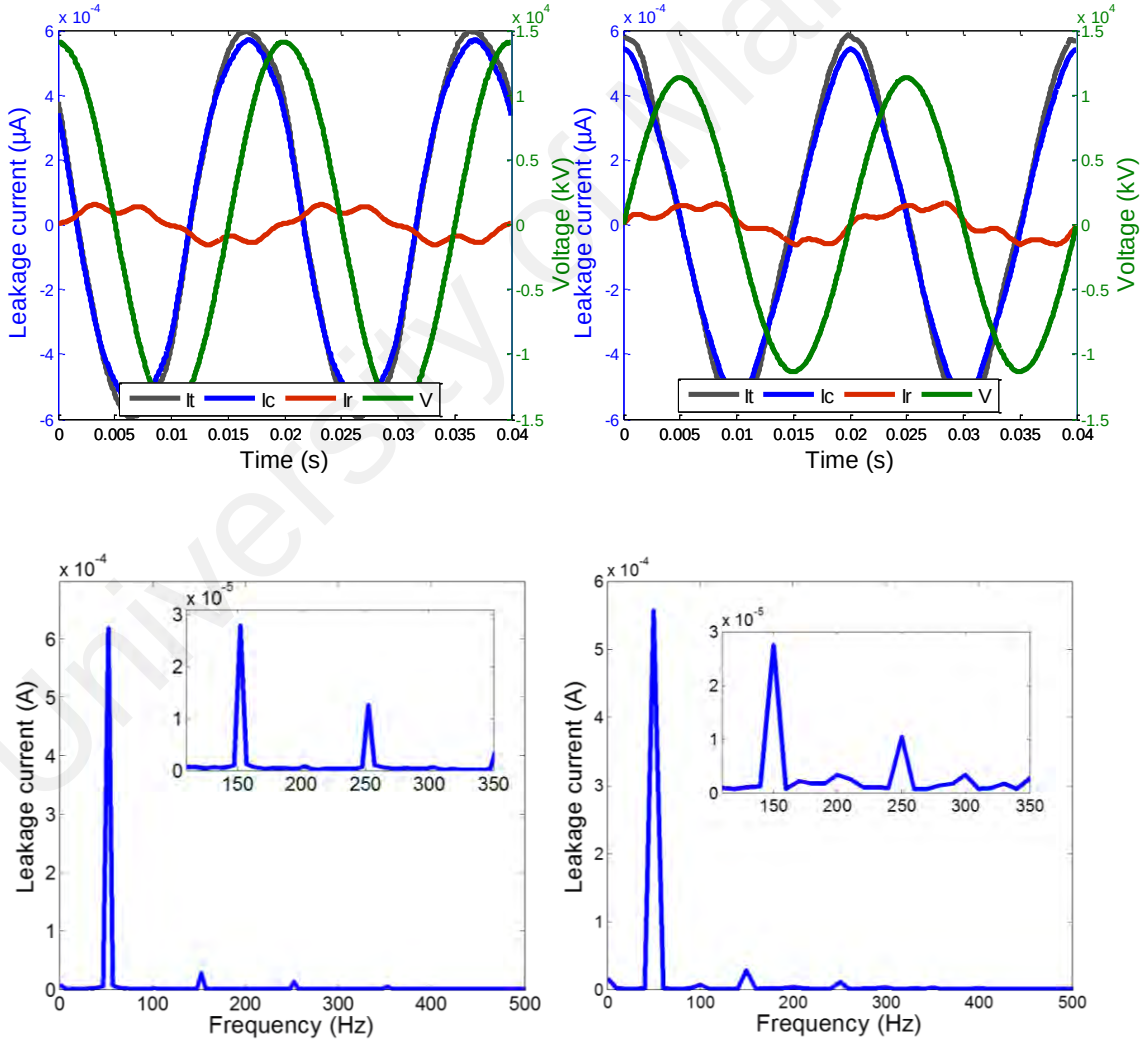

(a) (b)

Figure 4.13: Leakage current waveforms and harmonic components at 10kV$_{rms}$ applied voltage from the (a) measurement and (b) FEA model

4.4.2 Leakage current under different wetness conditions

The surge arrester was tested under different wetness conditions at $8kV_{rms}$ and at 26°C. Figure 4.14 shows the results of total leakage current value from measurement and simulation using the FEA model. From the results, it can be seen that the leakage current increases slightly when the arrester condition is wetter. This is due to the presence of water droplet, which increases the conductivity along the surge arrester surface, providing easier path for current to flow. Figure 4.15 shows the resistive and capacitive current components from the measured and simulated total leakage current. It can be seen that the resistive current component increases when there is more amount of water on the arrester surface. This humidification can also lead to moisture ingress of the surge arrester and degrade the lifetime of surge arrester (Metwally et al., 2017). However, there is not much variation in the capacitive current components under different wetness conditions.

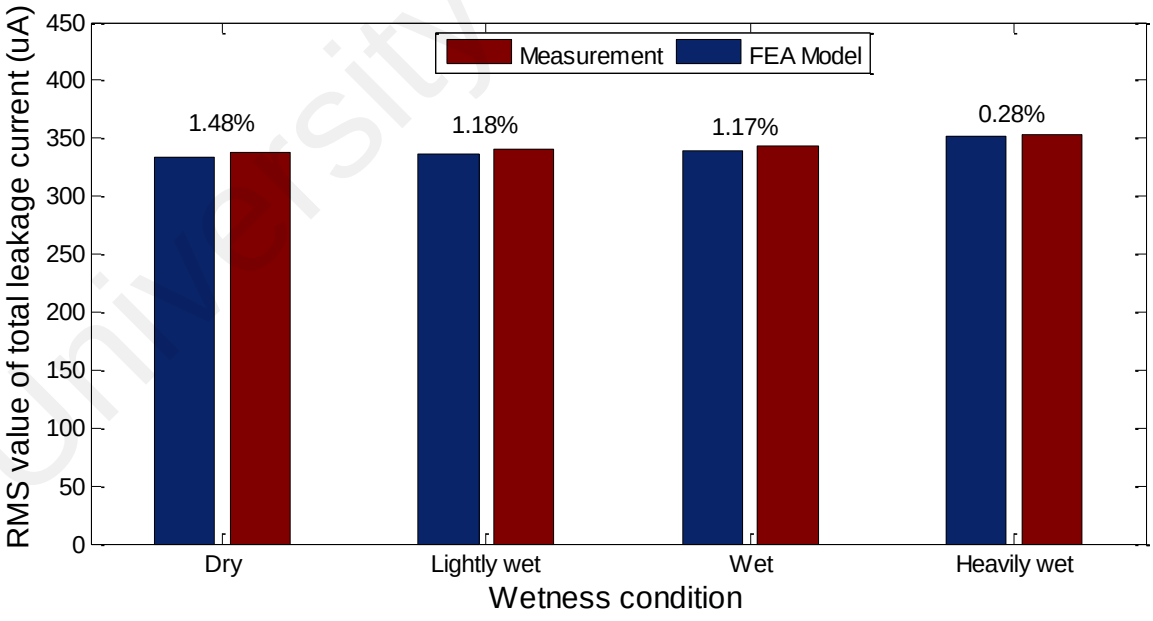

Figure 4.14: RMS value of the total leakage current between measurement and FEA model under different wetness conditions at $8kV_{rms}$

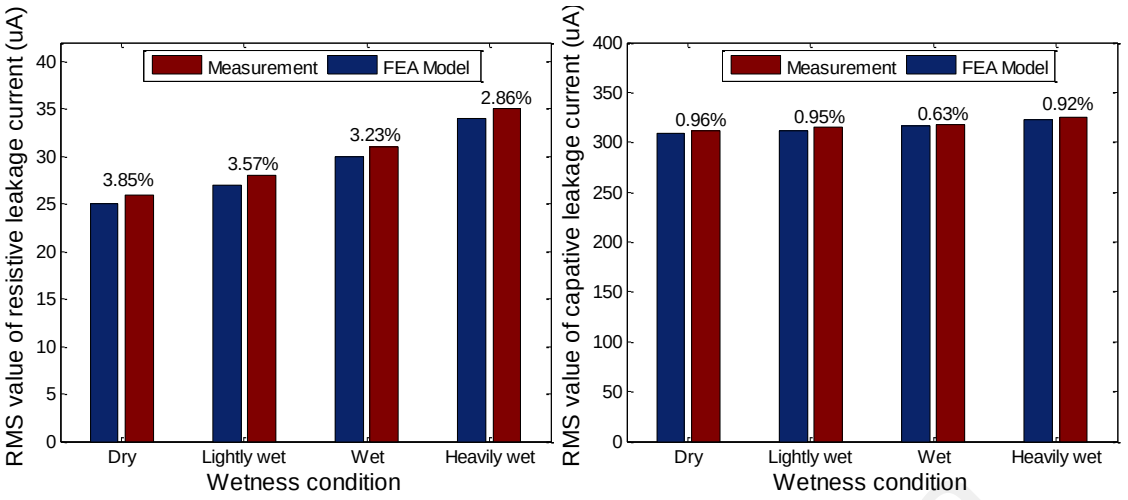

(a) **(b)**

Figure 4.15: RMS value of the leakage current between measurement and FEA model under different wetness conditions at 8kV$_{rms}$ for (a) resistive and (b) capacitive leakage current

The error between the measurement and simulation results using the FEA model is also shown in Figure 4.14 and Figure 4.15. The average percentage of errors between the measurement and simulation results determined by equation (4.1) are 1.03% for the total leakage current and 3.38% and 0.87% for resistive leakage current and capacitive leakage current respectively. The percentage of error for the FEA model compared to measurement is presented in Table 4.2. In Figure 4.16 (a) and (b), the waveforms of the applied voltage, total leakage current, capacitive leakage current and resistive leakage current with harmonic components of total leakage current were obtained using same methods; ITDAM for extraction and FFT for harmonic components.

Figure 4.16 (a) represents the results from the measurement whereas Figure 4.16 (b) represents the FEA model results. The total leakage current for measurement and FEA model for heavily wet surge arrester at 8kVrms are 352μA and 351μA whereas for capacitive and resistive leakage current are 322μA, 320μA, 34μA and 33μA accordingly. This indicates that the measurement and simulation results are in good agreement with each other. Again, this shows that the proposed FEA model for leakage current modelling

in the surge arrester under different wetness conditions in this work can be considered reasonable.

Table 4.2: Percentage error of FEA model leakage current compared to measurement

Wetness condition	Error compared to measurement (%)		
	Total leakage current	Resistive current	Capacitive current
Dry	1.48	3.85	0.96
Lightly wet	1.18	3.57	0.95
Wet	1.17	3.23	0.63
Heavily wet	0.28	2.86	0.92
Average	**1.03**	**3.38**	**0.87**

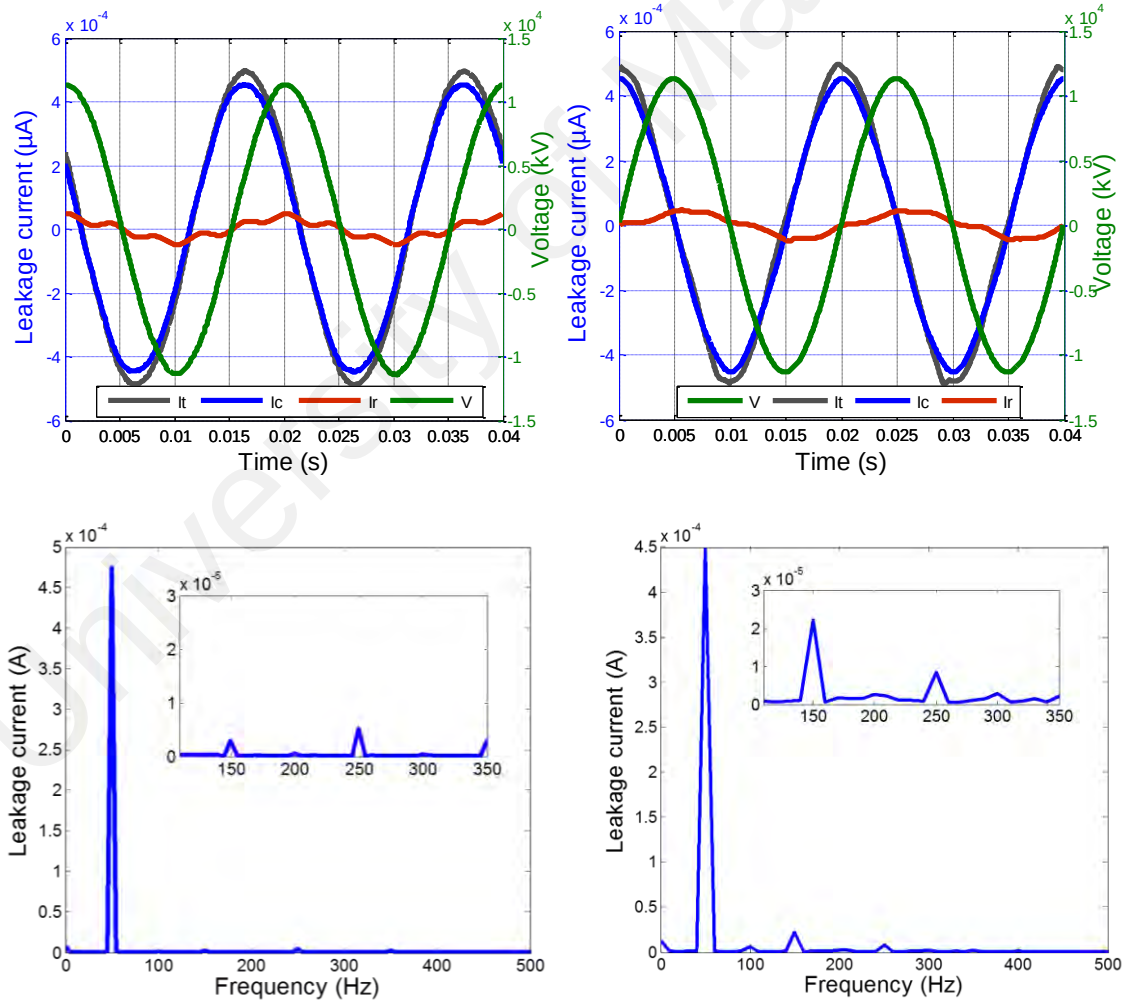

(a) **(b)**

Figure 4.16: Leakage current waveforms and harmonic components at 8kV$_{rms}$ applied voltage with heavily wet condition of surge arrester from the (a) measurement and (b) FEA model

4.4.3 Leakage current under different artificial pollution conditions

The leakage current behaviour of the surge arrester under different artificial pollution conditions is shown in Figure 4.17 and Figure 4.18. From the measurement, the surface of the surge arrester was contaminated with dry sand, wet sand, salt sand and salt water at $8kV_{rms}$. The salt sand is a blend of normal sand and salt, NaCl, with a ratio of 1:3 while the salt water is an emulsion of NaCl and water with a ratio of 1:3 with NaCl solution conductivity of 88 mS/cm. From the results, the presence of salt sand, salt water and wet sand on the surge arrester surface increases the total leakage current along the arrester surface. This is due to the higher conductivity along the surge arrester surface provided by the salt and water, providing easier path for current to flow.

Dry sand does not cause the leakage current to increase significantly because it has low conductivity. It can be concluded that increasing of leakage current is correlated to the increment of surface conductivity in pollution conditions (Faria, Martinez, & Queiroz, 2015; M. Khodsuz & Mirzaie, 2015). The error between the measurement and simulation results using the FEA model is also shown in Figures 4.17 and Figure 4.18.

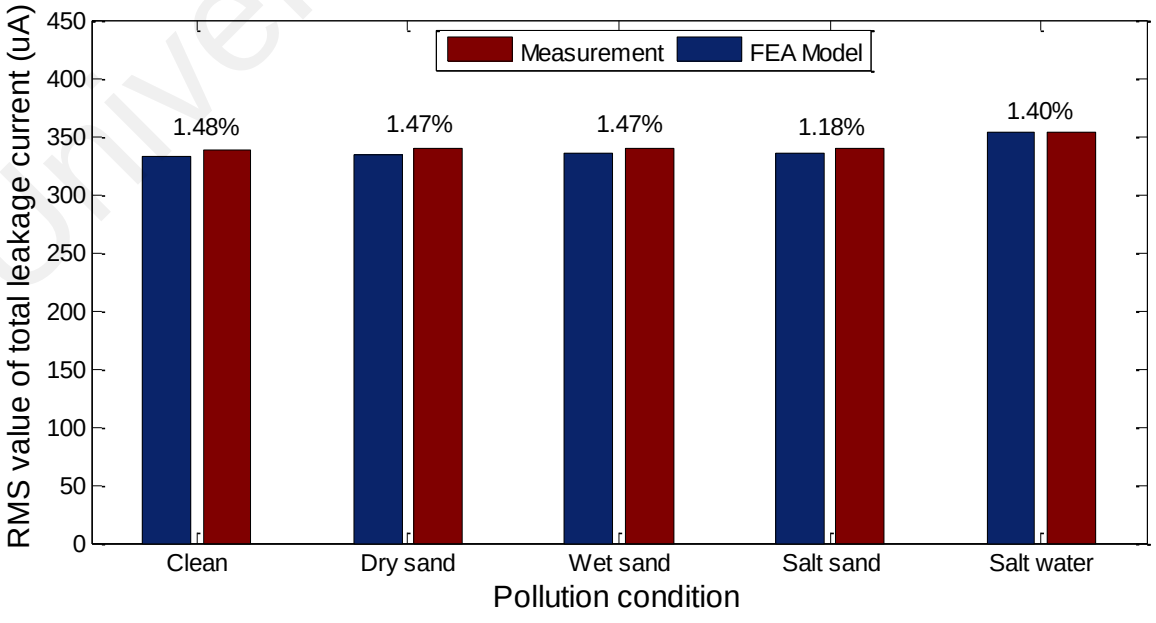

Figure 4.17: Comparison of RMS value of total leakage current between measurement and FEA model under different artificial pollution conditions

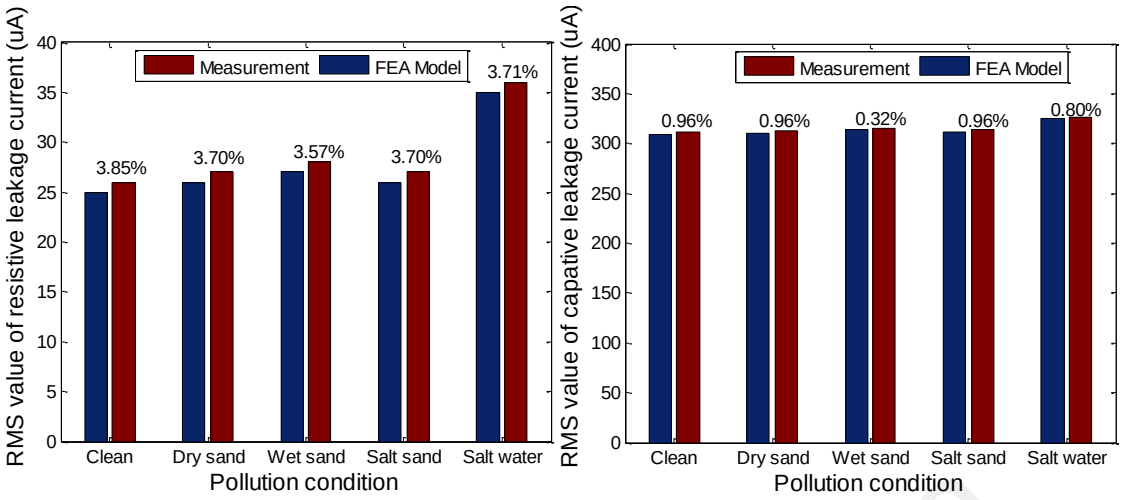

(a) **(b)**

Figure 4.18: Comparison of RMS value of leakage current between measurement and FEA model under different artificial pollution conditions at 8kV$_{rms}$ (a) Resistive (b) Capacitive

The average percentage of error is 1.40% for the total leakage current, 3.71% for resistive leakage current and 0.79% for capacitive leakage current as represent in Table 4.3. This shows that the measurement and simulation results are in good agreement with each other. Therefore, the proposed FEA model for leakage current modelling in surge arrester under different pollution conditions in this work can be considered acceptable.

Table 4.3: Percentage error of FEA model leakage current compared to measurement

Test sample condition	Error compared to measurement (%)		
	Total leakage current	Resistive current	Capacitive current
Clean	1.48	3.85	0.96
Dry sand	1.47	3.70	0.96
Wet sand	1.47	3.57	0.32
Salt sand	1.18	3.70	0.96
Salt water	1.40	3.71	0.80
Average	**1.40**	**3.71**	**0.79**

The waveforms for surge arrester polluted with salt water at 8kV$_{rms}$ applied voltage, total leakage current, resistive and capacitive leakage current are presented in Figure 4.19 with their harmonic components for measurement and FEA model. The total, capacitive

and resistive leakage current for measurement are 354μA, 326μA and 36μA and 353μA, 325A and 35μA for the FEA model. The total, capacitive and resistive leakage current increase around 16μA, 14μA and 10μA accordingly from the clean surface surge arrester. From the obtained harmonic waveform as described in Figure 4.19 (below each waveform), it can be realised that the fundamental, third and fifth harmonics influence the amplitude of the total leakage current under pollution with salt water. The increase of harmonic components and resistive current can lead to power loss, increase the temperature and therefore degrade the material that will possibly explode the surge arrester due to thermal avalanche.

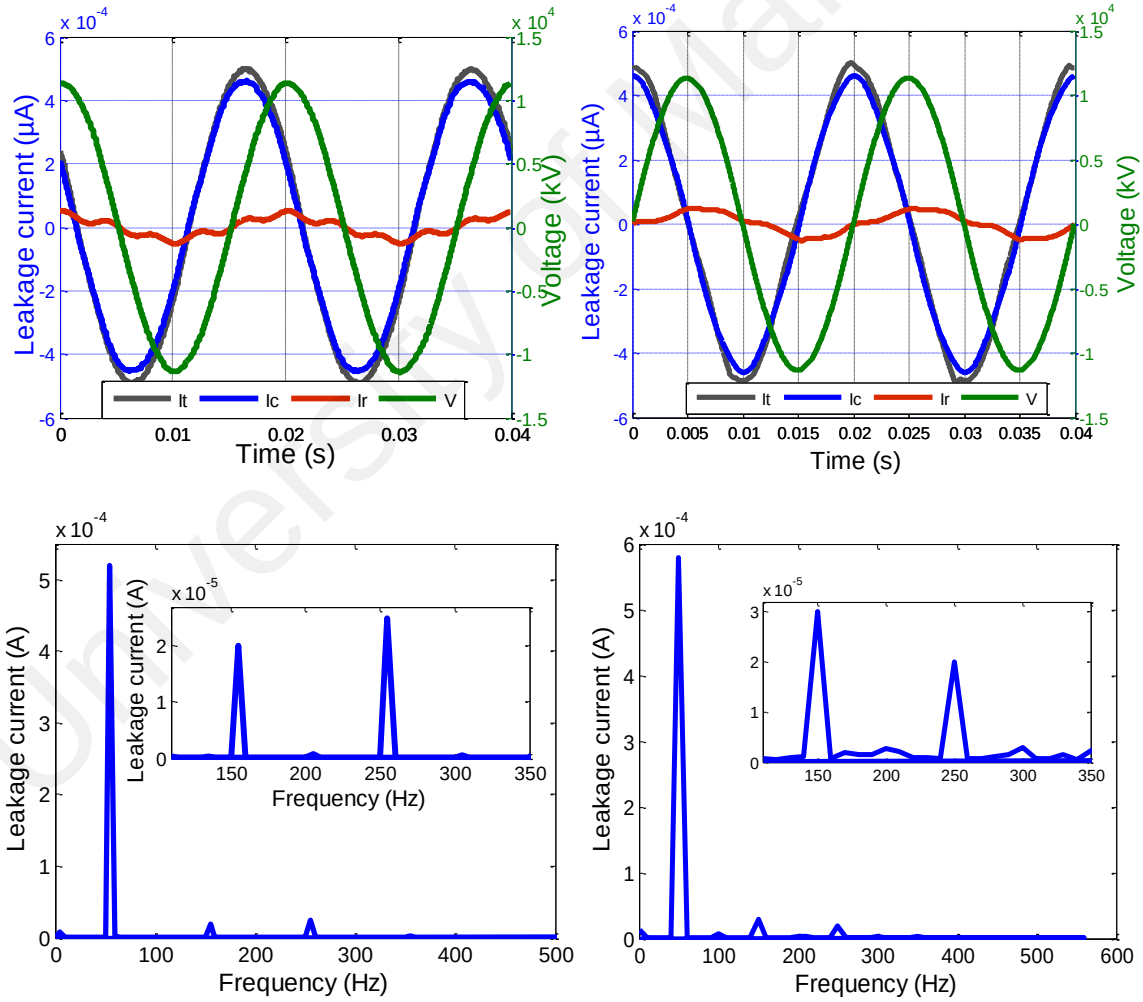

(a) **(b)**

Figure 4.19: Leakage current waveforms and harmonic components at 8kV$_{rms}$ applied voltage with salt water on the surge arrester from the (a) measurement and (b) FEA model

4.5 Optimisation results

In this work, designing a surge arrester with reduced leakage current was proposed using optimisation methods. The results obtained from the FEA model of the surge arrester were interfaced with MATLAB programming code to evaluate the objective function. This is also the main reason of choosing these two types of optimization method; imperialist competitive algorithm (ICA) and gravitational search algorithm (GSA). The results obtained were compared and analysed. Optimisation techniques were used to obtain a surge arrester design which yields the lowest leakage current through the arrester.

There are six parameters adjusted on the surge arrester. The parameters are the dimension of the aluminum block, aluminum base, curve of the housing shed, thickness of the silicone rubber, permittivity of the silicone rubber and glassfibre as presented in Figure 4.20. These parameters were selected because they have strong influence on the leakage current in the surge arrester. The size of the design can be changed while for the material permittivity, there is variation in the permittivity value of the glass and silicone rubber available in the market. The objective function of the problem is defined as the minimum leakage current that flows through the arrester as equation (4.2). The optimized leakage current through the surge arrester must be less than the leakage current through the original surge arrester design, which is 408μA at 9.5kV_{rms}, 50Hz.

$$f(h) = \text{mphint(model,'ec.normJ','selection', [3], 't', [0.004])} \quad (4.2)$$

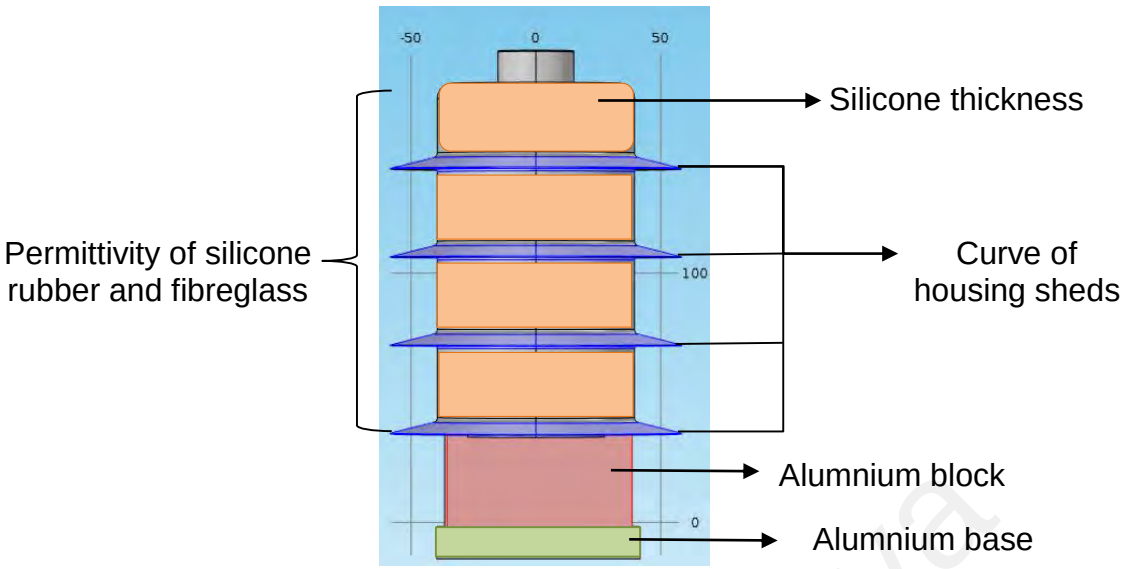

Figure 4.20: Parameters adjusted on the surge arrester

In order to examine the proposed technique, GSA and ICA were executed for five case studies. Five case studies of the optimisation were performed by using two and four variables. From the parametric study of the surge arrester, these parameters were carefully chosen and tuned for different cases. From the case studies that have been done, the leakage current is not affected by permittivity. Therefore, only four parameters have been optimized for each case. For Case 1, the parameters to be tuned are only the permittivity of the material, which are glassfibre and silicone rubber. For Case 2, the width of the ground terminals of the surge arrester was tuned, which are aluminium block and aluminium base. For Case 3, the thickness of the silicone rubber and curve of housing sheds were tuned. For Case 4 and Case 5, the tuned parameters are the combination of dimensions and permittivity. The descriptions of the case studies are summarised in Table 4.4.

Table 4.4: **Description of the case studies**

Case	Parameters to be tuned
Case 1	Permittivity value of glassfibre Permittivity value of silicone rubber
Case 2	Width of aluminium block (ground) Width of aluminium base (ground)
Case 3	Thickness of silicone rubber

	Curve of housing sheds
Case 4	Permittivity value of glassfibre Permittivity value of silicone rubber Width of aluminium block (ground) Width of aluminium base (ground)
Case 5	Thickness of silicone rubber Curve of housing sheds Width of aluminium block (ground) Width of aluminium base (ground)

4.5.1 Optimised parameters value of surge arrester

The lower and upper limits of each parameter used in optimisation were fixed based on the limits relative to the dimension and material properties of the surge arrester as shown in Table 4.5. The starting values in the optimization methods are chosen based on the actual surge arrester dimensions and must fulfil the IEC60815 standard, where the base of the surge arrester should have a minimum cross section of 35mm^2 and the arrester housing should have a suitable creepage distance. The existing value of the glassfibre permittivity and silicone rubber permittivity are 4.2 and 11.7 respectively. The width of the grounded aluminium block and base are 86mm and 70mm. The thickness of the silicone rubber is 3mm and the curve of the housing sheds is 0.4mm. The number of iterations used is 150.

Table 4.5: **Lower and upper limits of each parameter used in optimisation**

Parameter	Lower limit	Upper limit	Existing value
Permittivity of glassfibre	3.7	8	4.2
Permittivity of silicone rubber	11.0	12.9	11.7
Thickness of silicone rubber (mm)	1	6	3
Curve of housing sheds (mm)	0.05	0.8	0.4
Width of aluminum block (ground)	68	76	70
Width of aluminum base (ground)	80	90	86

Table 4.6 to Table 4.10 show the parameters obtained using GSA and ICA optimisation for five case studies. For Case 1 to Case 3, there are only two variables used

whereas four variables were used for Case 4 and Case 5. The outcomes show that Case 4 and Case 5 were able to reduce the leakage current more than the cases using two variables only. According to result of Case 1, which is varying the permittivity of the glassfibre and silicone rubber, it can be seen that the results obtained by GSA and ICA are quite similar. For ICA, the permittivity value of both materials is the same with the existing value. Case 2 shows the results of varying the width of the ground terminal, where the size obtained using ICA is larger than GSA and are the same with Case 3. The value for silicone thickness and curve housing sheds obtained from ICA is higher than GSA.

For Case 4, it shows that the permittivity value of glassfibre for GSA, 7.1873 is higher than ICA, 4.187 and its existing value, 4.2. The difference between GSA and ICA is around 3.0003. The permittivity of silicone rubber for both GSA and ICA, 12.319 and 12.303 respectively are higher than existing value, 11.7. For the width of the ground terminal, for GSA, it is lower than ICA for both block and base. For Case 5, the thickness of the silicon rubber of 3mm increases up to 4.924mm and 4.998mm for GSA and ICA. The curve of the housing sheds for both algorithm also increases from the existing value, which are 0.7996 for GSA and 0.8 for ICA. The value of the aluminium block for ICA is higher than GSA and the value of the aluminium base for GSA is lower than the existing value and ICA.

Table 4.6: Parameters obtained using GSA and ICA for Case 1

CASE 1	Existing value	GSA	ICA
Permittivity of glass	4.2	4.226	4.2
Permittivity of silicone rubber	11.7	11.859	11.7

Table 4.7: Parameters obtained using GSA and ICA for Case 2

CASE 2	Existing value	GSA	ICA
Width of aluminium block	70	75.594	76
Width of aluminium base	86	87.901	90

Table 4.8: Parameters obtained using GSA and ICA for Case 3

CASE 3	Existing value	GSA	ICA
Thickness of silicone rubber	3	3.412	4.995
Curve of housing sheds	0.4	0.67	0.75

Table 4.9: Parameters obtained using GSA and ICA for Case 4

CASE 4	Existing value	GSA	ICA
Permittivity of glass	4.2	7.1873	4.187
Permittivity of silicone rubber	11.7	12.319	12.303
Width of aluminium block	70	75.975	76
Width of aluminium base	86	85.708	90

Table 4.10: Parameters obtained using GSA and ICA for Case 5

CASE 5	Existing value	GSA	ICA
Thickness of silicone rubber	3	4.924	4.998
Curve of housing sheds	0.4	0.7996	0.8
Width of aluminium block	70	74.424	74.56
Width of aluminium base	86	83.279	86.716

4.5.2 Optimised leakage current value of surge arrester

The minimized leakage current using GSA and ICA for all case studies is shown in Figure 4.21. In this study, 150 iterations were used to acquire the results of the lowest leakage current, depending on the model and the number of parameters being used. Referring to the obtained results in Table 4.11, the leakage current is reduced for all cases.

According to Case 1, which is varying the permittivity of the materials only, it yields the leakage current value of 395.231μA from GSA and 394.101μA from ICA. In Case 2, when the width of grounded aluminium block and base of the surge arrester ground terminal was tuned, the leakage current obtained by GSA is higher than ICA, which is 384.820μA for GSA and 383.213μA for ICA. For Case 3, the results attained for GSA and ICA are 385.199μA and 384.764μA respectively. The percentage of reduction for

GSA and ICA compared to initial value of the leakage current is stated in Figure 4.26. The reduction for Case 1 is the lowest with 3.12% and 3.4% for GSA and ICA followed by Case 2 with 5.68% and 6.1% and finally Case 3 with 5.59% and 5.69%.

For Case 4, which is varying the permittivity of the materials and arrester dimension, it yields the leakage current value of 383.316μA from GSA and 382.927μA from ICA, which is lower than the leakage current from the original arrester design. This shows a reduction of 6.05% and 6.15% in the leakage current obtained by GSA and ICA respectively compared to the original arrester design. In Case 5, which is varying the dimensions of the arrester, the leakage current obtained by GSA is higher than ICA, which is 375.34μA for GSA and 374.073 μA for ICA. This shows a reduction of 8.00% and 8.32% in the leakage current obtained by GSA and ICA respectively compared to the original arrester design. As a conclusion, it can be conclude that ICA have better result compared to GSA. Therefore, ICA is more suitable in optimizing the surge arrester design with interfacing with FEA model. In general, it can be seen that by changing the width of alumnium base and block will affect the leakage current. This is because the value of leakage current is taken on the ground surface of the surge arrester which detected on the aluminium block and base. From all five cases, it shows that the value of the leakage current obtained using ICA is slightly lower than GSA.

Table 4.11: Total leakage current for all cases

Case	Total leakage current (μA)		
	Existing value	GSA	ICA
Case 1	408	395.231	394.101
Case 2	408	384.82	383.213
Case 3	408	385.199	384.764
Case 4	408	383.316	382.927
Case 5	408	375.417	374.073

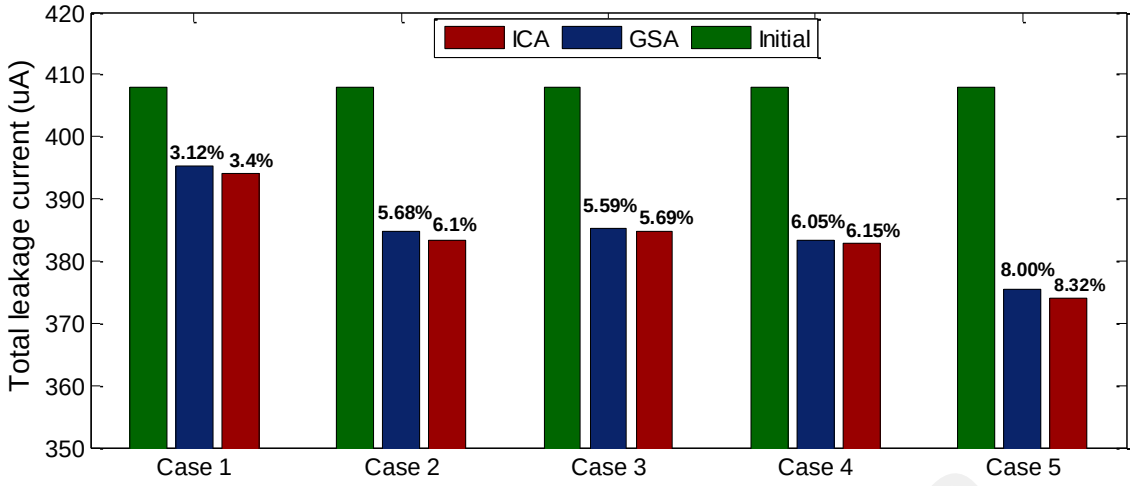

Figure 4.21: Total value of leakage current obtained using GSA and ICA

The convergence curves of ICA and GSA for Case 1 to Case 5 are shown in Figure 4.22. As can be seen, the objective function value, which is the leakage current across the arrester, using both GSA and ICA is reduced for all cases. The optimization have been run for 10 times and the results taken from the average results. Moreover, for all cases, the value of the leakage current from ICA is lower than GSA. As can be seen from these figures, the best value of the objective function, i.e. the lowest leakage current, is achieved by ICA from Case 5. However, it can be seen that the attained results illustrate the performance of GSA is relatively simple compared to ICA and generally indicates that GSA converges slightly faster than ICA. Since only 150 iterations are used, therefore, the curves are not smooth for all cases. In general, more iterations used, more smooth the curves will be. However, in this study, the curves also related to the meshing of FEA model which causes some error. For example, the element or triangular size of the meshing changed to smaller or finer elements in a FEA model to obtain smoother and discrete curves.

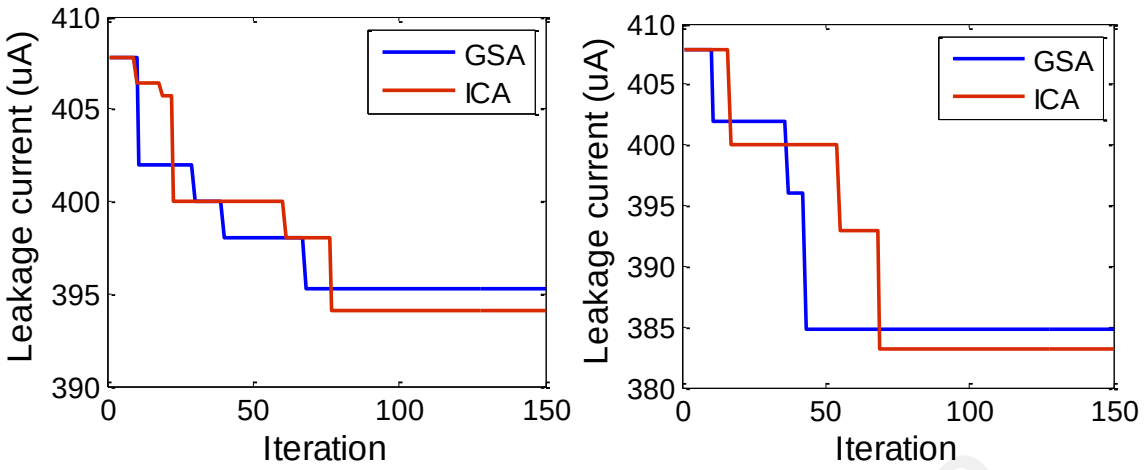

(a)

(b)

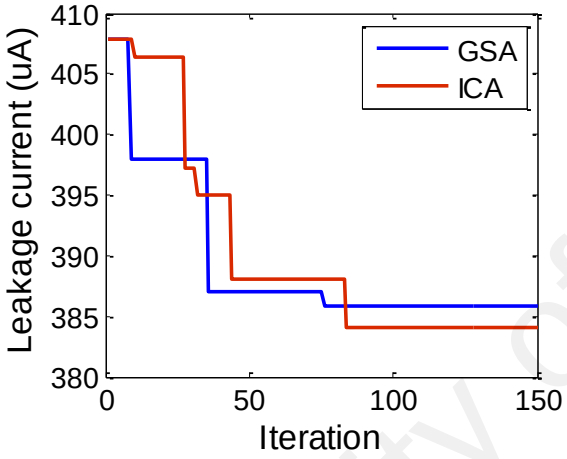

(c)

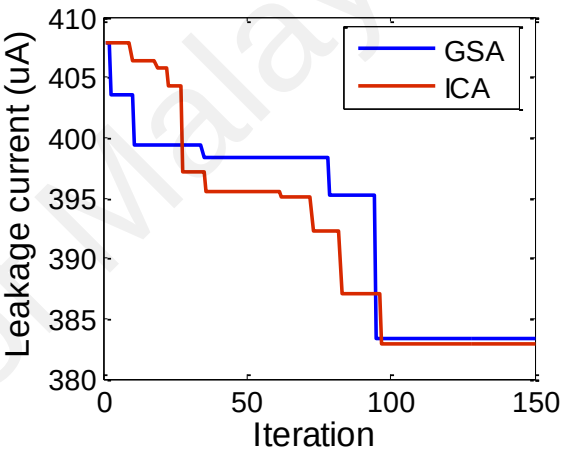

(d)

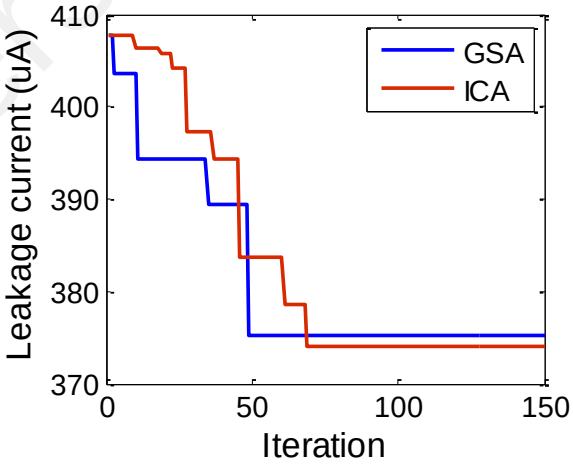

(e)

Figure 4.22: Convergence curve of GSA and ICA for (a) Case 1 (b) Case 2 (c) Case 3 (d) Case 4 and (e) Case 5

4.6 Optimised design of surge arrester model

From Figure 4.21, it can be observed that ICA for Case 5 shows the best result in reducing the leakage current with to 374.073μA. Hence, a new FEA model was developed according to the parameters obtained using ICA from Case 5. The thickness of the silicone rubber was set to 4.998mm and the curve of housing shed was set to 0.8mm. The ground aluminium block and base were fixed to 74.56mm and 86.716mm respectively. Figure 4.23 and Figure 4.24 illustrate the comparison between original design and optimised design of surge arrester.

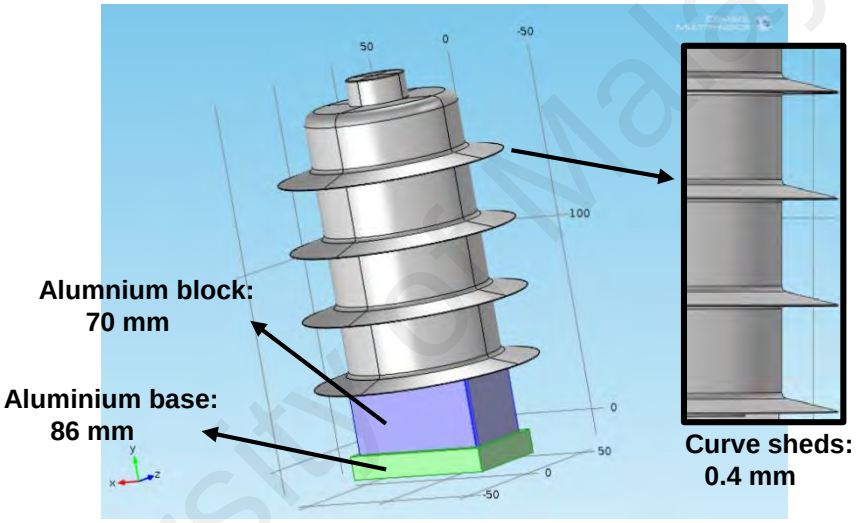

Figure 4.23: Original surge arrester

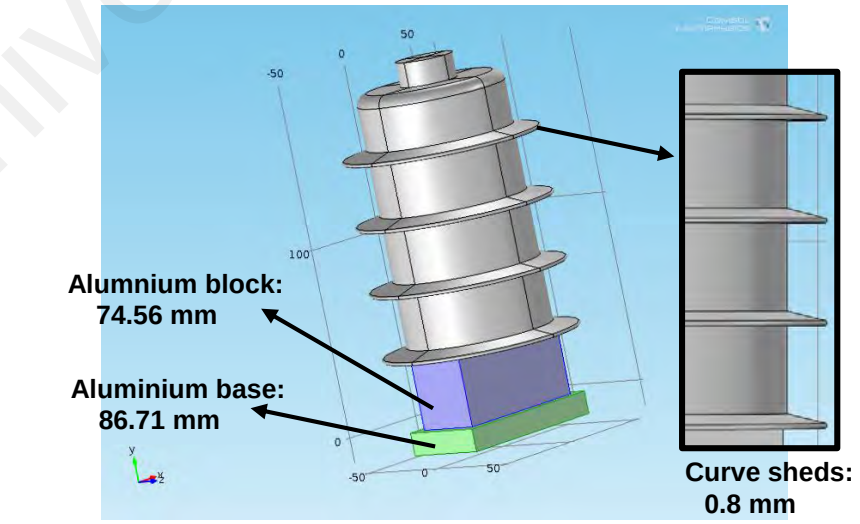

Figure 4.24: Optimised design of the surge arrester model

The electric potential, current density and electric field distributions were simulated at $9kV_{rms}$ applied voltage amplitude and presented in Figure 4.25 to Figure 4.27. It can be seen that the distribution of the electric potential, current density and electric field are high at the terminal of the surge arrester because the voltage is applied at the terminal. This is shown by the red colour scale for the electric potential and current density whereas more contour lines for the electric field. By comparing Figure 4.26 and Figure 4.27 with Figure 4.2 and Figure 4.3 in Section 4.2, the current density and electric field distribution are reduced.

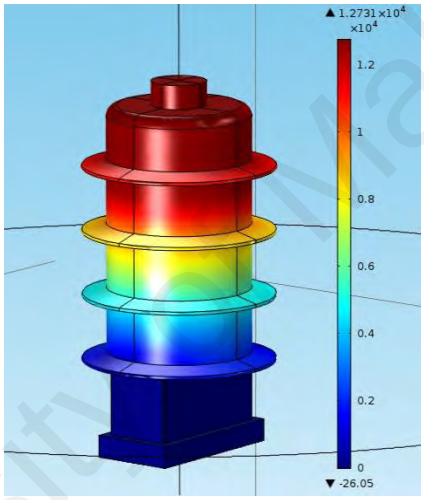

Figure 4.25: Electric potential distribution from the surge arrester FEA model

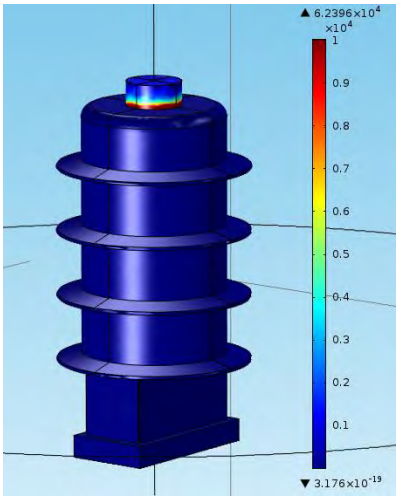

Figure 4.26: Current density distribution from the surge arrester FEA model

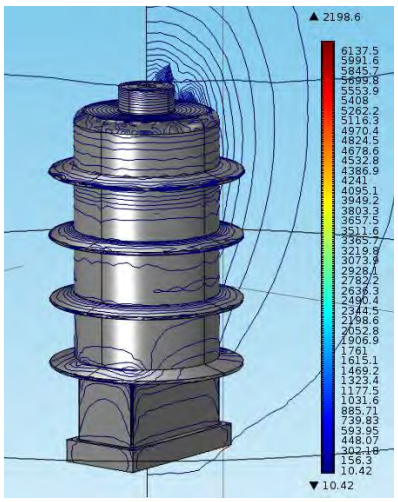

Figure 4.27: Electric field distribution from the surge arrester FEA model

The resistive and capacitive current were extracted from the obtained total leakage current by using ITDAM and the waveforms are presented in Figure 4.28. From the obtained waveform simulated at $9kV_{rms}$, the value of the leakage current for the optimised design of surge arrester reduces around 6.08%, 15.63% and 6.17% for the total leakage current, resistive current and capacitive current respectively, as tabulated in Table 4.12. Since surge arresters are affected by several conditions as shown in Section 4.4, the optimised design of the surge arrester was simulated and analysed under various conditions, which include different applied voltage amplitudes, wetness conditions and artificial pollution conditions. The optimised surge arrester model was simulated and compared with the original surge arrester model.

Table 4.12: Comparison of leakage current for original and optimised surge arrester model at $9kV_{rms}$

Leakage current type	Leakage current (uA)		Percentage of reduction (%)
	Original model	Optimised model	
Total	378	355	6.08
Resistive	32	27	15.63
Capacitive	348	325	6.17

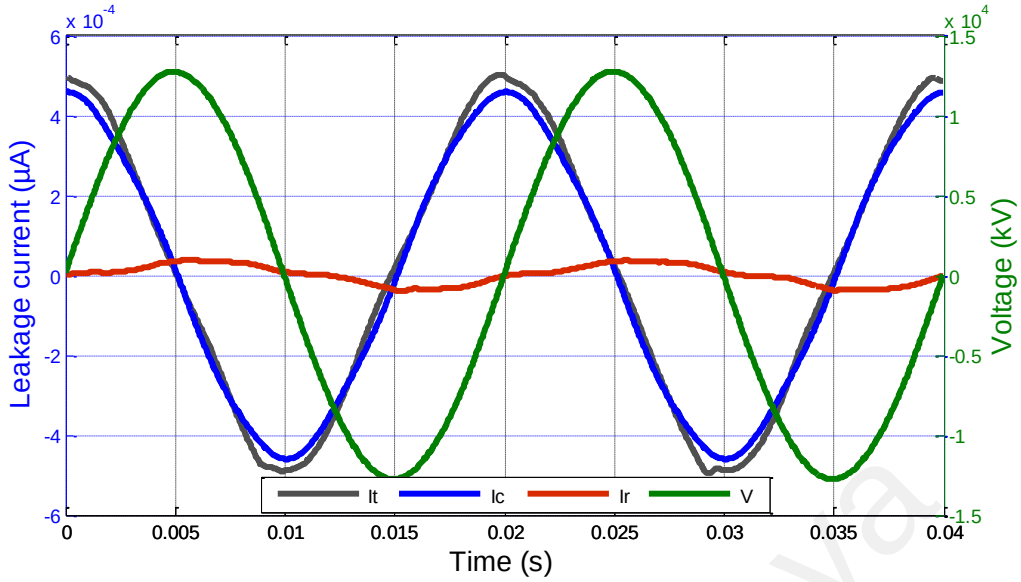

(a)

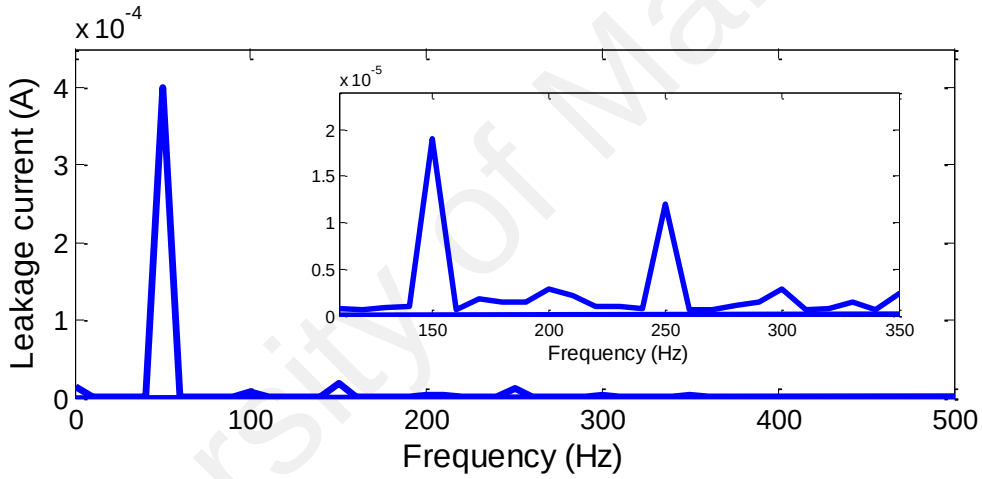

(b)

Figure 4.28: (a) Leakage current waveforms and (b) harmonic components at 9kV$_{rms}$ applied voltage

4.6.1 Optimised surge arrester model under various applied voltage amplitudes

The voltage was applied between 6kV and 10kV on the optimised surge arrester model in FEA software. From the results obtained, the leakage current increases linearly when the applied voltage is increased. Figure 4.29 and Figure 4.30 represent the total, resistive and capacitive leakage current from the simulation results of the original and optimised designs of the surge arrester model under different applied voltage amplitudes. From these figures, the results show that the leakage current is reduced in the new design of the

surge arrester compared to the original surge arrester design from 6kV to 10kV. The percentage of reduction for total, resistive and capacitive leakage current are calculated in Table 4.13 and stated in Figure 4.29 and Figure 4.30. The average percentages of reduction from the original to optimised surge arrester are 8.28%, 7.34% and 15.97% for total, capacitive and resistive leakage current respectively. Therefore, this indicates that the surge arrester design has been successfully improved using imperialist competitive algorithm (ICA).

Table 4.13: Average percentage of reduction by optimised design surge arrester under various applied voltages

Leakage current	Average percentage of reduction (%)
Total	8.28
Resistive	15.97
Capacitive	7.34

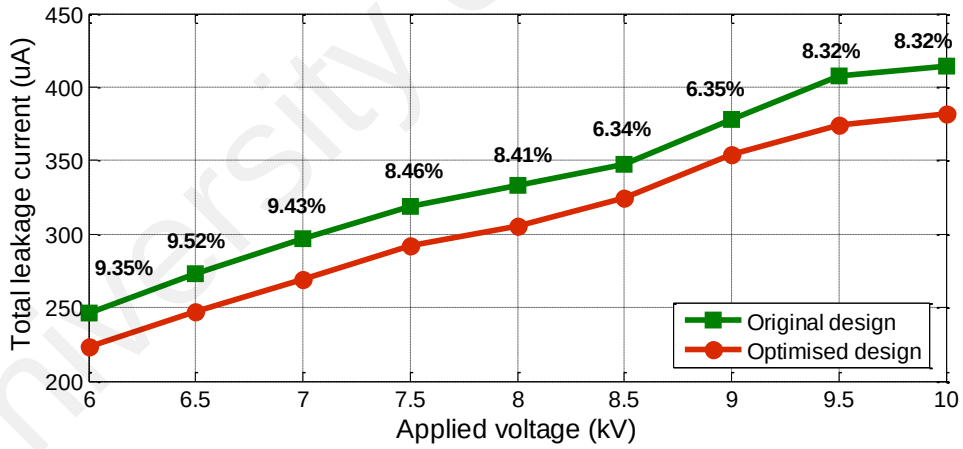

Figure 4.29: Total leakage current under different applied voltages for original and optimised surge arrester design

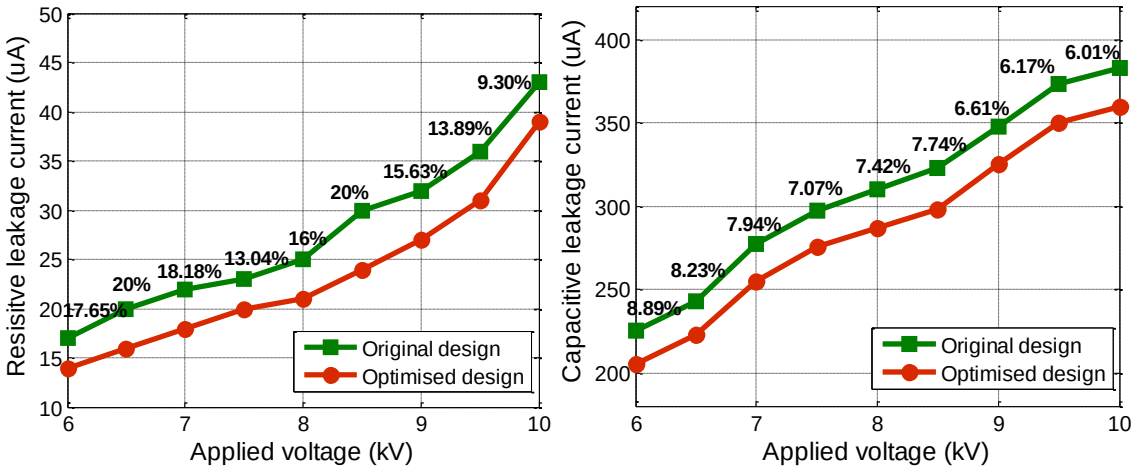

(a) **(b)**

Figure 4.30: Leakage current under different applied voltages for original and optimised surge arrester design; (a) resistive and (b) capacitive component

4.6.2 Optimised surge arrester under wetness conditions

The leakage current of the optimised surge arrester design developed using FEA software for dry and wetness conditions at $8kV_{rms}$, lightly wet, wet and heavily wet are reduced from the original design by 8.45%, 13.14% and 7.30% respectively for total, resistive and capacitive leakage current, as shown in Table 4.14. Referring to Figure 4.31 and Figure 4.32, the lines show that the optimised design has smaller leakage current compared to the original design, where the percentage of leakage current reduction for the optimised design are shown above the line. Therefore, again, this signs that the optimised design of the surge arrester model has been effectively enhanced using imperialist competitive algorithm (ICA).

Table 4.14: Average percentage of reduction by optimised design surge arrester under different wetness conditions

Leakage current	Average percentage of reduction (%)
Total	8.45
Resistive	13.14
Capacitive	7.30

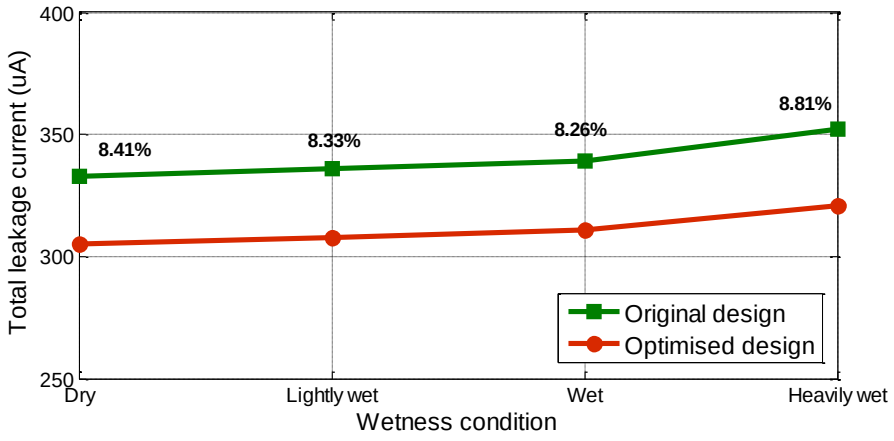

Figure 4.31: **Total leakage current under different wetness condition for original and optimised surge arrester design**

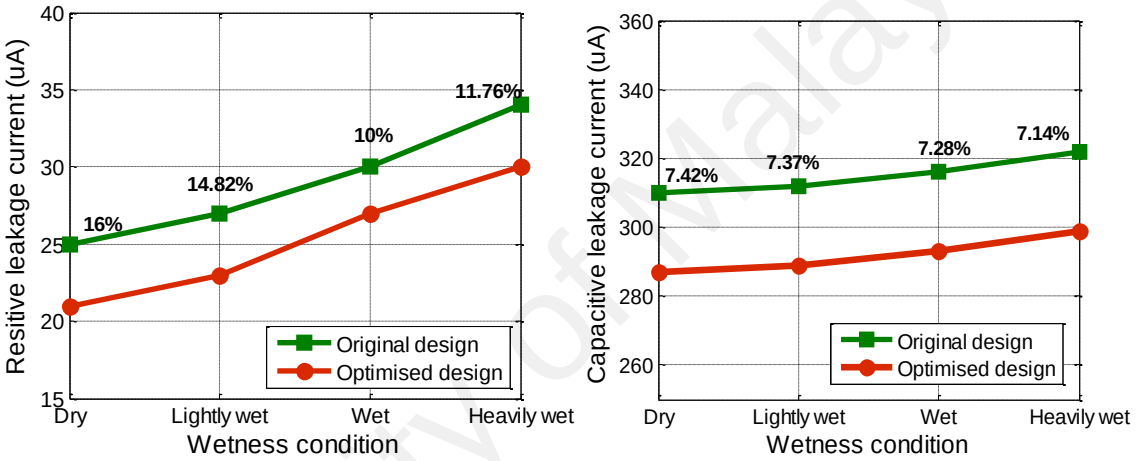

(a) **(b)**

Figure 4.32: Leakage current under different wetness condition for original and optimised surge arrester design; (a) resistive and (b) capacitive component

4.6.3 Optimised surge arrester under artificial polluted conditions

The optimised surge arrester has also been examined under polluted conditions as analysed in Section 4.43. The optimised surge arrester design was simulated using FEA software at $8kV_{rms}$ for clean and polluted conditions, where the surface of the arrester housing was contaminated with dry sand, wet sand, salt sand and salt water. From the simulation results, the percentage of reduction of the total, resistive and capacitive leakage current from the original design of the surge arrester are 8.46%, 14.6% and 7.33% respectively, as tabulated in Table 4.15. The percentages of reduction for every type of artificial pollutions are shown in the Figure 4.33 and Figure 4.34 above the green line (for

original design). Again, these results indicate that optimised design of the surge arrester model is enhanced in terms of reducing leakage current by using ICA.

Table 4.15: Average percentage of reduction by optimised design surge arrester under polluted conditions

Leakage current	Average percentage of reduction (%)
Total	8.46
Resistive	14.60
Capacitive	7.33

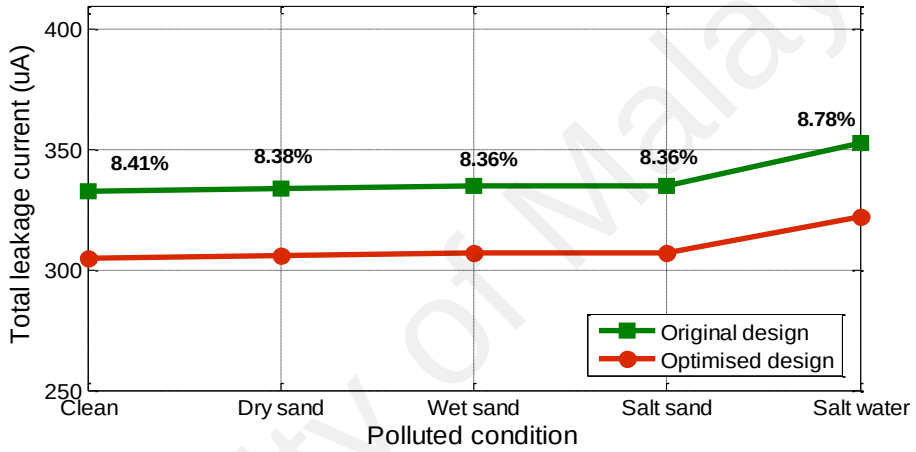

Figure 4.33: Total leakage current under polluted condition for original and optimised surge arrester design

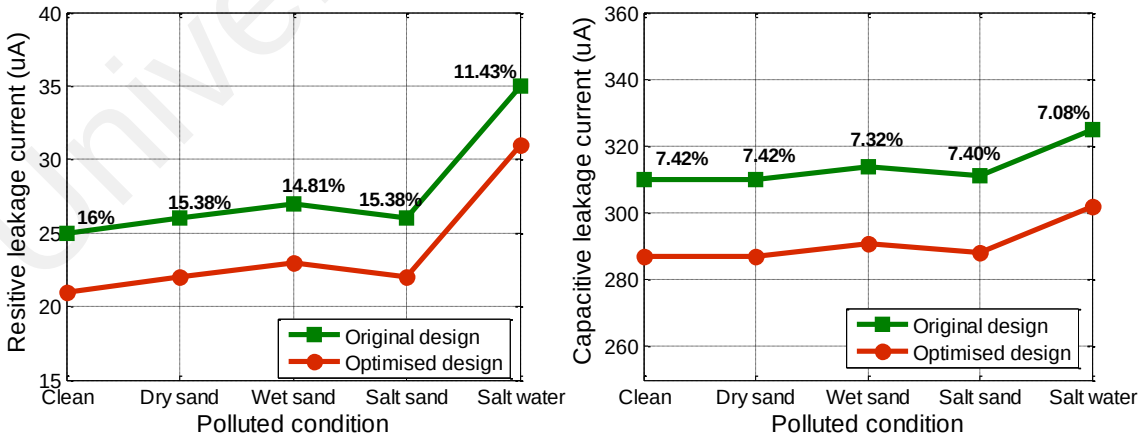

(a) **(b)**

Figure 4.34: Leakage current under polluted condition for original and optimised surge arrester design; (a) resistive and (b) capacitive component

Since polluted surface of the surge arrester influences the fundamental and third harmonic of the total leakage current (Metwally et al., 2017), fast Fourier transform (FFT) was used to obtain harmonic components on the optimised surge arrester design under salt water pollution at $8kV_{rms}$. The results were compared with the original design surge arrester. Figure 4.35 presents the harmonic components on the total leakage current for the fundamental and third harmonic of the surge arrester with clean and polluted surge arrester surface with salt water for the original and optimised surge arrester model.

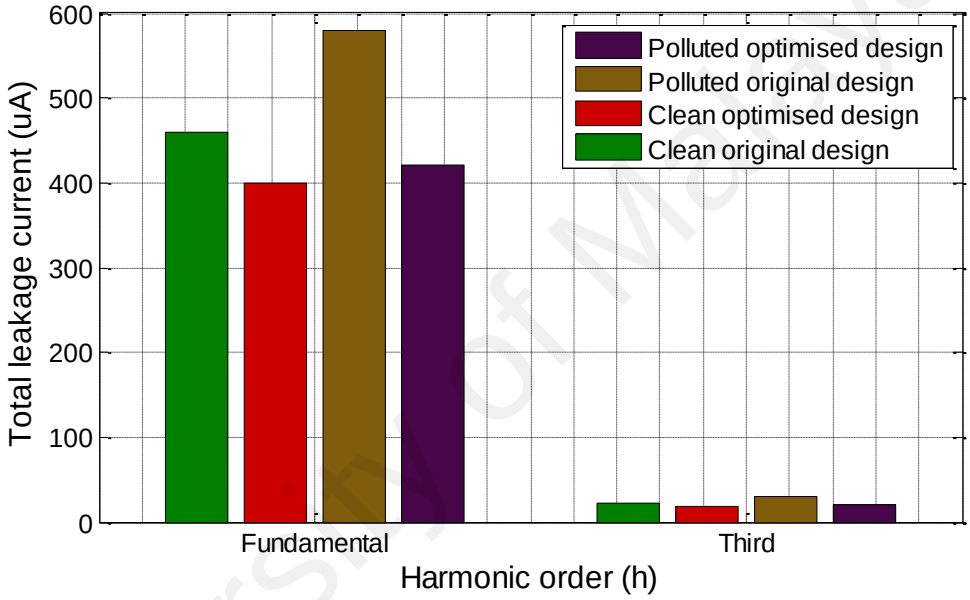

Figure 4.35: Harmonic components from the original and optimised surge arrester design under clean and polluted surface

From the obtained results, the magnitude of the fundamental and third harmonic for the optimised and original surge arrester design is smaller than under the pollution condition. For the original design, the percentage increases around 21.42% for fundamental harmonic when the surge arrester was polluted with salt water whereas for the optimised design, the percentage increases to 4.76%. For the third harmonic under polluted surface, the percentage increases to 26.67% and 5% for the original and optimised design respectively. In general, it can be seen that the optimised design of the surge arrester has lower harmonic components compared to the original surge arrester

design. Hence, it is clear that the optimised surge arrester design has been achieved in reducing leakage current and also harmonic components.

4.7 Summary

In this chapter, the results that have been obtained from this work and the explanations of each result have been discussed and evaluated. These include the leakage current measurement results, simulation results, optimization results of the surge arrester models and comparison between the measurement and simulation results. The simulation and experiment results indicate that the leakage current of surge arrester are influenced by many parameters including the applied voltage amplitude, wetness and artificial pollution conditions. The leakage current increases with increasing applied voltage and wetness of the surge arrester surface.

From the optimization results, the parameters set as the variables for ICA are thickness of the silicone rubber, the curve of the housing sheds and aluminium blocks. ICA yields better results in reducing the leakage current during normal condition than GSA. Based on the outcomes, the optimised design of the surge arrester can reduce around 8% of the total leakage current from the original design of the surge arrester model. The effectiveness of the optimised design of surge arrester was verified by developing the model in FEA software for different settings and conditions.

CHAPTER 5: CONCLUSIONS AND RECOMMENDATIONS

5.1 Conclusions

In this work, the effect of different applied voltage amplitudes, wetness conditions and artificial pollution conditions on the surge arrester leakage current has been successfully evaluated using measurement and simulation model. It was found that the leakage current increases when the applied voltage amplitude is higher, wetness level is higher and pollution condition is worse.

A three-dimensional 11 kV surge arrester model was successfully developed in finite element analysis (FEA) software and was employed to obtain the total, resistive and capacitive leakage current during normal operation under different conditions of the applied voltage, wetness and pollution conditions. The model was used to identify the surge arrester parameters, which are influenced by these conditions. The leakage current amplitudes and signals obtained from the simulation of FEA model were also compared with the measurement results. It was found that the results obtained using the proposed FEA model are within reasonable agreement with the measurement results. Thus, the proposed FEA model for leakage current modelling in surge arrester in this work can be considered reasonable.

From the FEA model of the surge arrester that has been developed, it was found that the material conductivity is affecting the leakage current significantly under different applied voltage amplitude, wetness condition and pollution condition. Hence, physical parameters of the surge arrester that influence the leakage current under different conditions of the surge arrester have been identified from the FEA model. The proposed model can also help in improvement of surge arrester design through the assessment of leakage current.

A surge arrester design has also been successfully improved using two optimisation methods, which are gravitational search algorithm (GSA) and imperialist competitive algorithm (ICA). The parameters set as the variables are the thickness of the silicone rubber, the curve of the housing sheds and the width of the ground terminal of the surge arrester. It was found that the surge arrester design obtained using ICA has lower leakage current than GSA and the original design of the surge arrester. Therefore, ICA can be considered a preferred optimisation method over GSA in designing surge arresters with lower leakage current. Consequently, this can lead to the improvement of surge arrester designs under different applied voltages and polluted conditions.

From the obtained results, it was shown that the leakage current from the original surge arrester design could be reduced by only a few percentage using optimisation techniques. However, a small change could improve the life of the surge arrester slightly but experiments are required to assess the actual improvement. Other ways of reducing the leakage current in the future are by improving the condition monitoring methods and reducing pollution on the surge arrester.

5.2 Recommendations

Recommendations for the future work are as follows:

1) Additional improvements on the FEA model can be done by considering omitted assemblies of the ZnO surge arrester such as the zinc oxide wall, stainless steel rod, disc string and drilled holes.
2) In this study, the best optimisation design of the ZnO surge arrester is focusing on reducing leakage current that flow through arrester. However, the design also can be improve by adding measurement tan delta value. By measuring tan delta value, the overheating of the surge arrester can be reduced and hence reducing the

degradation of the surge arrester. Many insulating substances have dielectric constant greater than unity and have dielectric loss when subjected to AC voltage. This loss depends on the magnitude of the voltage stress and on the frequency of the applied voltage.

REFERENCES

3-4-11, I. W. (1992). Modeling of metal oxide surge arreste. *IEEE Transactions on Power Delivery, 7*(1), 302-309.

A. Gakiya Kanashiro, & al., e. (2011). Diagnostic of Silicon Carbide Surge Arresters Using Leakage Current Measurements. *IEEE Latin America Transactions*.

Abdul-Malek, Z., Novizon, & Aulia. (2008, 1-3 Dec. 2008). *A new method to extract the resistive component of the metal oxide surge arrester leakage current.* Paper presented at the 2008 IEEE 2nd International Power and Energy Conference.

Abdul Latiff, N. A., Illias, H. A., Abu Bakar, A. H., Abd Halim, S., & Dabbak, S. Z. (2018). Design technique for leakage current reduction in surge arrester using gravitational search algorithm and imperialist competitive algorithm. *COMPEL-The international journal for computation and mathematics in electrical and electronic engineering, 37*(1), 357-374.

Akbar, M., & Ahmad, M. (1999). Failure study of metal-oxide surge arresters. *Electric Power Systems Research, 50*(2), 79-82.

Almeida, C. A. L. (2009). Intelligent Thermographic Diagnostic Applied to Surge Arresters: A New Approach. *IEEE Transactions on Power Delivery, 24*.

B., A. (2008). Parameter identification of ZnO surge arrester models based on genetic algorithms. *Electric Power Systems Research*.

Bakar, A., Halim, A., Zainal Abidin, A., Illias, H. A., Mokhlis, H., Abd Halim, S., . . . Tan, C. K. (2016). Determination of the striking distance of a lightning rod using finite element analysis. *Turkish Journal of Electrical Engineering & Computer Sciences, 24*(5).

Baran, M. E., & Wu, F. F. (1989). Network reconfiguration in distribution systems for loss reduction and load balancing. *Power Delivery, IEEE Transactions on, 4*(2), 1401-1407.

Bassi, W., & Tatizawa, H. (2016). Early prediction of surge arrester failures by dielectric characterization. *IEEE Electrical Insulation Magazine, 32*(2), 35-42.

Bhattacharya, A., & Roy, P. K. (2012). Solution of multi-objective optimal power flow using gravitational search algorithm. *Generation, Transmission & Distribution, IET, 6*(8), 751-763.

Bok-Hee Lee, Sung-Man Kang, Ju-Hong Eom, & Kawamura, T. (2003). A Monitoring Device of Leakage Currents Flowing through ZnO Surge Arreters. *The Japan Society of Applied Physics*.

C. Lin, W. Lee, C. S., & W.Whu. (2008). A varistor-polymer composite with nonlinear electrical-thermal switching properties. *Ceram International, 34*, 131-136.

C.A. Christodoulou, L. Ekonomou, G.P. Fotis, P. Karampelas, & Stathopulos, I. A. (2009). Parameters' optimisation for surge arrester circuit models. *IET Science, Measurement & Technology*.

Chrzan, K. L. (2004). Influence of moisture and partial discharges on the degradation of high-voltage surge arresters. *European Transactions On Electrical Power*.

Coleman, V. A., & Jagadish,. (2000). *Basic Properties and Applications of ZnO.*

D.H. Kim, A. Abraham, & Cho, J. H. (2007). A hybrid genetic algorithm and bacterial foraging approach for global optimization, *Information Sciences, 177*, 3918–3937.

Duman, S., So, x, nmez, Y., Gu, x, . . . keren, N. (2012). Optimal reactive power dispatch using a gravitational search algorithm. *Generation, Transmission & Distribution, IET, 6*(6), 563-576.

Esmat Rashedi, Hossein Nezamabadi-pour , & Saryazdi, S. (2009). GSA: A Gravitational Search Algorithm. *Information Sciences, 179*, 2232–2248.

Esmat Rashedi, Hossein Nezamabadi-pour *, & Saryazdi, S. (2009). GSA: A Gravitational Search Algorithm. *Information Sciences*(179), 2232–2248.

F. Tian, Q. Lei, X. W., & Wang, Y. (2011). Effect of deep trapping states on space charge suppression in polyethylene/ZnO nanocomposite, *Applied Physics Letters, 99*.

Faria, I. P. d., Martinez, M. L. B., & Queiroz, A. A. A. d. (2015). Electrical performance evaluation of plasticized polyolefin formulation developed for manufacturing surge arresters housings. *IEEE Transactions on Dielectrics and Electrical Insulation, 22*(6), 3429-3441.

G. Heger, H.J. Vermeulen, J.P. Holtzhausen, & Vosloo., W. L. (2010). A comparative study of insulator materials exposed to high voltage AC and DC surface discharges. *IEEE Transactions on Dielectrics and Electrical Insulation, 17*.

Glotic, A., Joze Pihler, Janez Ribic, & Stumberger., G. (2010). Determining a Gas-Discharge Arrester Model's Parameters by Measurements and Optimization. *IEEE Transactions on Power Delivery*.

Group, I. W. (1992). Modeling of metal oxide surge arresters, *IEEE Transactions on Power Delivery*.

Gubanski, S. M., Vlastos, & E, A. (1990). Wettability of naturally aged silicon and EPDM composite insulators. *IEEE Transactions on Power Delivery*.

Hamed Zeinoddini-Meymand, Behrooz Vahidi, Ramezan Ali Naghizadeh, & Moghimi-Haji, M. (2013). Optimal Surge Arrester Parameter Estimation Using a PSO-Based Multiobjective Approach. *IEEE Transactions on Power Delivery, 28*.

Harid, N., Bogias, A. C., Griffiths, H., Robson, S., & Haddad, A. (2016). A Wireless System for Monitoring Leakage Current in Electrical Substation Equipment. *IEEE Access, 4*, 2965-2975.

Hazlee Azil Illias, S. A. H., Ab Halim Abu Bakar, Hazlie Mokhlis. (2014). Determination of surge arrester discharge energy using finite element analysis method. *IET Science, Measurement & Technology*.

Heinrich, C., & Hinrichsen, V. (2001). Diagnostics and monitoring of metal-oxide surge arresters in high-voltage networks-comparison of existing and newly developed procedures. *IEEE Transactions on Power Delivery, 16*(1), 138-143.

Hinrichen, V. (Ed.). (2006). *Metal Oxide Surge Arrester* (1st ed.): Siemens.

Hoang, T. T., Cho, M.-Y., Alam, M. N., & Vu, Q. T. (2018). A novel differential particle swarm optimization for parameter selection of support vector machines for monitoring metal-oxide surge arrester conditions. *Swarm and Evolutionary Computation, 38*, 120-126.

Hosseini, S. H., & Gharadaghi, Y. (2017). New Modeling of Metal Oxide Surge Arresters. *Electrical Engineering*, 25-34.

Illias, H., Chen, G., & Lewin, P. L. (2017). Comparison between three-capacitance, analytical-based and finite element analysis partial discharge models in condition monitoring. *IEEE Transactions on Dielectrics and Electrical Insulation, 24*(1), 99-109.

Illias, H. A., Bakar, A. H. A., Mokhlis, H., & Halim, S. A. (2012). Calculation of inductance and capacitance in power system transmission lines using finite element analysis method. *PRZEGLĄD ELEKTROTECHNICZNY, 10a*(88).

Illias, H. A., Chen, G., & Lewin, P. L. (2011). The influence of spherical cavity surface charge distribution on the sequence of partial discharge events. *Journal of Physics D: Applied Physics, 44*(24), 245202.

Ivan Paulo de Faria, Manuel Luis Barreira Martinez, & Queiroz, A. A. A. d. (2015). Electrical Performance Evaluation of Plasticized Polyolefin Formulation Developed for Manufacturing Surge Arresters Housings. *IEEE Transactions on Dielectrics and Electrical Insulation*.

J.D. Farmer, N.H. Packard, & Perelson, A. S. (1986). The immune system, adaptation and machine learning. *Physica, 2*, 87–204.

Jazebi, S., Hadji, M. M., & Naghizadeh, R. A. (2014). Distribution Network Reconfiguration in the Presence of Harmonic Loads: Optimization Techniques and Analysis. *IEEE Transactions on Smart Grid, 5*(4), 1929-1937.

Jinliang, H., Shuiming, C., Rong, Z., Jun, H., & Chenggang, D. (2006). Development of polymeric surge ZnO arresters for 500-kV compact transmission line. *Power Delivery, IEEE Transactions on, 21*(1), 113-120.

K.S. Tang, K.F. Man, S. Kwong, & He, Q. (1996). Genetic algorithms and their applications *IEEE Signal Processing Magazine, 13*(6), 22-37.

K.Steinfeld. (2000). Design of Metal-Oxide Surge Arresters with Polymeric Housings.

Khodsuz, M., & Mirzaie, M. (2015). Evaluation of ultraviolet ageing, pollution and varistor degradation effects on harmonic contents of surge arrester leakage current. *IET Science, Measurement & Technology, 9*(8), 979-986.

Khodsuz, M., & Mirzaie, M. (2016). An improved time-delay addition method for MOSA resistive leakage current extraction under applied harmonic voltage. *Measurement, 77*, 327-334.

Khodsuz, M., Mirzaie, M., & Seyyedbarzegar, S. (2015). Metal oxide surge arrester condition monitoring based on analysis of leakage current components. *International Journal of Electrical Power & Energy Systems, 66*, 188-193.

Khorani, V., Razavi, F., & Disfani, V. R. (2011). A Mathematical Model for Urban Traffic and Traffic Optimization Using a Developed ICA Technique. *Intelligent Transportation Systems, IEEE Transactions on, 12*(4), 1024-1036.

Latiff, N. A., Illias, H. A., Bakar, A. H., & Dabbak, S. Z. (2018). Measurement and Modelling of Leakage Current Behaviour in ZnO Surge Arresters under Various Applied Voltage Amplitudes and Pollution Conditions. *Energies, 11*(4), 875.

Lee, B.-H., & Kang, S.-M. (2005). A new on-line leakage current monitoring system of ZnO surge arresters. *Materials Science and Engineering: B, 119*(1), 13-18.

Liao, R., Wang, Z., Sun, C., Gu, L., Yan, P., & Yang, B. (2000, 2000). *The harmonic analysis method and its application in the on-line detection of electric equipment insulation.* Paper presented at the Proceedings of the 6th International Conference on Properties and Applications of Dielectric Materials (Cat. No.00CH36347).

Lira, G. R. S., & Costa, E. G. (2013). MOSA Monitoring Technique Based on Analysis of Total Leakage Current. *Power Delivery, IEEE Transactions on, 28*(2), 1057-1062.

Lira, G. R. S., Costa, E. G., & Ferreira, T. V. (2014). Metal-oxide surge arrester monitoring and diagnosis by self-organizing maps. *Electric Power Systems Research, 108*, 315-321.

Lu, J., Xie, P., Fang, Z., & Hu, J. (2018). Electro-Thermal Modeling of Metal-Oxide Arrester under Power Frequency Applied Voltages. *Energies, 11*(6), 1-13.

Lundquist, J., Stenstrom, L., Schei, A., & Hansen, B. (1990). New method for measurement of the resistive leakage currents of metal-oxide surge arresters in service. *IEEE Transactions on Power Delivery, 5*(4), 1811-1822.

Luo, Y. F. (2003). *Study on metal-oxide-arrester on-line monitoring distributed- control-system.* (M.Eng Eng.), School Elect. Eng., Xi'an Jiao tong University, Xi'an, China.

M, P., & G.C, P. (2002). Application of a New SurgeArrester Model in Protection Studies Concerning Switching Surges. *IEEE Power Engineering Review, 22*(9).

M. Dorigo, V. Maniezzo, & A. Colorni. (1996). The ant system: optimization by a colony of cooperating agents. *EEE Transactions on Systems, Man, and Cybernetic, 26*(1), 29-41.

M.K. Yalla1, V. P. (2012). A new modified shifted current technique to diagnose the surge arrester condition. *Int. J. Eng. Res. Technol.(IJERT), 1-5*.

M.R. Aghaebrahimi, Shariatinasab, R., & Ghayedi, M. (2012). Optimal Design of Grading Ring of Surge Arresters Due to Electric Field Distribution. *IEEE Transactions on Power Delivery*.

Martinez, J. A., & Durbak, D. W. (2005). Parameter Determination for Modeling Systems Transients—Part V: Surge Arresters. *IEEE Transactions on Power Delivery*.

Meshkatoddini, M. R. (2018). *Study of the Electric Field Intensity in Bushing Integrated ZnO surge Arresters by Means of Finite Element Analysis*.

Metwally, I. A., Eladawy, M., & Feilat, E. A. (2017). Online Condition Monitoring of Surge Arresters Based on Third-Harmonic Analysis of Leakage Current. *IEEE Transactions on Dielectrics and Electrical Insulation, 24*(4).

Miguel, P. M. (2014). Comparison of Surge Arrester Models. *IEEE Transactions on Power Delivery*.

Mohammad Ali Atefi, Majid Sanaye-Pasand, & Bahari, S. (2013). Preventing Transformer Energizing Resonant Overvoltages Using Surge Arrester Temperature Rise Index and Controlled Closing Method. *IEEE Transactions on Power Delivery*.

Mousavi, S., Feizifar, B., & Onal, E. (2017). A Wide-Range Model for Surge Arresters: Verification Analysis. *Energy Procedia, 141*, 460-464.

Nafar, M., Gharehpetian, G. B., & Niknam, T. (2011). A novel parameter estimation method for metal oxide surge arrester models. *Sadhana, 36*(6), 941-961.

Naidu, M., & Kamaraju, S. (2006). *High Voltage Engineering* (Third ed.). Singapore: Mc Graw Hill.

Novizona, Maleka, Z. A., Nouruddeen Bashira, & Asilah, N. (2013). Thermal Image and Leakage Current Diagnostic as a Tool for Testing and Condition Monitoring of ZnO Surge Arrester. *Jurnal Teknologi*.

Ohki, Y. (2014). Advanced Directly Molded Type Polymer-Housed Surge Arresters. *IEEE Electrical Insulation Magazine, 29*.

PINCETI P., & M, G. (1999). A simplified model for zinc oxide surge arresters. *IEEE Transactions on Power Delivery, 14*(2), 393-398.

Pinto, J. D., Coimbra, A. P., Antunes, C. L., & e Moura, A. M. (1998). *Thermal analysis of a ZnO surge arrester using the finite element approach.* Paper presented at the Power System Technology, 1998. Proceedings. POWERCON'98. 1998 International Conference on.

R. Arora, & Mosch, W. (Eds.). (2011). *High Voltage and Electrical Insulation Engineering*. New Jersey: John Wiley & Sons.

Rashedi, E., Nezamabadi-pour, H., & Saryazdi, S. (2011). Filter modeling using gravitational search algorithm. *Engineering Applications of Artificial Intelligence, 24*(1), 117-122.

Reza Shariatinasab, Farid Ajri, & Daman-Khorshid, H. (2013). Probabilistic evaluation of failure risk of transmission line surge arresters caused by lightning flash. *IET Generation, Transmission & Distribution*.

Safari, M., & Sarvi, M. (2014). Optimal load sharing strategy for a wind/diesel/battery hybrid power system based on imperialist competitive neural network algorithm. *Renewable Power Generation, IET, 8*(8), 937-946.

Said, A. (2018). Analysis of 500kV OHTL polluted insulator string behavior during lightning strokes. *International Journal of Electrical Power & Energy Systems, 95*, 405-416.

Seyyedbarzegar, S. M., & Mirzaie, M. (2016). Thermal balance diagram modelling of surge arrester for thermal stability analysis considering ZnO varistor degradation effect. *IET Generation, Transmission & Distribution, 10*(7), 1570-1581.

Shinji Ishibe, Masafumi Mori, Masahiro Kozako, & Hikita, M. (2014). A New Concept Varistor With Epoxy/Microvaristor Composite. *IEEE Transactions on Power Delivery*.

Shirakawa, S., Endo, F., Kitajima, H., Kobayashi, S., Goto, K., & Sakai, M. (1988). Maintenance of surge arrester by a portable arrester leakage current detector. *IEEE Transactions on Power Delivery, 3*(3), 998-1003.

Sp, Y.,E, ck, L., Gjonaj, E., Gersem, H. D., Weiland, T., . . . Hinrichsen, V. (2016). Electroquasistatic-Thermal Modeling and Simulation of Station Class Surge Arresters. *IEEE Transactions on Magnetics, 52*(3), 1-4.

Steinfeld K., Gohler R., & D, P. (2003). *High Voltage Surge Arrester for Protection of Series Compensation and HVDC Converter Stations*. Paper presented at the The 4th International Conference on Power Transmission and Distribution Technology, Berlin.

T. Takada, Y. Hayase, Y. T., & Okamoto, T. (2008). Space charge trapping in electrical potential well caused by permanent and induced dipoles for LDPE/MgO nanocomposite. *IEEE Transactions on Dielectrics and Electrical Insulation, 15*.

Teyssedre, G., & Laurent, C. (2013). Advances in High-Field Insulating Polymeric Materials Over the Past 50 Years. *IEEE Electrical Insulation Magazine, 29*.

Valsalal, P., Usa, S., & Udayakumar, K. (2011). Modelling of metal oxide arrester for very fast transients. *Science, Measurement & Technology, IET, 5*(4), 140-146.

W. Du, & Li, B. (2008). Multi-strategy ensemble particle swarm optimization for dynamic optimization. *Information Sciences 178*, 3096–3109.

Woodworth, J. (2010). History of Arresters on Power Systems 1965 - Present. *ArresterWorks*.

X. Wang, D. M. Tu, C. L., & Du, Q. G. (2008). Insulation performance and microstructure in modified polyethylene by MPE. *Journal of Applied Polymer Science, 107*.

Xu, Z. n., Zhao, L. j., Ding, A., & Lu, F. c. (2013). A Current Orthogonality Method to Extract Resistive Leakage Current of MOSA. *IEEE Transactions on Power Delivery, 28*(1), 93-101.

Zhang, C., Kester, J. J., Daley, C. W., & Rigby, S. J. (2010). *Electric field analysis of high voltage apparatus using finite element method.* Paper presented at the Electrical Insulation and Dielectric Phenomena (CEIDP), 2010 Annual Report Conference on.

Zeinoddini-Meymand, H., Vahidi, B., Naghizadeh, R. A., & Moghimi-Haji, M. (2013). Optimal surge arrester parameter estimation using a PSO-based multiobjective approach. *IEEE Transactions on Power Delivery*, *28*(3), 1758-1769.

LIST OF PUBLICATIONS AND PAPERS PRESENTED

List of ISI journal papers:

1) N.A.A. Latiff, H.A. Illias, A.H.A. Bakar, S.A. Halim and S.Z. Dabbak, "Design technique for leakage current reduction in surge arrester using gravitational search algorithm and imperialist competitive algorithm," *International Journal for Computation and Mathematics in Electrical and Electronic Engineering (COMPEL)*, Vol. 37, No. 1, pp.357-374, 2018.
2) N. Latiff, H. Illias, A. Bakar, and S. Dabbak, "Measurement and Modelling of Leakage Current Behaviour in ZnO Surge Arresters under Various Applied Voltage Amplitudes and Pollution Conditions," *Energies*, vol. 11, no. 4, p. 875, Apr. 2018.

List of conference papers:

1. Latiff, N. A. A., Illias, H. A., Abu Bakar, A. H., "Condition monitoring of discharged ZnO surge arrester on temperature distribution under various design conditions," *International Conference on Condition Monitoring and Diagnosis 2016*, pp.1-4, Xian, China, September 2016.
2. Latiff, N. A. A., Illias, H. A., Dabbak, S. Z., "Measurement of leakage current in 11kV Zinc Oxide surge arresters," *2016 MyHVnet Colloquium*, Johor Bahru, Malaysia, Jan 2016.
3. Latiff, N. A. A., Illias, H. A., Abu Bakar, A. H., "Analysis of Leakage Current on 11kV Zinc Oxide Surge Arrester Using Finite Element Method," *International Power Engineering and Optimization Conference*, Malacca, Malaysia, March 2015.

List of posters:

1. Latiff, N. A. A, and Illias, H. A., "Leakage Current Analysis of Various Parameters on 11kV Surge Arrester Designs," *COMSOL Conference 2015*, Kuala Lumpur, Malaysia, November 2015.
2. Latiff, N. A. A, and Illias, H. A., Analysis of Leakage Current on 11kV Zinc Oxide Surge Arrester using Finite Element Method," Postgraduate Day 2015, Kuala Lumpur, Malaysia, May 2015.